

Departament de Física, Facultat de Ciències
Universitat Autònoma de Barcelona
January 2008

Electron beam lithography for Nanofabrication

A scanning electron microscope (SEM) image of a circular, porous structure, likely a nanofabricated component. The structure has a complex, interconnected network of fibers or filaments forming a mesh-like pattern. The central part of the structure is darker, suggesting a different material or a shadow effect. The overall appearance is that of a highly porous, spherical or cylindrical object.

PhD Thesis by

Gemma Rius Suñé

Directed by Francesc Pérez-Murano and Joan Bausells

*The cover image corresponds to a
PMMA residual found after the
stripping of the resist layer.*

*Even though it seems a new planet,
it is 1 μ m in diameter.*

This memory reflects part of the work performed at the Nanofabrication Laboratory of the IMB–CNM during the past 5 years, based on Electron Beam Lithography (EBL).

Nanofabrication is a very active area of research, as can be noticed from the number of publications that appear continuously and from the number of running R&D projects. Most of the work is realized in the framework of three European research projects.

Novopoly project deals with the development of new polymer materials for applications in micro and nano systems. The development of a new EBL resist is framed in this project.

Within NaPa, Emerging Nanopatterning methods, the development of NEMS fabrication with EBL is used to realise discrete nanomechanical devices. They are used to characterize the performance of resonating nanostructures and signal enhancement is achieved by their integration in CMOS circuits.

The aim of Charpan is the development of a new patterning tool based on several charged particle species. The incidence of charged particle beams on devices is studied to evaluate potential effects induced during fabrication.

Carbon nanotube (CNT) based devices contribute to some tasks of national projects Crenatun and Sensonat. In particular, the technology for fabrication of high performance CNT field-effect transistors and their preparation for sensing applications is established.



Directors:

Pr. Francesc Pérez-Murano

Pr. Joan Bausells Roigé

Tutor UAB:

Jordi Pascual Gainza

Els doctors Francesc Pérez-Murano i Joan Bausells, ambdós Professors d'Investigació del Consejo Superior de Investigaciones Científicas (CSIC) a l'Institut de Microelectrònica de Barcelona (IMB-CNM),

CERTIFIQUEN

que la present memòria titulada "Electron beam lithography for Nanofabrication" ha estat realitzada sota la seva direcció per na Gemma Rius Suñé

Bellaterra, gener 2008

Departament de Física, Facultat de Ciències,
Universitat Autònoma de Barcelona



Preface

Acknowledgements

1	Introduction	1
1.1	Towards the nanometer scale.....	1
1.2	Nanotechnology and nanofabrication	3
1.3	Nanopatterning. Nanolithographic techniques.....	6
1.4	Nanoapplications. Nanometric devices.....	10
1.4.1	Nanodevices. From micro- to nano-electronics.	11
2	Electron Beam Lithography	17
2.1	Lithographic technique	17
2.1.1	Introduction to the concept.....	17
2.1.2	Instrumental	18
2.1.3	Characteristics.....	19
2.1.4	Limitations	19
2.1.5	Resolution and applications	20
2.2	Instruments for SEM based lithography	21
2.2.1	SEM based system	21
2.2.2	Electron source.....	22
2.2.3	SEM column	23
2.2.4	Chamber and stage	27
2.2.5	Computer control	27
2.2.6	Vacuum system.....	29
2.3	Exposure procedure	30
2.3.1	Equipment	30
2.3.2	Procedure	31
2.3.3	Deflection calibration.....	32
2.3.4	Positioning	33
2.3.5	Focusing.....	36
2.3.6	Pattern design.....	37
2.3.7	Exposure conditions.....	39
3	Electron beam irradiation of resists	47
3.1	Exposure effect	47
3.1.1	Organic resists.....	48
3.1.2	Resist processing.....	51
3.1.3	Modeling the effect of exposure	52
3.2	Poly(methyl methacrylate). A positive resist.....	59
3.2.1	Simulations on PMMA	61
3.2.2	Exposure results in PMMA.....	64
3.2.3	Methacrylic resists	70
3.3	Epoxy based resists. Negative resists.....	72
3.3.1	Simulations on SU8	73
3.3.2	Electron beam lithography on thick layers of mr-L 5005 XP	75
3.3.3	Electron beam on thin layers: mr-EBL 6000.1 XP and ma-N 2401.....	79
3.3.4	Post-lithography processing: etch resistance.....	88
3.4	Proximity effect correction	95
3.4.1	Proximity effect.....	95
3.4.2	Theoretical model. Proximity function	97

3.4.3	Methodology for Proximity Effect Correction parameter.....	99
3.4.4	Experimental Proximity Effect Correction parameters.....	101
3.4.5	Computer-based Proximity Effect Correction. NanoPECS.....	105
3.4.6	Results of Proximity Effect Correction on PMMA.....	106
3.4.7	Results of Proximity Effect Correction on mr-EBL 6000.1 XP.....	111
4	Fabrication of nanomechanical devices.....	119
4.1	Introduction to nanomechanics.....	119
4.2	Fabrication process.....	122
4.3	Fabrication of discrete nanomechanical devices.....	123
4.4	Fabrication of CMOS-integrated nanomechanical devices.....	130
4.5	Focused Ion Beam fabrication combined with Electron Beam Lithography.....	136
5	Fabrication of Carbon Nanotube based devices by EBL.....	143
5.1	Introduction to carbon nanotubes.....	143
5.2	Fabrication of CNTFETs.....	146
5.2.1	Contacting deposited CNTs.....	147
5.2.2	Contacting CVD grown CNTs.....	150
5.3	Electrical characterization.....	154
5.3.1	Electrical measurements set up.....	157
5.3.2	Results for semiconducting and metallic contacted CNTs.....	158
5.3.3	Device performance overview.....	168
5.4	Sensors based on CNTFETs.....	169
5.4.1	CNT protection, passivation.....	170
5.4.2	Liquid measurements.....	172
5.4.3	Set up for CNT based measurement systems.....	175
5.5	Local and oriented growth of CNTs for fabrication of devices.....	177
5.5.1	Negative resist.....	178
5.5.2	Positive resist.....	179
5.5.3	Zeolites deposition.....	180
6	Study of the effect of charged particle irradiation on electronic nanodevices	189
6.1	Effect of Electron Beam on CMOS integrated circuits and devices.....	190
6.1.1	Damage during fabrication of CMOS-NEMS.....	192
6.1.2	Electron Beam induced motion of NEMS.....	197
6.2	Atomic Force Microscopy based characterization techniques.....	203
6.2.1	Electrical Force Microscopy.....	204
6.2.2	Kelvin Probe Force Microscopy.....	210
6.3	Electron Beam exposure on CNTFETs.....	213
6.3.1	Electrical characterization.....	213
6.3.2	Electrical Force Microscopy and Kelvin Probe Force Microscopy on exposed CNTFET devices.....	217
6.3.3	Electrostatic simulations.....	220
6.3.4	Comparison to MOS results and theoretical analysis.....	221
6.3.5	Design of ion beam induced experiments on CNTFETs.....	223
7	Conclusions.....	231

Glossary

Scientific CV

Preface

Electron beam lithography (EBL) has consolidated as one of the most common techniques for patterning at the nanoscale meter range. It has enabled the nanofabrication of structures and devices within the research field of nanotechnology and nanoscience.

EBL is based on the definition of submicronic features by the scanning of a focused energetic beam of electrons on a resist. The nature of electrons and the development of extremely fine beams and its flexible control provide the platform to satisfy the requirements of Nanofabrication. Use of EBL for the development of a wide range of nanostructures, nanodevices and nanosystems has been, and continues to be, crucial for the applications of mask production, prototyping and discrete devices for fundamental research and it relies on its high resolution, flexibility and compatibility with other conventional fabrication processes.

The purpose of this thesis is to advance in the knowledge, development and application of electron beam lithography in the areas of micro/nano systems and nanoelectronics. In this direction, this memory reflects part of the work performed at the Nanofabrication Laboratory of the IMB–CNM during the past 5 years. Since there was no previous experience on EBL at CNM, the need for developing a set of processes has determined partially the work and it is represented in this document.

The variety of topics that concern to nanoscience and nanotechnology is enormous. Chapter 1 briefly sintetizes nanoscale related aspects. This section aims to frame the contents of this thesis, coherently. Also for completeness, it is intended to address the specific subjects under discussion or contained in the following chapters and it is based or oriented to the experimental results that will be presented.

Chapter 2 is a general overview of the electron beam lithography (EBL) technique from the point of view of the system and the physical interaction of the process. In particular, the characteristics of the scanning electron microscope (SEM) and specifications of the lithographic capabilities of the system that is used are presented.

In chapter 3, irradiation effect on resists is studied. The chemical behaviour of different polymeric materials is correlated with theoretical simulations for two types of resists: methacrylic based positive resists and epoxy based negative resists. The first is used for validation of the modelization and to describe the general performance of EBL on different conditions. The second covers the experiments oriented to establish the performance parameters of a new resist and comparison with another existing negative electron beam resist. Proximity effect correction concludes with the correlation of theory and experimental results for both types of resists, positive and negative.

Chapter 4 is an example of the fabrication and optimization of a micro/nanosystem for sensing at the nanoscale. In particular, nanoresonators are developed with two approaches (EBL and Focused ion beam (FIB)) and enhanced response is achieved by their integration on CMOS circuitry.

Chapter 5 presents carbon nanotube (CNT) based devices that are realized and implemented for applications in nanoelectronics and sensing. First, different fabrication approaches for contacting CNTs are discussed. Then, the results of electrical characterization of the devices are presented. Finally, technology development for the use of these devices for sensing is established.

The last chapter embraces all the previous sections and pays attention to the effect of electron beam on the devices. In particular, electron induced effect is studied on nanomechanical structures integrated in circuits and CNT based devices, in order to evaluate EBL based fabrication, SEM characterization or more fundamental aspects. Advanced characterization techniques are used together with simulations, both assessing a deeper understanding of the results. Electrical measurements and Atomic Force Microscopy (AFM) based techniques are used to characterise the effect of the electron irradiation by changes in their performance characteristics, charging, surface potential imaging, current measurements, etc.

Main results and solved challenges are summarized in the conclusive chapter 7 that finishes with this document.

In summary, this thesis provides advances in EBL-based technological processes. A new negative electron beam resist is characterised and available to be used for nanofabrication. Optimization of EBL is accomplished by using proximity effect correction methods. Integration of nanomechanical structures into CMOS circuits is established, as it is, the fabrication of CNT-based devices. And finally, the study of charged beam effects on devices complements previous issues to evaluate the feasibility of beam-based fabrication methods. In addition, this memory contains not only a description of the main results, but also it is intended to provide information on electron beam based nanofabrication processes that can serve as documentation for future research in this area.

Acknowledgements

From the time working at the CNM I have had the opportunity to get in touch with the scientific research, in the field of nanotechnology and in the context of a well-equipped infrastructure. I would like to thank to all who made it possible, whatever their implication.

Firstly, thanks to my two co-directors, Pr. Francesc Pérez-Murano and Pr. Joan Bausells, to assess me along the thesis development and, specially, during the writing period.

My gratitude to the committee for accepting to attend my PhD defense: Dr. Xavier Borrisé, Pr. Emilio Lora-Tamayo, Dr. Adrian Bachtold, Dr. José M^a de Teresa and Pr. Albert Romano.

In addition, I would like to mention the coordinators and researchers that I have met in the frame of the projects I have been involved in. In special, thank you so much to Dr. Hans Loeschner, Pr. Eli Kolodney, Pr. Emilio Lora-Tamayo and Pr. Francesc Pérez-Murano for the confidence you deposited on me.

Aquesta tesi no hagués estat possible sense la participació del Francesc. Gràcies, un cop més, per haver-me contagiats el teu entusiasme per la investigació i per haver-me transmés moltes de les coses que he après aquí. Agraixo molt la confiança i haver-me motivat, encoratjat i estimulat, dia a dia, durant tot aquest temps.

Vull agrair molt sincerament tots aquells que m'heu facilitat i ajudat a la feina: Josep Montserrat, Marta Gerbolés, Raquel Palencia, Amelia Barreiro, Adrian Bachtold, Libertad Solé, Jordi Llobet, Josep Tarradas, Roger Llopis, Marta Duch, Montse Calderon, Annabel Muñoz, Elisenda Benet, José Rus, Carles Mateu i tants altres.

Juntament amb tots ells, voldria també destacar un gran nombre de gent amb la que he col·laborat estretament en el desenvolupament de les diverses tasques de la nostra recerca: Xavier Borrisé, Iñigo Martín, Philippe Godignon, Joan Bausells, Julien Arcamone, Servane Blanqué, Francesca Campabadal, David Jiménez, Ferney A. Chaves, M^a José Esplandiú, Guillermo Villanueva, Cristina Martín, etc. En particular, al Jordi Fraxedas i l'Albert Verdaguer els vull donar les gràcies, tant per tot el que he après amb ells, com per positivar(-me) i recolzar-me en certs moments de dificultat.

Encara que alguns ja heu estat citats, hi ha molta altra gent al CNM (i rodalies) de qui guardaré un agradable record de la companyia i amistat que hem compartit durant aquest temps: Joan Vilà, Xavi Jordà, Xavi Moreno, Gemma Gabriel, Albert Gutés, Rodrigo Gómez, Maria Villarroya, Pierre, Ignasi, Pepe, Marta Duch, Anna Tàrrega, Joel, Narcís ... i, és clar, aquells amb els q he compartit despatx: Marc Sansa, Nadia, Giulio, Marta Fernández, Olga, Andreu, etc!

Aquells que més m'estimo, els meus pares, aprofito per dedicar-los aquest treball i espero que així rebin l'homenatge que es mereixen per haver-me suportat (en totes els seus significats ...) sempre. A la resta de la família i, en particular, al Jordi i l'Eva, els remeto des d'aquí el meu afecte incondicional.

Per acabar, envio una forta abraçada a tota la gent amb la que tinc la sort d'estar en contacte o que tinc el privilegi de conèixer: companys del Varium, Meri, Aida, Javi, Sílvia, Artur, Carina, Sergi, Mon, Marc, Christian, etc (disculpeu q no us pugui citar a tots!).

Un petó ben fort!!

This thesis is framed in the research area of nanotechnology and nanoscience. Introduction chapter defines the aspects that the field of nanometer scale dimensions deals with. Its relation with nanotechnology and nanofabrication, together with main application areas are briefly described. A discussion about nanopatterning methods connects to the rest of the thesis. Electron beam is the common feature of all the results that are presented.

1 Introduction

1.1 Towards the nanometer scale

For most of those who are not much involved in science, measurable dimensions end at about the millimeter length. Micrometer size is roughly understandable or imagined thanks to daily used devices, such as computers or mobile phones, containing microchips. From here, people jump directly to the particle and atomic scale where things are simply out of our reach. The same for things named with prefix nano- which appear to be as magic, but attractive and fascinating, as atomistic things.

A nanometer (nm) is one-billionth of a meter (10^{-9} m) or one-millionth of a millimeter. As an example, among natural things, red blood cells are some thousands of nanometer wide and DNA is few nanometers in diameter. Now, handmade things are also reachable at nanometer length scale (1-100) nm, in one, two or three dimensions (1). These are the targets of nanoscience and nanotechnology. The key concept is the control over the matter, devices, structures, molecules, etc. They are intentionally shaped or manipulated at this length scale.

Indeed, materials and structures fabricated in this range lead to a new kind of science, since they are placed in the transition region between truly atomic systems and bulk materials. New features arise from the fact that their sizes are comparable to many physical parameters. Device performance and properties of some materials can show properties or phenomena that have never been seen before. Therefore, new models are required to refine or discard classical models, even a compromise between quantum and classical theories needs to be established for some cases (2).

An idea of nanoscale world could be thought as the place where nanoscience and nanotechnology are working together for a common feature, building up such tiny things. Nanoscience studies new materials, structures and devices and manipulates them at the atomic, molecular and macromolecular scale. It accesses to properties and functions that behave different from the bulk or macroscopic version of them. This behaviour is because of their size and it contributes to fundamental research. Nanotechnology is the ability to manipulate these materials, to design and fabricate the structures, devices and systems and to characterise their performance. Both branches are indissoluble and certainly feed each other. They share, the theoretical advances from nanophenomena, the knowledge from characterization, novel applications from nanomaterials and innovative devices and systems from nanofabrication.

Another important aspect comes from its multidisciplinary nature. Collaboration between traditionally separated disciplines is essential, to reach integration and synergic relations. In addition, development of computer technologies and communications support its advance. The different fields involved make necessary an easier access to a great amount of information. Improvement in the communication networks, such as internet, have been crucial for the flux and interchange of knowledge.

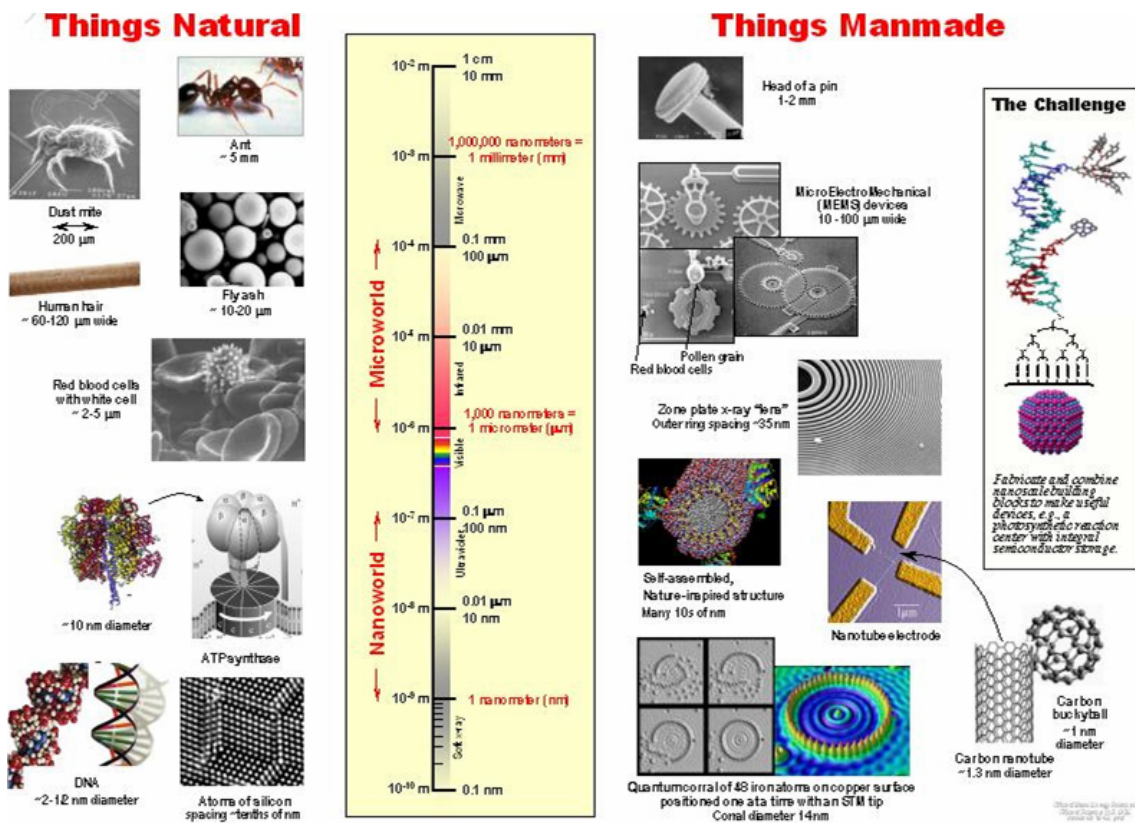


Figure 1.1. Nanometer scale chart (3). Natural things are compared to man made things in terms of dimensions.

1.2 Nanotechnology and nanofabrication

Nanotechnology is the ability to control and manipulate matter at the nanoscale and, therefore, it consists of the design, production, characterization and application of materials, devices, structures and systems from the submicron to atomic dimensionality (4).

Traditionally, the physics approach to science has been using a top-down development for understanding the intimate properties of matter, this is breaking it progressively into smaller basic building blocks. But, now a growing interest is also centered in the knowledge of how atoms and molecules tend to arrange forming complex systems, the so called bottom-up approach (2). From a technological point of view, top-down way means the control of shape and size from bulk material to create smaller structures as desired. Bottom-up works with the assembly of basic matter units to form larger units of good quality (4). Nanotechnology appears when both approaches converge to achieve their results in the same length size, the nanoscale, and a hybrid way of manufacture arises.

From the point of view of semiconductors industry, nanotechnology can be seen as the natural evolution of microtechnology. Microelectronics progress is based on shrinking device dimensions in order to get faster, more powerful and less power consumption systems. In consequence, cost decreases whereas device performance is improved (5).

Certainly, the term nanotechnology is first used in 1974 by Taniguchi (6) to name the ability to engineer materials at the nanometer level. First structures were then fabricated with EBL under 100 nm size. In spite of the fact that fabrication techniques are developed to achieve such nanoelectronic devices, mesoscopic or quantum effects dominate their performance. Thermal limitations also arise and should be taken into account. Due to this, new materials are seen as a solution and they might be found or they belong to the nanometer scale range.

The concept of nanotechnology was created even before by Richard Feynmann in his lecture “There is plenty of room at the bottom” in 1959. The main idea he presented is that he had visualised the possibility to manipulate atoms and molecules. But, since early 80s nanotechnology does not take off. For some, 1981 is considered the starting point with the invention of the scanning tunnelling microscope (STM) by Binnig and Rohrer (7) (Figure 1.2, left). Others place it in 1985 with the discovering of the buckminsterfullerene (C_{60}) by Kroto et al (8) (Figure 1.2, right). It is also thanks to the invention of AFM in 1986 and new materials, such as promising carbon nanotubes (CNT) in 1991 (9) that the discipline gets relevant. The idea that new things and phenomena are accessible embraes and motivates scientific research and development (10).

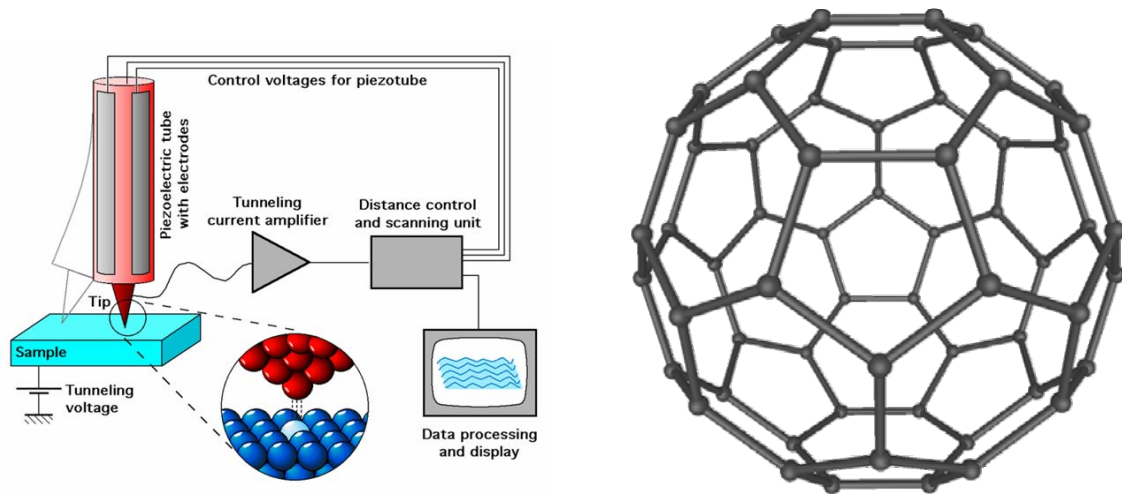


Figure 1.2. (Left) Configuration for a STM. It probes the density of states of a material using tunneling current and is based on the quantum tunneling. (Right) Buckminsterfullerene is formed by 60 carbon atoms arranged in the form of a ball.

The potential of nanoscaled structures opens a broad range of opportunities in terms of fundamental and applied science. The experimental challenges belong to nanotechnology and are concerned to synthesis, manipulation and characterization. Theory, modeling and simulations play an important role in nanoscience and nanotechnology to assist knowledge advances and technical improvements. As an example, theoretical models to predict and understand the interaction between measuring tool and measured structure are really useful (11). They survey the limitations of the characterization technique, but can also suggest novel applications or phenomena.

Besides, nanostructures are now able to integrate materials once incompatible. For nanometer feature size, some principles of physics, chemistry and biology are feasible to be studied. Their exploitation shows similarities between physical, chemical and biological systems in the atomic and molecular level. That is the case of nanobiotechnology (12), where even different approaches are developed. Innovative ways of using biological materials, imitation of nature to enable the use of synthetic materials, hybrid devices combining biomaterials at the nanoscale or biological systems characterized with nanoscale probes are among the studied subjects and the research is oriented to develop a wide number of different applications.

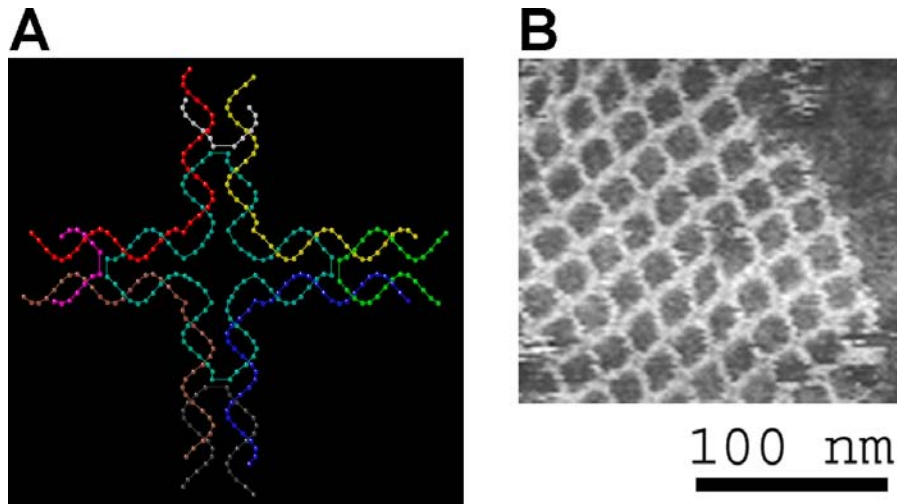


Figure 1.3. Self-assembled DNA nanostructures. (Left) DNA tile structure consisting of four branched junctions serve as the primary building block for the assembly of the DNA nanogrids shown in (B). (Right) An atomic force microscope image of individual DNA tiles self-assembled into a highly ordered periodic two-dimensional DNA nanogrid (13).

Manufacturing in nanotechnology embraces bottom-up and top-down techniques. The fabrication of complex systems hold both approaches to work together. Bottom-up is mainly focused to develop materials in the form of particles and molecules, crystals, films and tubes or experimental atomic and molecular devices. For this purpose, chemical synthesis, self-assembly and positional assembly are used, respectively.

On the other side, top-down approach is based on three elements: patterning, etching and depositing in order to define whole fabrication processes. Nanofabrication is in charge of manufacturing structures at nanoscaled dimensions, but also works to achieve macroscopic systems from nanoscale components or electromechanical systems engineered from devices with dimensions in the nanoscale range. The typical tools of a nanofabrication laboratory can be classified into two categories, those that precisely engineer matter (etching and depositing) and those that define the shape of the elements to be engineered (patterning, mainly lithographic techniques). Among others, plasma etching, reactive ion etching (RIE), evaporation, sputtering, chemical vapor deposition (CVD), optical lithography, molecular beam epitaxy (MBE), SPM or EBL are examples of currently used processes (14).

In the framework of nanofabrication, processes are expected to perform with such a precision and resolution that environmental conditions have to be under control. Therefore, the laboratory work is in general performed in special facilities. The concept of Clean Room (from the original french version, *Salle Blanche*) comes from the semiconductors industry. This is devoted to maintain low levels of airborne particles, acoustic noise, vibrations and electromagnetic interference, besides constant temperature and relative humidity. In this conditions, some uncertainties in the different processes are minimized. Dust particles are crytical since they are often many times bigger than desired structures. Clean Rooms are usually classified in terms of Class, this is, the maximum quantity of particles permitted per air volume (15) (Figure 1.4).

Class	US FED STD 209E cleanroom standards (maximum number of particles/ft ³)				
	≥ 0.1 μm	≥ 0.2 μm	≥ 0.3 μm	≥ 0.5 μm	≥ 5 μm
1	35	7	3	1	
10	350	75	30	10	
100		750	300	100	
1,000				1,000	7
10,000				10,000	70
100,000				100,000	700

Figure 1.4. Clean Room classification by Classes.
Nanofabrication Laboratory at the IMB-CNM-CSIC is Class 100.

1.3 Nanopatterning. Nanolithographic techniques

Once defined the conventional idea of (micro)fabrication, it is worth to remark that the above description corresponds to the concept of planar processing (16). This technology is led by silicon based industry and, indeed, places lithography as the cornerstone of microelectronics. It has been mentioned that fabrication is based on three steps: patterning, depositing and etching. Lithography, as a patterning tool, defines mainly two dimensional (2D) features that will be transferred to the substrate by subsequent processes. Combination of deposition and etching and superimposition of patterning levels allows to fabricate the 3D structured devices. The number of levels of lithography usually quantifies the complexity of the whole process and of its devices. Feature sizes determine the density of the integrated circuit (IC).

The Moore law (17) expresses the time evolution of minimum printable feature size without cost increment, in particular, doubling the number of transistors/chip every 1.5 years. Since ICs are based on transistors, this development is directly linked to the transistor density and, hence, economically interesting: same fabrication cost leads to increased number of devices. In spite of this, Moore evolution seems limited and it is expected to be reduced in about 10 years. From one side, this was the initial motivation for investment in lithographic techniques development. On the other side, quantum effects on transistor gate and performance drop due to interconnection scaling down, force to search for alternative lithographies or new device fabrication strategies, such as quantum devices or bottom-up manufacture. A general overview of the existing patterning techniques is next presented, paying attention to their characteristics and field of application.

Patterning techniques

Patterning techniques can be classified in different categories from different points of view. The most usual way is to separate them as a function of the interface used to define the features. The method for pattern definition can be masked lithography, direct writing or mold processing. Other visions focus on the use (or not) of resist, resist based techniques versus resistless techniques, or their throughput, serial versus parallel processes.

Traditionally, optical lithography (photolithography) monopolizes microelectronics fabrication because it is an easy processing, parallel and material compatible technique in silicon machining. However, the resolution for conventional sources is about 180 nm, since it is limited by the wavelength of light and the optical diffraction phenomena (18). Besides, it depends on other techniques for the mask fabrication and alignment is sometimes done manually. The efforts of microfabrication to further diminish feature size are centered to the development of extreme UV lithography and X-ray lithography, but they encounter some inconvenients. Light sources are more expensive and X-rays tend to penetrate conventional metal masks. Other technological options for IC miniaturization require the density increase of dopants, which is not feasible due to clustering and nonuniformities at wafer scale (19).

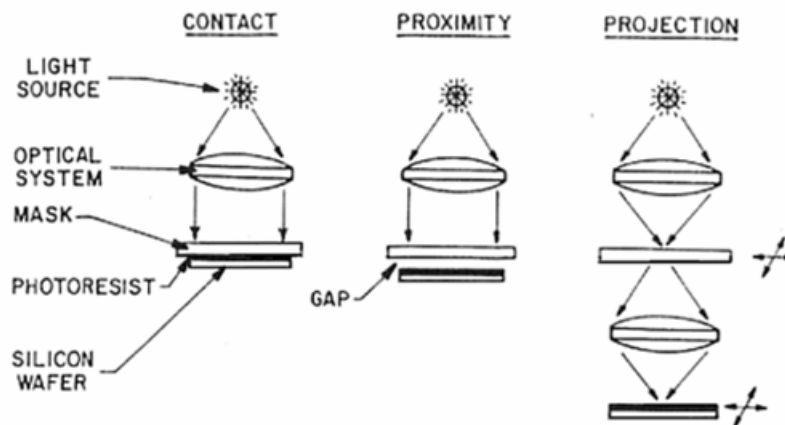


Figure 1.5. Methods of exposure in optical lithography: contact, proximity and projection.

In the context of nanofabrication, this topic is even more crucial and delicate. In fact, now IC fabrication and nanotechnology diverge in defining and using patterning strategies. The wide variety of materials involved in nanoresearch restricts many combinations of processes and techniques. The required resolution to define features is far beyond the standard lithography minimum printable feature size. Often, the pursuit of individual manipulation of matter or flexibility in the pattern design, invalidate some of the existing methods.

Next generation lithographies

Due to this, the development of the so called next generation lithographies (NGL) is ongoing in the scope of many companies (20) or research projects. Other emerging lithographies are also pursued, as the alternative to photolithography for nanoapplications. A wide range of non-optical nanopatterning techniques are now available and they try to cover most part of applications, within their own characteristic limitations. The choice of the proper process often depends on the final product, for this, specific patterning tools are devoted to production, prototyping or fundamental research. These techniques share the common property that they are able to define features or manipulate matter at the nanoscale range.

Among NGLs, three types are consolidated and even continue to be improved or invested in: Extreme UV (EUV) lithography, X-ray lithography and charged particle-beam lithography. For the first two, besides the above mentioned limitations, the mask use can be inconvenient.

Charged particle-beam techniques include EBL and ion beam lithography. For both, the resolution is really high and they are quite flexible in terms of design, particle species, depth of focus, etc. On the other side, limited throughput, surface damage or price may limit their use. One of the advantages of NGLs might be attributed to the possibility of some of them to directly define features in 3D, such as proton beam writing or FIB. More details about these tools are included along present document (Chapters 2, 3, 4).

Emerging nanopatterning methods

Concerning to emerging patterning methods, in some way, they are more oriented to specific applications. They can be classified between soft lithography (21) and nanoimprinting, scanning probe lithographies (SPL) or 3D lithography.

In the case of soft lithography, it is based on the pattern transfer of a stamp, mold or mask made of elastomer material. This set of patterning techniques collects several different strategies (replica molding, micro-contact printing, molding in capillarities, etc). In general, two branches can be distinguished: strictly soft lithography, which uses molds fabricated in polymeric materials, and imprinting techniques, comprising both thermal and UV nanoimprint, which use solid and rigid stamps. They present useful advantages for nanofabrication, such as capability to pattern non planar substrates, compatibility with some innovative materials, low cost or large area covering.



Figure 1.6. Nanoimprint Lithography (NIL) equipment from Obducat at the Nanofabrication Laboratory in the CNM.

SPLs are based on the wide variety of proximal probe microscopes available. STM, AFM or scanning near-field optical microscopy (SNOM) are tools mainly for scientific purposes due to their slow operation and sequential processing. Main

difference with the previous techniques is the direct interaction of the probe with the substrate to pattern. Certainly, SPL technique offers some unique properties very useful for nanometric structures and devices. Its imaging resolution reaches atomic level, two orders of magnitude beyond SEM, and as a patterning tool it depends on the probe, sample surface and strategy, but resolution may be confined to less than 10 nm. Besides this, the electrons interact at low energy, which avoid damage or proximity effects, and is able to perform many different actions, like oxidation, mechanical patterning (scratching), single atom placement and removal, resist elimination of ultrathin layers, etc. Otherwise, the processing time for the direct modification of a surface is about 30 times larger than its analogous by electron beam (22) and confirms SPL application as a basic research tool. Many efforts are dedicated to perform parallel use of scanning probes, as it is the case of Millipede by IBM (23).

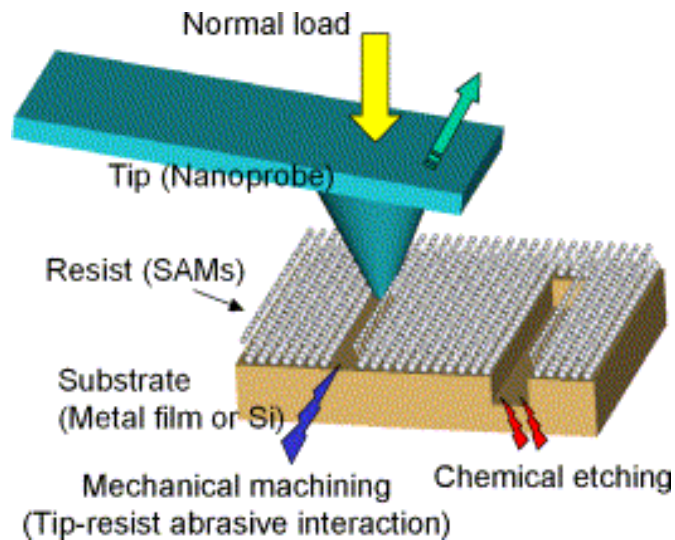


Figure 1.7. Schematic of mechano-chemical scanning probe lithography (MC-SPL) process (24).

Although soft lithography defines 3D structures, 3D lithography methods refer to few specific techniques that pattern from direct or masked beams. As examples, holographic lithography or stereolithography are among the more efficient ones.

Resistless nanopatterning methods

In nanotechnology and nanoscience, often the use of a resist as the media transfer is inconvenient and great efforts are also focused to develop resistless patterning techniques. Examples, such as nanostencil, are based on the use of mask or templates to define the features. However, maskless methods contribute to define flexible patterning techniques. Scanning probe systems comprise existing Dip Pen or Millipede, but also beam based systems exist. Some examples are laser based techniques or particle beams, such as focused ion beam (FIB) or electron beam induced deposition (EBID). Under continuous development, maskless patterning by projection methods using various particle beams is achieved in the Charpan project (25), which CNM is involved in.

1.4 Nanoapplications. Nanometric devices

Nanoscience and nanotechnology are exceptional for their multidisciplinary nature. The different disciplines work alone mostly in the development of innovative materials and they appear as products in the form of nanoparticles, nanostructure synthesised materials, nanotubes or molecule self assembled materials. The range of use of nanomaterials is widespread along an immense variety of uses. Potentially, they might be used in medicine, chemistry, environment, consumer goods, etc, for example, in drug delivery and tissue engineering, catalysis and filtration, food, optics, textiles or cosmetics. The ethical issues of already feasible products need to be considered before use. As well as it happens with genetics research, ethical concerns may cause controversy due to the consequences of their applications.

The cooperation between different fields is even more interesting and origins a continuously increasing number of novel devices, applications and phenomena. Nanodevices are oriented to cover at least the topics of microfabrication, but translated to the nanoscale. Interdisciplinary collaboration in this length scale range results absolutely necessary, since both fabrication techniques and device performances are pushed to the limit.

Nanotechnology supports nanodevice fabrication in order to implement the applications in three different ways. It engineers materials to make functional structures, to establish interfaces between macroscopic world and nanoitems or to build platforms where self assembly of molecules could be possible. The challenge lies in the intrinsic limitations of the whole process. Device itself sets bounds to the fabrication sequence and tolerances, but also technological limitations or access to the proper/convenient instruments is not always possible. Nanofabrication often requires a clever combination of existing technologies. Otherwise, their development or the introduction of new strategies are unavoidable. Indeed, creativity plays an important role in this field and leads to innovative devices. Working together with the tools of nanotechnology, novel applications and phenomena are reachable.

The list of nanodevices that are under study or development may be neverending. Just few examples to illustrate the scope of the field, apart from nanoelectronics applications that will be presented in the next subsection.

Towards the electromechanical systems, the aim continues to be achieving higher sensitivity sensors. In the case of nanoelectromechanical systems (NEMS), faster responsivity determines the dimensions of the movable part and the device characteristics up to a limit that often affects not only to the fabrication. Electromechanical systems are structures with mechanical movement induced by electrical, magnetic or other forces. At the nanoscale, fabrication is certainly a challenge, but actuation and registration may be even more limiting. The integration with CMOS circuitry is presented as a successful solution (26). Among the potential applications, optomechanical and electromechanical signal processing or mass detection with enhanced properties of resolution, sensitivity, etc, are already demonstrated (27).

Nanobiotechnology area is another topic with a broad range of possibilities to be developed. It comprises applications as diverse as the synthesis of new molecules, the study of protein systems or fighting against viruses and bacteria (28). Among this field a wide interest is centered around biosystems for achieving versatile and complete analytical tools. Often known as lab-on-a-chip systems, the basis remains in the use of IC technologies to achieve analytical instruments for chemistry and biotechnology. The characteristics of this devices are based on their real use. They are designed to be small,

portable and robusts and to be able to perform measurements in parallel. The possibility to automatize their control and massive fabrication makes them ideal for many control analysis in medicine, environment, etc. Microarray and microfluidic chips have faster response and diminish the quantity of analite biomaterial needed. However, the downscaling presents some difficulties. At the nanoscale some of those nanosystems are more complicated and it is not clear if further miniaturization is possible with the same objective. For example, it is said that nanofluidics might change its role and explode a more fundamental research. For this, interrogating single molecules might not be so commercially applied, but it apports basic knowledge by specialised characterization (29). Scaling down devices often changes how they perform. But, it not only invalidates some of the theoretical laws they are based on, again technical impediments can stop their development (30).

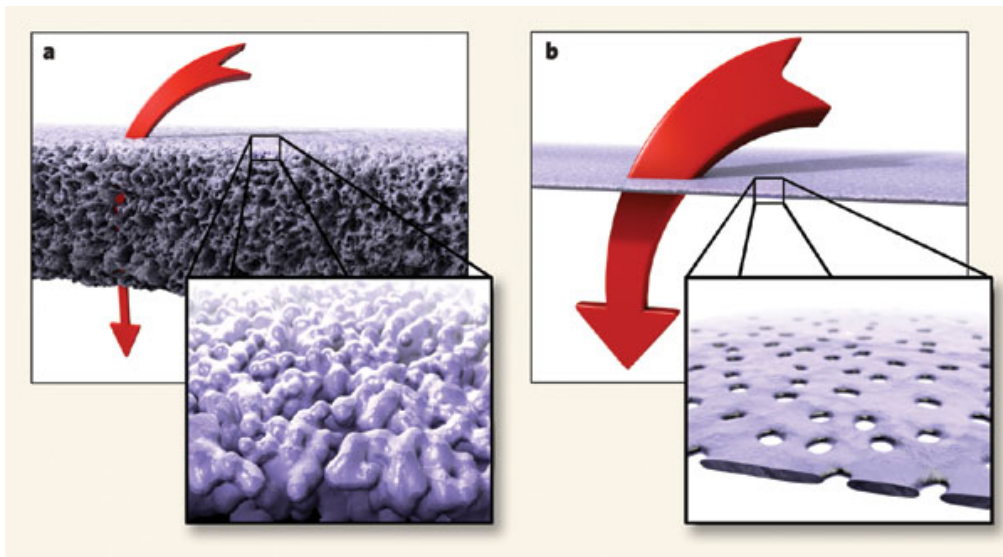


Figure 1.8. (Left, a) The nanoscale nodules that make up a conventional ultrafiltration membrane form a significant restriction to flow. (Right, b) The ultrathin porous nanocrystalline silicon membranes allow efficient protein separation without restricting the flow as much (31).

Nanometrology, energy or information and communication applications are other fields where development of other nanometric devices are in the pursuit of nanotechnology and nanoscience. The more exotic and fancy configurations that one imagines, the more possibilities open to innovation.

1.4.1 Nanodevices. From micro- to nano-electronics.

Originally, microfabrication is triggered for the implementation of devices to satisfy semiconductors industry needs. As mentioned, the development of such technologies and processes is focused to obtain, first, simple miniaturised devices, then ICs with increasing device production, reliability and complexity, i.e. increasing density (by shrinking dimensions), lowering cost, etc (Figure 1.9). Besides electronic devices and VLSI manufacturing, other areas are in the scope of microfabrication, such as magnetic storage, optoelectronics, micromechanical systems or biochips (also known as, lab-on-a-chip) (16).

Beyond conventional microelectronics technology, nanoelectronics arises as an outcome from these fabrication techniques, but again it is not the only one and many other application areas are undertaken. Besides, electronics scaling down seems to reach its limits with existing technologies and alternatives are searched in new materials (32).

In the field of nanoelectronics, circuit functions equivalent to those of CMOS circuits are pursued. Novel materials use and improved device performance are the final goals of innovating configurations. Two different types of devices can be presented, solid state and single molecule based devices. Within the first, some examples are single electron transistors (SET), quantum dots (QD) or resonating tunneling devices. Others like CNT based transistors, introduce the use of promising materials to the topic. Single molecule based devices are not easily fabricated and might be feasible with SPL techniques.

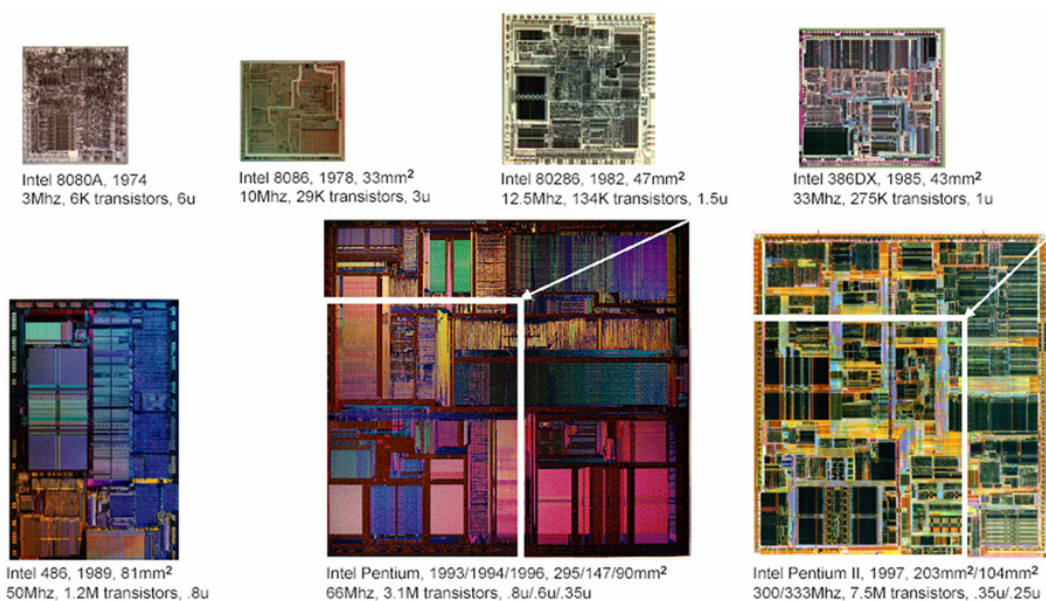


Figure 1.9. Successive generations of ICs developed by Intel Corp. (www.intel.com). Down scaling transistor dimensions allows to integrate higher number of devices per chip.

Optoelectronics is using the tools of ICs manufacture to the microfabrication of semiconductor lasers, light emitting diodes or waveguide devices. Similarly, nanofabrication allows to develop nanophotonic devices such as photonic crystals in 1, 2 or 3D, with the increased difficulty of feature sizes and density.

The growth of information storage, which is even faster than transistor development in ICs, is possible thanks to microfabrication evolution and, now, nanofabrication techniques. Microfabrication processes are important since they are used in the manufacturing of the heads used for reading and writing. Advances in these processes, from one side, and recording media development, on the other, lead to the possibility of manufacturing storage units arrays of high density even with quantised or discrete magnetic units.

Nanofabrication is a very active area of research, as can be noticed from the number of new publications that appear continuously and from the number of running R&D projects. Specifically, most of the work has been realized in (and has been conditioned by) the framework of three European research projects: Novopoly, NaPa and Charpan.

Novopoly project (Novel functional polymer materials for MEMS and NEMS applications, NMP3-CT-2005-013619) deals with the development of new polymer materials for applications in micro and nano systems (resist processing and applications). The development of a new EBL resist has been framed in this project.

Within NaPa (Emerging nanopatterning methods, NPM4-CT-2003-500120) the development of NEMS fabrication with EBL has been used to fabricate discrete nanomechanical devices. They have been used to characterize the performance of resonating (submicronic) structures and signal enhancement has been achieved by their integration in CMOS circuits.

Within Charpan (Charged Particle Nanotech, NPM4-CT-2004-515803-2), the development of a new patterning tool based on several charged particle species is undertaken. The incidence of charged particle beams on devices has been studied to evaluate potential effects induced during fabrication.

Finally, carbon nanotube (CNT) based devices contribute to some tasks of national projects Crenatun (Crecimiento de Nanotubos de Carbono Unidireccional, INTRAM-FRON 200550F0151) and Sensorat (Tecnología para sistema sensores y electrodos basados en nanotubos de carbono, NAN2004-09306-C05-01). In particular, the technology for fabrication of high performance CNT field-effect transistors and their preparation for sensing applications has been established.

References

- (1) Various authors
EPA Nanotechnology White Paper
(2005)
- (2) B. Appleton
Brave new nanoworld
ORNL Review **32** (3) (1999)
- (3) www.nanotechbc.ca/main/10008/
- (4) Various authors
Nanoscience and nanotechnologies
The Royal Society and the Royal Academy of Engineering (2004)
- (5) M. Ventra et al
Introduction to nanoscale science and technologies
Springer, ISBN 1402077203 (2004)
- (6) N. Taniguchi
On the Basic Concept of 'Nano-Technology'
Proc. Intl. Conf. Prod. Eng. Tokyo, Japan Society of Precision Engineering (Part II) (1974)
- (7) R.J. Behm, N Garcia, and H. Rohrer
Scanning Tunneling Microscopy and related Methods
Proceedings: NATO ASI, Dordrecht, Holland: Kluwer **184** (1989)
- (8) H. W. Kroto, J. R. Heath, S. C. Obrien, R. F. Curl, and R. E. Smalley
C-60 - Buckminsterfullerene
Nature **318** (6042), 162-163 (1985)
- (9) S. Iijima
Helical Microtubules of Graphitic Carbon
Nature **354** (6348), 56-58 (1991)
- (10) J.K. Gimzewski
Nanotecnologia (...)
KRTU (2006)
- (11) P. Cummings
New tools for nanoscience
ORNL Review **38** (3) (2005)
- (12) Various authors
Nature's way
ORNL Review **38** (3) (2005)
- (13) M. Strong

- Protein Nanomachines**
PLoS Biol **2** (3), e73 (2004)
- (14) Various authors
Nanofabrication in the Clean Room
ORNL Review **38** (3) (2005)
- (15) D.L. Tolliver
Handbook of contamination control
Noyes publications, ISBN 0815511515 (1988)
- (16) Z. Cui
Micro-nanofabrication
Higher education press, ISBN 7040176637 (2005)
- (17) www.public.itrs.net
The international technology roadmap of semiconductors
- (18) E.L. Wolf
Nanophysics and nanotechnologies
Wiley-VCH, ISBN 352740407 (2004)
- (19) M. J. Madou
Fundamentals of microfabrication: the science of miniaturization (2nd edition)
CRC Press, ISBN 0 8493 0826 8497 (2002)
- (20) F. Watt, M. B. H. Breese, A. A. Bettiol, and J. A. van Kan
Proton beam writing
Materials Today **10** (6), 20-29 (2007)
- (21) Y. N. Xia and G. M. Whitesides
Soft lithography
Annual Review of Materials Science **28**, 153-184 (1998)
- (22) K. Wilder, C. F. Quate, B. Singh, and D. F. Kyser
Electron beam and scanning probe lithography: A comparison
Journal of Vacuum Science & Technology B **16** (6), 3864-3873 (1998)
- (23) G. Binnig et al
The “Millipede” – Nanotechnology Entering Data Storage
Handbook of Nanotechnology, Ed Bharat Bhushan, Springer-Verlag (2002)
- (24) I.H. Sung and D.E. Kim
Nano-scale patterning by mechano-chemical scanning probe lithography
Applied Surface Science **239** (2), 209-221 (2005)
- (25) Charpan
Charged Particle Nanotech
NPM4-CT-2004-515803-2

- (26) J. Arcamone
Integration of nanomechanical sensors on CMOS by nanopatterning methods
PhD Thesis, July 2007, Universitat Autònoma de Barcelona

- (27) K. L. Ekinici and M. L. Roukes
Nanoelectromechanical systems
Review of Scientific Instruments **76** (6) (2005)

- (28) K.E. Drexler
Molecular engineering: An approach to the development of general capabilities for molecular manipulation
Proc Natl Acad Sci USA **78**, 5275–5258 (1981)

- (29) H. Craighead
Future lab-on-a-chip technologies for interrogating individual molecules
Nature **442**, 387-392 (2006)

- (30) D. Janasek et al
Scaling and the design of miniaturized chemical-analysis systems
Nature **442**, 374-379 (2006)

- (31) A. van den Berg and M. Wessling
Nanofluidics: Silicon for the perfect membrane
Nature **445**, 726 (2007)

- (32) W. Hoenlein, G. S. Duesberg, A. P. Graham, F. Kreupl, M. Liebau, W. Pamler, R. Seidel, and E. Unger
Nanoelectronics beyond silicon
Microelectronic Engineering **83** (4-9), 619-623 (2006)

The main instrumental aspects of EBL are described in this chapter. First, the general characteristics of the technique are summarized. Then, direct writing EBL is presented by the description of the different elements of the system. Finally, a brief description of lithographic capabilities introduced to the SEM is included. In particular, the general procedure for exposure is generally schematized.

2 Electron Beam Lithography

2.1 Lithographic technique

2.1.1 Introduction to the concept

The origins of the use of lithography date from the 17th century in applications of ink imprinting (1). Nowadays, the techniques and applications of lithography have been diversified, but the concept keeps valid. Lithography is the process to transfer a pattern from one media to another (2).

Photolithography uses light as the transfer media and it is widely used in technological processes. As a matter of fact, its characteristic high yield makes it ideal for semiconductors industry, in particular, applied to silicon technology in the fabrication of integrated circuits (3).

Electron beam lithography appeared in the late 60s and consists of the electron irradiation of a surface that is covered with a resist sensitive to electrons by means of a focused electron beam. The energetic absorption in specific places causes the intramolecular phenomena that define the features in the polymeric layer.

This lithographic process, capable of creating submicronic structures, comprises three steps: exposure of the sensitive material, development of the resist and pattern transfer. It is important to consider that these should not be realized independently and the final resolution is conditioned for the accumulative effect of each individual step of the process (4). A great number of parameters, conditions and factors within the different subsystems are involved in the process and contribute to the EBL operation and result.

In a direct write EBL system, the designs are directly defined by scanning the energetic electron beam, then the sensitive material is physically or chemically modified due to the energy deposited from the electron beam. This material is called the resist, since, later, it resists the process of transference to the substrate. The energy deposited during the exposure creates a latent image that is materialized during chemical

development. For positive resists, the development eliminates the patterned area, whereas for negative resists, the inverse occurs. In consequence, the shape and characteristics of the electron beam, the energy and intensity of electrons, the molecular structure and thickness of the resist, the electron–solid interactions, the chemistry of the developer in the resist, the conditions (time, T ,...) for development and the irradiation process, from the structure design to the beam deflection and control, are determinant for the results, in terms of dimensions, resist profile, edge roughness, feature definition, etc.

2.1.2 Instrumental

In the context of fabrication, lithography comprises several different techniques that can be classified, among others, as a function of the equipment, the nature or agent that induces the process, the phenomena, interaction or reaction that takes place, etc.

Specifically in the framework of nanotechnology, i.e. in the submicron feature range, it is considered that this diversity is reduced to just a few techniques, instruments and applications that are capable of defining structures at that length scale. As a result, photonic techniques or projection systems are usually not resolute enough nor capable to accomplish nanofabrication requirements and it is thanks to charged particle beams or direct manipulation methods that nanostructuring is feasible (5).

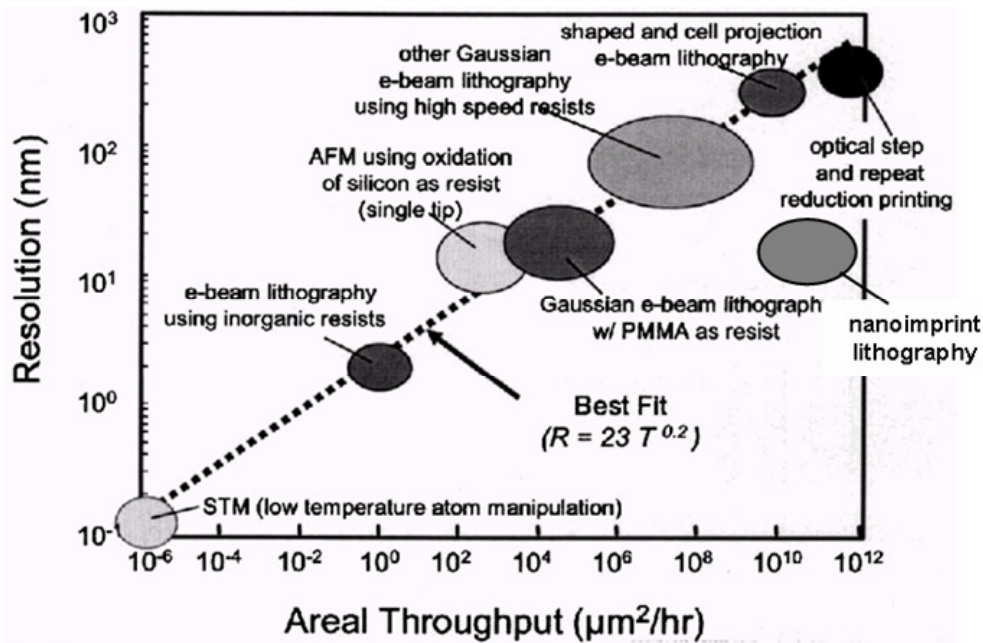


Figure 2.1 Resolution of different lithographic techniques as a function of productivity (Adapted from (5)).

One of the valid alternatives is the technique of EBL based on a scanning electron microscope (SEM). It consists of a direct write system, in contrast with projection systems that require the use of masks to define the patterns, and uses the narrow electron beam of the microscope, the same that is used on SEM inspection, to acquire high resolution images. As it will be explained next, for EBL an (electronic) interface is attached to the SEM in order to control the deflection and interruption of the beam. Other EBL-system elements are the material sensitive to the electron exposure (resist) and the developer solution. The SEM provides the rest of integrating parts of the

system: the electron source, the focusing system and the support for the sample substrate.

It is worth noting that both the specifications of the SEM and of the additional modules, in addition to the resist, the developer, the environmental conditions and the specific exposure parameters can strongly determine the operation and performance of the lithographic process.

2.1.3 Characteristics

EBL has been considered one of the more flexible methods that can undertake the realization of submicronic devices. Therefore, it is possible to be applied for nanofabrication and for the production of masks for other lithographic techniques.

Its versatility has been obtained thanks to the successive development of the different components and elements that are involved in the process, this is, the beam generation, the system, the process, the resist and the operation system (2).

The advances in the beam characteristics embrace from the development of more stable and cold emission filaments to the decrease of the effective beam diameter until a few nanometers. In addition, the main limitation of photolithography resolution, the effect of diffraction, is not present for electronic radiation.

Concerning to the system, great advances have been achieved thanks to the development of the electron optics of the SEM column, which is in charge of the formation and displacement control of the beam. Also important are the improvements related with the vacuum system or the possibility to integrate motorized supports.

The use of computers facilitates the automation of certain actions, both for the administration of SEM parameters and focus or for the interface of design and the control of lithography execution. The consequences of computer assistance are indeed remarkable. The designs that can be patterned are almost unlimited and they can be fast and easily modified in situ, an advantageous difference from masked lithographies. In addition, it allows to realize simple and precise alignment, flexible field calibration with high accuracy in the dimensional control and positioning on prestructured features.

In relation to the resists, polymethyl methacrylate (PMMA) continues to be the most widely used even if it was one of the first materials originally tested for EBL. The reason relies on its high resolution and easy processing. However, currently there exist other resists that are more convenient for some specific applications.

To conclude, the use of EBL has been simplified and reaches higher resolution since the phenomena and processes involved attain deeper comprehension. There can be found a large number of studies to elucidate the mechanisms and the rhythm of electron-matter interactions, the chemical performance of the resist or the transport and diffusion processes during development. As a result, simulation and models adequately correlate with the experimental results and contribute to make EBL more effective.

2.1.4 Limitations

Once the positive characteristics of EBL have been described, the properties and factors that limit the technique should be mentioned. Limiting factors refer to the aspects that constrict the capability of EBL, specially in the area of nanofabrication, and, in consequence, those that condition the approach and operation of the process.

The system specifications introduce inherent limitations, such as geometric aberrations. The maximal area of the writing field, the numerical aperture and the resolution are restricted from the diameter and shape of the beam in the focus point. The electron source has determined characteristics of brightness, emission, uniformity, stability and life time. The mechanic support provides limited positioning precision, in addition, to finite displacement speed and time for loading and downloading the samples. The lithographic capabilities are characterized by their maximal velocities of beam deflection and switch on/off, together with determined transmission rate of design and exposure data and finite capacity for data storage.

On the other hand, there are factors inherent to the process that cause the exposure phenomena, this is, the beam-resist interaction and the polymer characteristics. The Coulomb interaction is related with the beam current and strongly conditions the final resolution of EBL. The resist introduces certain requirements in terms of dose and pre and post exposure processing that are necessary for adequate results and also its molecular structure limits the resolution. The minimum feature size and maximal pattern density is considered to be highly determined by the massive and charged nature of electrons that causes a certain delocalization of the delivered radiation.

The disadvantages determined by the equipment are also significant. The SEM is an expensive instrument due to the technology that integrates, but also for the cost of its maintenance. In addition to the electron optics and the gun, working at high vacuum level is both slow and expensive. Compared to photolithography, it is considered to have rather low productivity, since the writing speed and transfer rate for the design data are limited, it is a serial process and often partially manual (3).

For very high resolution processes, the important number of parameters and complexity of operation and phenomenology of the subsystems involved cause low reproducibility in the EBL result. For nanolithography, often the precision and dimensions of the features and structures to be patterned are comparable to the maximal resolution of the technique.

2.1.5 Resolution and applications

For both science and technology, it is generally required to establish the specifications of a fabrication technique or those of a measurement system, determining the minimum structure or dimension that is capable to implement or to resolve. Nevertheless, some authors consider this criteria very subjective to define resolution. Hence, for EBL some propose the maximal line density as the measure for resolution, this is the minimum space between two lines that is possible to be defined (6, 7). This viewpoint is analogous to the commonly used in optical systems, where resolution is defined as the minimum distance between two points that can be distinguished.

Whatever the criteria it is chosen, the resolution of EBL is considered to be determined by the combination of four factors: the delocalization between electrons and resist molecules during exposure due to Coulomb interaction, the secondary electrons dispersion in the resist layer, the backward scattered radiation caused by electron collisions with the substrate, and the molecular structure of the resist and the molecular dynamics of development process. Each individual factor is at the same time conditioned by the specifications, characteristics and properties of various parameters.

In conclusion, the limiting factor of EBL resolution is not attributed to the optical system nor to the backward electron dispersion (except for densely packed patterns), but to the resolution resulting from the resist molecule and its interaction with

incoming electrons, to the range of secondary electrons and to the postexposure process. In fabrication, the methods to transfer the patterns to the substrate are crucial and determinant. It is often difficult to establish an exact value, so generally speaking it is considered that features of a few tens of nanometers (10-20 nm) can be fabricated almost controllably and repeatedly based on EBL.

In order to conclude this general overview of EBL characteristics, the main applications that derive from its properties are collected. Due to the advantages and limitations of the technique, EBL is highly efficient to complement photolithography in the semiconductors and ICs industry and for nanotechnology. Mainly, it is used in four areas: mask fabrication, prototyping, fabrication of a small number of specific structures or research and development of fundamental science applications (3).

In consequence, EBL allows to obtain electronic devices, optics components, calibration standards for AFM or a great diversity of structures suitable for research in materials science, energy, medicine, etc.

2.2 Instruments for SEM based lithography

2.2.1 SEM based system

As mentioned, one of the system configurations for direct writing EBL is based on a SEM and lithographic capabilities attachment. The process can be redefined as the gaussian circular beam that exposes one unique point at a time (8). The characteristics and parts that constitute this technique are presented next.

An schematic diagram of the typical configuration is presented in Figure 2.2. It consists of a complex system that is devoted to realize a great variety of structures of precise and high resolution dimensions, in small quantities and determined positions of the sample substrate.

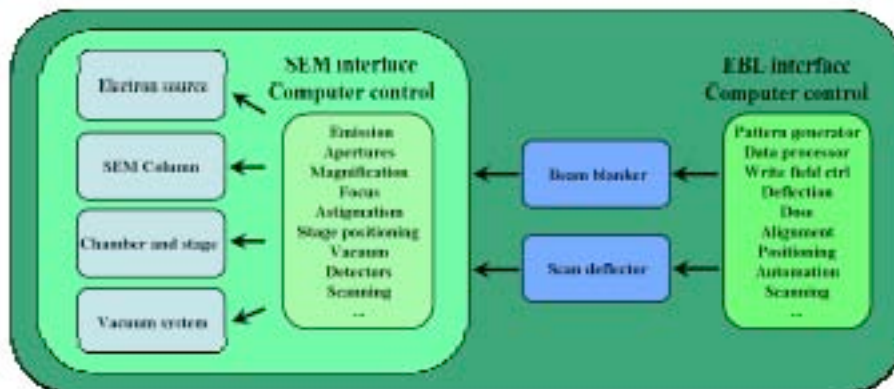


Figure 2.2 Schematic of an EBL system controlled by PC.

This task determines the technical requirements of the different parts that integrate the EBL system. The SEM provides a beam with emission stability, perfectly circular and minimal diameter. This is accomplished working at ultra high vacuum (UHV) level conditions. The control of beam deflection keeps beam integrity and, at the

same time, precise enough operation to define the design exactly, dimensionally calibrated and accurately positioned on the sample. In addition to this, the beam blanking should be fast enough to avoid imprecisions and the mounting stage might allow exact positioning. All these aspects require a computer based system control that is capable of managing all subsystems, fast and simultaneously.

2.2.2 Electron source

The electron source (gun) is a portion of the electron optics of the SEM, but its significance warrants a detailed explanation. It is composed of one or two electrodes that extract and accelerate to certain energy the electrons pulled off from the filament. For high resolution, the effective size of the source and the emission energy bandwidth might be small, which determines field emission sources (in comparison to thermoionic sources) as the most convenient sources for SEM and EBL (9). Due to this, next description is centered in the characteristics of field emission sources.

Analogous to light sources, the virtual size of the source, the brightness and energy dispersion characterize electron beam sources (3).

The virtual size of the source determines the demagnification that has to be applied by the SEM column. The smaller the virtual size is, the smaller the beam spot on the sample with a minimum number of lenses. In consequence, column configuration can be simplified and higher resolution is expected.

The beam brightness is equivalent to the intensity in conventional optics. High value is desired to minimize exposure process time, but experimentally, high resolution lithography is accomplished only with lower beam intensities.

The energetic dispersion refers to the energy distribution of emitted electrons. A wide spectrum is equivalent to white light, whereas a reduced energy distribution is analogous to a laser. The minimum dispersion is required to reduce chromatic aberrations.

Source type	Filament material	Brightness (A/cm ² /rad)	Source size	Energy dispersion (eV)	Vacuum level (Torr)	Filament temperature (K)
Tungsten thermoionic	W	~10 ⁵	25 μm	2-3	10 ⁻⁶	~3000
LaB ₆ thermoionic	LaB ₆	~10 ⁶	10 μm	2-3	10 ⁻⁸	~2000-3000
Thermic field emission (Schottky)	Zr/O/W	~10 ⁸	20 nm	0.9	10 ⁻⁹	~1800
Cold field emission	W	~10 ⁹	5 nm	0.22	10 ⁻¹⁰	Ambience

Figure 2.3 Characteristics of different types of filaments (10).

Field emission sources are about 5-20 nm virtual size, have good and stable emission intensity and reduced energetic dispersion. In addition, filament temperature is lower than thermoionic sources, but require UHV.

The mechanism for electron extraction on field emission sources relies in the application of an electric field, high enough to enable electrons to traverse the surface potential barrier. Since the emitter works very close to the extraction electrode and at low voltage, the tip radius has to be sharp and made of a material with reduced work function. Tungsten tips provide the extremely high fields necessary for electron extraction. Intensity fluctuations in the beam current caused by tip absorption are reduced with UHV.

Finally, the thermoionic field emission sources (Schottky) are the best option. This device combines the best characteristics of field emission sources with the characteristic properties of thermic sources. Thermic sources emission occurs by heating of conductive material. The combination of both approaches allows to obtain electron emission at 1800 K. It is less sensitive to environmental conditions and the source life time is increased.

In particular, one configuration of thermal field emission is composed of a tungsten needle covered by a zirconium oxide layer. The needle emits electrons, whereas the covering layer reduces work function (from 4.6 to 2.48 eV) and replenishes the material rejected from the tip.

2.2.3 SEM column

The three main components of the SEM column are the electron source, the objective lenses and the beam deflection unit. Once the beam is formed, the electron optics is responsible of focusing and steering the beam.

The physics principles that explain the operation of the column are simple and can be described using the basic laws of electromagnetism. Electrons do behave as waves under determined conditions, which implies that can be focused and manipulated analogous to the classical optics systems (geometric optics). At the same time, electrons maintain the characteristic properties of classical charged particles.

From the second law of Newton, $\mathbf{F} = m \cdot d^2\mathbf{r}/dt^2$, the trajectory and speed of electrons can be controlled by external forces, more precisely, by electromagnetic forces.

The Coulomb law expresses that the force exerted by an electric field on an electron, $\mathbf{F}_E = -e \cdot \mathbf{E}$, is parallel and opposite to the applied field. Lorentz law, $\mathbf{F}_M = -e \mathbf{v} \times \mathbf{B}$, describes the force acting on an electron travelling in a magnetic field as perpendicular to the force and to the particle speed (11). In general, both forces are not used simultaneously to steer the electron beam.

Electrostatic lenses usually produce higher aberrations, therefore magnetic lenses are preferred to focus the beam. An electron with certain tangential velocity respect to the optical axis (the beam axis) interacts with the radial magnetic force that is created by the coil. In consequence, the electron experiences a force that leads it towards the beam axis (12).

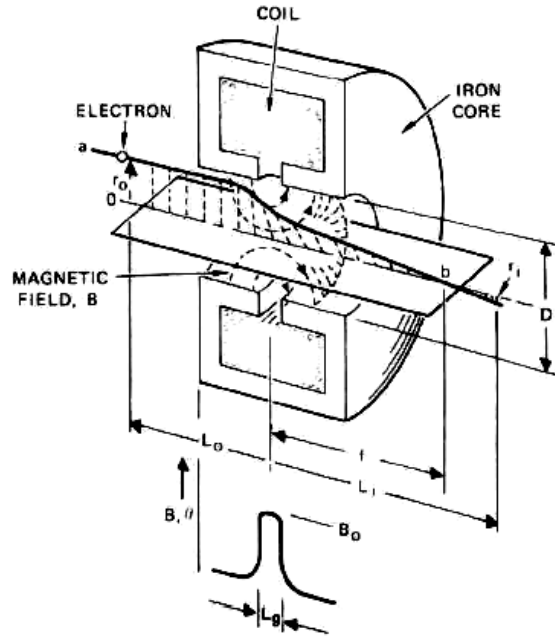


Figure 2.4 Section of a magnetic electron lens (3).

Neglecting the actual aberrations that exist in the beam trajectories, electrons are focused to a certain distance, f , from the center of the lens, determined by magnetic field B_0 , the gap L_g , the ratio $e/m = \eta$ and the electron velocity (expressed by the potential V_0).

$$f \cong \frac{8V_0}{L_g \eta B_0^2} \quad (2.1)$$

Electrostatic lens operation, to force electrons to converge in some point of the optical axis, is similar to magnetic lens one. The realization is accomplished by three plates provided with a central aperture. Central plate has variable potential and the first and third plate are connected to the ground (3). In general, electrostatic lenses are used as condenser lenses of the electron gun, since the distortions inherent to these lenses are less critical here.

The deflection unit is in charge of deviating the beam through the sample surface, within what is called the scan field. Ideally, the minimum degradation of beam is desired, i.e. precise deflection, constant beam size and no hysteresis.

Similarly to the focusing lenses, deflection can be realized both electrostatically or magnetically. It is implemented with coils and plates that create fields perpendicular to the optical axis. The magnetic deflection again introduces less distortions, but the electrostatic deflection has faster response. In addition, deflection unit is usually placed at the end of the column, which means that interaction with metallic conductive portions should be avoided. Shielding is used to minimize parasitic currents. The introduction of dynamic corrections, by means of the beam driving software, solves the main existing aberrations.

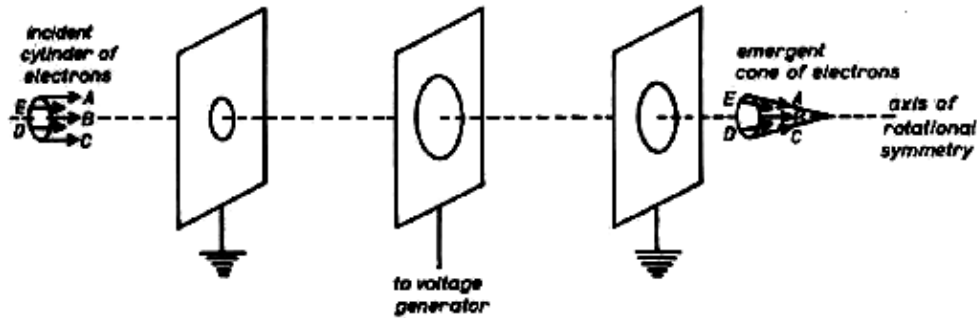


Figure 2.5 Scheme of an electrostatic lens (3).

The rest of elements that constitute the column are the apertures, astigmaters and the beam blaker.

The holes that beam traverse along the column are called apertures. There are two kinds depending on their function: for limiting the beam or to interrupt it. Those used to limit the beam determine the amount of beam current and the convergence angle α (which is the angle of the beam respect to the sample surface). Due to this, apertures are very important, since they conditionate the effect of lens aberrations and, consequently, the resolution. The aperture that intercepts the deflected beam, performs the switch on and off of the beam on the sample.

The beam blaker is comprised by a pair of plates connected to an amplifier with fast response. The potential applied to the beam deflects it far from the column axis until the beam passes through the aperture mentioned above. For EBL by vector scan strategy, it is important that the time necessary for interrupting the beam is very short compared to the time that it takes to irradiate a pixel on the sample. In addition, it is basic that beam does not move during pixel exposure, in order to avoid distortions on the exposed design.

The imperfections in fabrication and assembling of the column are the cause of astigmatism, causing that, for each sample surface position, focus conditions are slightly different. This means that the ideal circular section of the beam becomes elliptic and, consequently distorts the image. Concerning to lithography, beam shape does not correspond to the model used for calculating the exposure dose, therefore the pattern to be transferred is also distorted from the original design. The astigmator system is responsible of correcting beam shape to be circular again. It consists of four or eight poles that surround the optical axis. Adjustment is performed by the balance of electrical signal of the poles.

Concerning to the SEM, the detectors used for high resolution images should be mentioned. Typically, backward scattered or low energy secondary electrons are collected to reconstruct the sample surface. The imaging resolution is crucial for focusing, deflection calibration and alignment marks detection. Another important component for EBL systems is the Faraday cup that is used to measure the beam current and hence, to adjust the electron dose during the exposure.

The description of the column ends with the characteristics and limitations of the electron optics, which determines beam resolution. Different from conventional optical lenses, electromagnetic lenses are only converging. In reference to aberrations, their quality is so poorer that field size and convergence angle (numerical aperture) are limited. From electron source specifications, the beam diameter as a function of virtual source and column reduction is determined.

The distortions caused by the column arise as spherical aberrations (astigmatism) and they are originated in both the lenses and the deflectors. Chromatic

aberrations appear when electrons present a certain energetic spectra. This may be caused in the beam source itself, but also can be increased by the so-called Boersch and Loeffler effects, where energetic distribution increases as a result of electron collisions (13). Both phenomena contribute to decrease the precision of lenses and deflectors.

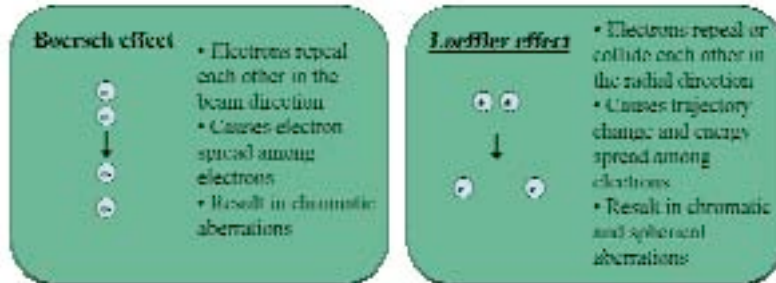


Figure 2.6 Interelectronic interactions of the beam of electrons, caused by Coulomb force (13).

From quantum mechanics, the resolution limit (2.2) caused by diffraction can be determined: it is significantly lower to the one of the light used for photolithography because of the wavelength attributed to energetic electrons.

$$\lambda_{e^-} = \frac{1.226}{\sqrt{V_{e^-}}} \text{ (nm)} \quad (2.2)$$

In general, the theoretical effective beam can be expressed as the quadratic sum of each contribution and optimal point is a compromise between all involved factors. For high resolution, the use of high magnification and beam energy is combined with low energetic dispersion and short focal distance. In consequence, write field is smaller and beam current should be reduced, what means that exposure process is slower, throughput is limited, and flexibility is constrained.

Beam size (d)	
$d = (d_s^2 + d_\alpha^2 + d_c^2 + d_\lambda^2)^{1/2}$	
• virtual source, $d_s = d_f/M$	d_f , source size; M, magnification
• spherical aberration, $d_\alpha = \frac{1}{2} C_s \alpha^3$	C_s , spherical aberration; α , beam convergence angle; C_s proportional to f , where f , focal distance
• chromatic aberration, $d_c = C_c \alpha \Delta E/V_e$	C_c , chromatic aberration; ΔE , energetic dispersion and V_e beam acceleration voltage
• diffraction limit, $d_\lambda = 0.6 \lambda/\alpha$	$\lambda = 1.2 / \sqrt{V_e}$, electronic wave length

Figure 2.7 Expression of the different contributions of the size of electron beam diameter.

2.2.4 Chamber and stage

The lithographic process is performed in the SEM chamber. There are different sample holders where the samples can be fixed by screws, stickers or silver paint, and also sample holders specially designed to fit to the shape and dimensions of silicon technology wafers. It is often convenient to have simultaneous access to the sample, the one that will be patterned, and to the calibration and correction standards for write field and focus. This allows to refine the adjustment just before exposure and, thus, to optimize the resolution.

Concerning to the chamber, the dimensions and mobility determine the size and accessibility of the sample that can be patterned. The equipment used can lodge up to 6" wafers and movement is possible for XYZ, rotation and tilt. The capabilities of the system benefit from precise and motorized controlled displacements.

In addition it can be equipped with a CCD (charge coupled device) camera to visualize inside the chamber and to assess the control of sample positioning. Another important aspect related to the chamber is the presence of vibrations and electromagnetic noise that can distort the beam. Support is isolated from mechanical vibrations, which is even more critical for high resolution EBL than it is for conventional lithography. At the same time, computer monitors, transformers and vacuum pumps are kept separate or controlled and shielding is used to avoid interferences (3).

2.2.5 Computer control

The operation of direct write EBL relies on the delivery of the electron dose: the resist, sensitive to electrons, is exposed sequentially according to the design elements (14). The offline data processor determines the order, geometry and size of irradiation. Computer based control is responsible of design, exposure rhythm (beam deflection speed), adjustment of exposure field (size and compensation of position, rotation and orthogonality) and stage positioning.

The lithography is performed by scanning the designed pattern, cell by cell, with the electron beam of circular section. In general, the design features are fragmented into rectangles or parallelograms and beam irradiation is executed with control over deflection and switch on and off of the beam (Figure 2.8).

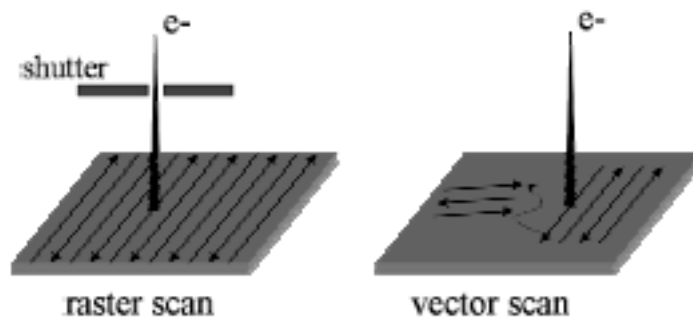


Figure 2.8 Comparison between raster and vector scan techniques in direct writing EBL.

Vector scan mode is time efficient, since the beam only is scanned in the areas that should be patterned. On the contrary, for raster scan mode the beam is driven all over the working area and shape is controlled switching on and off the beam. Compared to conventional lithography, both methods are serial and, therefore, fabrication yield is low. As a matter of fact, all microscopes (optical, electronic, probe or scanning based) adapted for writing have the common limitations of reduced working area and low throughput.

Another characteristic of this method is the flexibility to access, control or adjust most of process parameters. The way to steer the beam takes advantage of the possibility to determine the coils performance, which are used by SEM to scan the sample surface during imaging. Analogic control of the potentials deflects the beam from the beam axis (where potential/current is zero) until maximal deflection angle (measure of working area). It is implemented by using a PC with a card for digital to analogic conversion (DAC) and connection to the deflection system of the SEM (Figure 2.9).

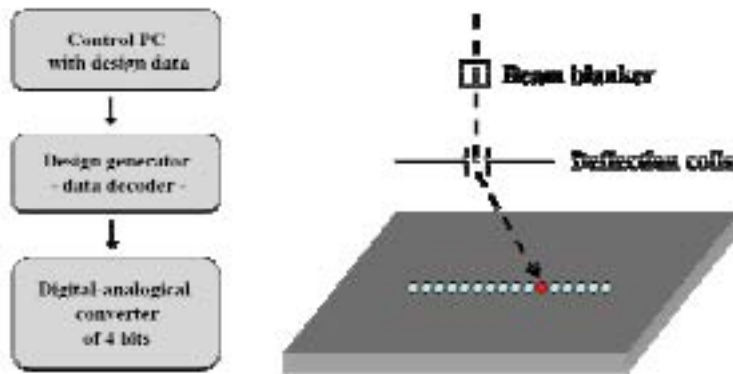


Figure 2.9 Structure of the beam blanking and deflection system.

A simplified methodology is the following. The deflection in one dimension with a DAC of 4 bits allows to define 16 different positions (2^4). This is due to the 16 different values that DAC can determine on potential. Each value determines a pixel orixel (picture or exposure element, respectively). Hence, to write a line (ab) the computer switches on the beam in determined position (pixel a), deflects the beam at determined speed until the other position (pixel b) and switches the beam off.

Real systems are more complicated, since designs are two dimensional and higher resolution is desired. With DAC of 16 bits for each axis, accessible area is defined by 65536 x 65536 positions, that constitute the field. The field is the maximal area that can be exposed with the beam deflection. Spacing between pixels in a determined field is,

$$\text{Interpixel spacing (metric unit)} = \text{Field size (metric unit)} / 65536$$

From this concept it is easy to extrapolate the importance of choosing field size, exposure parameters and design for high resolution applications.

The gaussian vector scan mode is the evolution of the method presented above. The original design is fragmented in subelements that will be continuously exposed by

the beam of gaussian intensity profile (Figure 2.10). For each subelement the beam is switched off and it is directly driven to the next portion. In order to operate with this strategy, two DACs are used: one to conduct the deflector that locates the beam in the corner of each subelement and the second to drive the beam within the subelement.

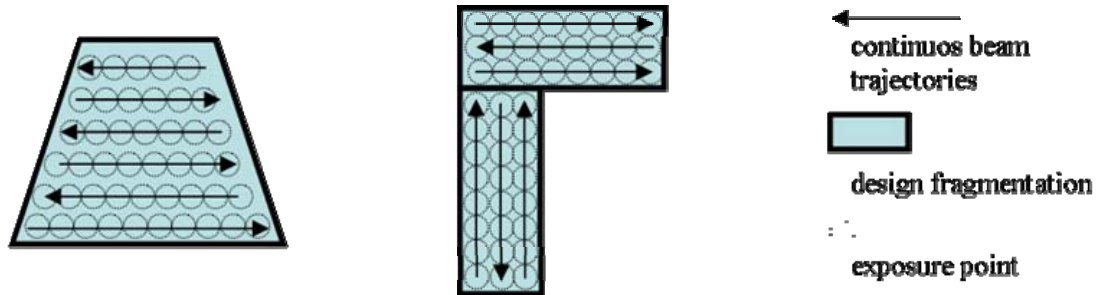


Figure 2.10 Representation of fragmentation and scan direction of the designs (15).

If the area of the design is bigger than the field size, a second fragmentation of the design has to be done. Due to this, motorized support and positioning system by laser interferometric stage is convenient, to optimize the stitching precision.

The operation of beam exposure is completed with the determination of beam speed. Dose is the amount of charge per unit area that receives the resist. The exact value to fully expose the whole resist thickness and to precisely define its shape and dimensions is specific for each resist and its intrinsic characteristics. During irradiation, dose is adjusted by determining the time that beam remains in each pixel (called area dwelltime). The expression that is used to determine the set of exposure parameters during exposure is presented in the next section. Beam deflection speed is limited by the bus transmission speed, since the management of design data by the PC is faster than the converter.

Another limitation of these systems is the tolerance of scanning coils, which are not designed for the random displacements of vector scan mode. The uncertainties can be reduced choosing a proper settling time in exposure parameters. The chamber, the support and its displacements or positioning are other limiting factors. The planarity of sample holders and the precision of minimum displacement can be the cause of distortions. Manual alignment is very useful, but slows down the process.

Summarizing the system performance, the applicability of EBL is restricted by stitching, alignment, automation and data transfer rate of the designs.

2.2.6 Vacuum system

As it has been remarked during SEM column description, it is not only convenient, but necessary to work in high vacuum conditions inside the column. The beam performance and resolution is strongly conditioned by the performance of the vacuum system.

In general, SEMs are equipped with two vacuum levels. Inside the column, UHV (in the order or lower than 10^{-9} mBar) is maintained, whereas the chamber level is less strict (lower than 10^{-5} mBar).

It is accomplished by means of three vacuum pumps. Usually a first rotary pump is used to supply the vacuum level that allow the operation of the second pump. It is

typically a turbomolecular pump that implements the chamber vacuum level. Inside the column, an ionic pump is used to reach the UHV required for the beam operation. The SEM includes a valve that isolates the column when chamber is vented to load samples.

2.3 Exposure procedure

2.3.1 Equipment

The Nanofabrication Laboratory at the IMB is equipped with a SEM from Zeiss, model LEO 1530, Gemini column (Figure 2.11). It is based on a Schottky field emission filament made of tungsten. It works at low temperature and it is outstanding for its emission stability, very convenient for lithography. The microscope nominal resolution is 1 nm at 20 keV beam energy and 2.1 nm at 1 keV, and acceleration voltage range is 0.1 – 30 kV. Magnification varies from 20x to 900kx, six apertures are available, 7.5, 10, 20, 30, 60, 120 μm in diameter, two detectors (Inlens, for backward scattered electrons and SE2 for secondary electrons) are used, 6" wafers can be introduced in the chamber and stage movements are motorized in XYZ and rotation. The computer interface works under WindowsNT.

Lithographic capabilities comprise external beam blower and beam deflection system provided by Raith GmbH. The beam blower abruptly deflects the beam by the application of a voltage of 200 V. The maximal frequency of switch on and off is around 2.6 MHz with transitory time of 10 ns. The control over the beam during exposure is accomplished by Elphy Plus program. It integrates the beam deflection system, the hardware for design, calibration and control of exposure conditions. The program is graphics oriented and enables different configurations adapted to each user preferences and for each lithographic task.

All the experiments of EBL included in this thesis have been performed with the equipment described above. EBL system has been operated in Clean Room conditions, Class 100, where temperature is 22°C and relative humidity ranges, typically, from 30 to 60 %.



Figure 2.11 EBL system at the Nanofabrication Laboratory in the IMB-CNM.

2.3.2 Procedure

The procedure for the exposure comprises several steps: design of the pattern and determination of exposure coordinates, calibration of working field (WF, write field), definition of reference systems (SR) for positioning and alignment, determination of actual beam current to establish the exposure conditions, optimization of focus and irradiation. Each lithographic system is determined by its own exposure procedure and actions sequence. The flux diagram in Figure 2.12 schematizes the operation of the system at the IMB-CNM.

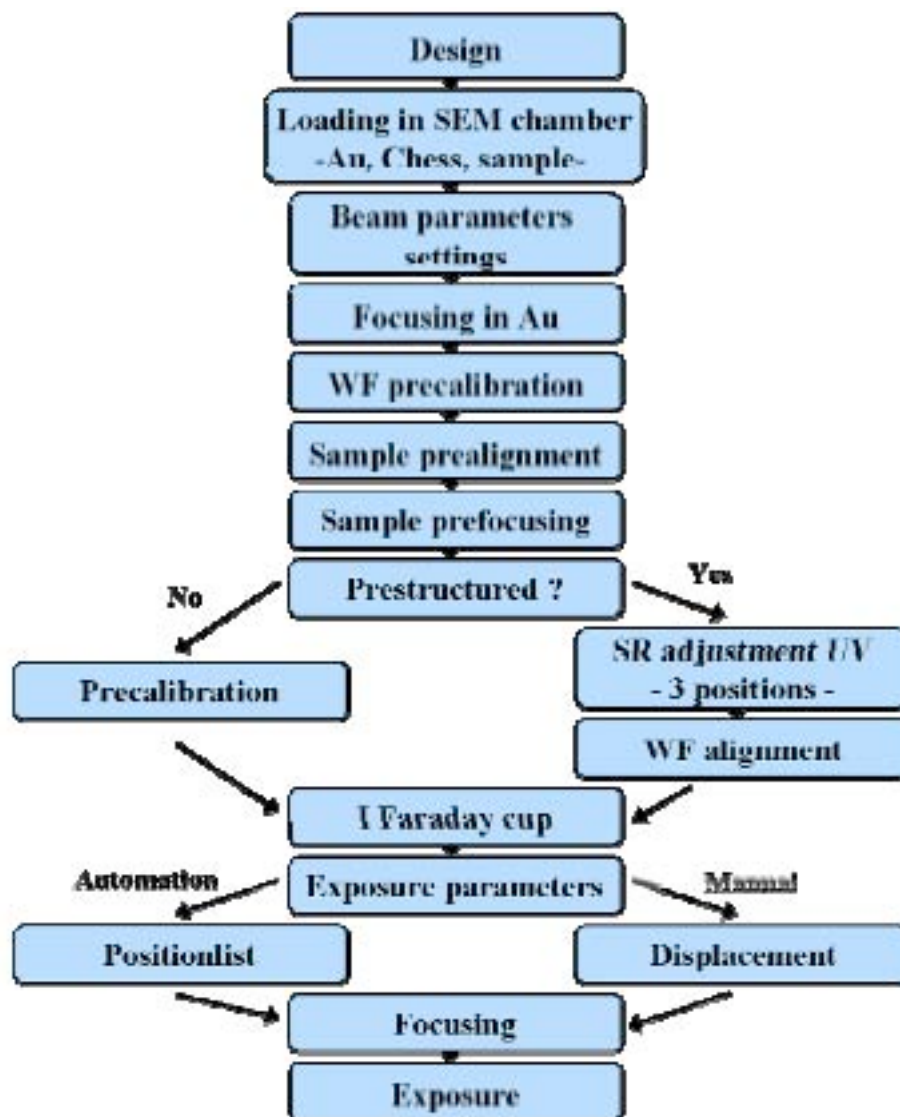


Figure 2.12 Flux diagram of the exposure procedure.

2.3.3 Deflection calibration

The calibration of deflection is necessary to determine the value that quantifies each coordinate/position on the surface of the substrate with the beam deflection respect to the optical axis. As presented in previous section, the precise control of beam displacement is realized by means of variable potentials applied to the deflection coils, separately for X and Y axis. To define the patterns through the lithographic interface, this equivalence should be defined.

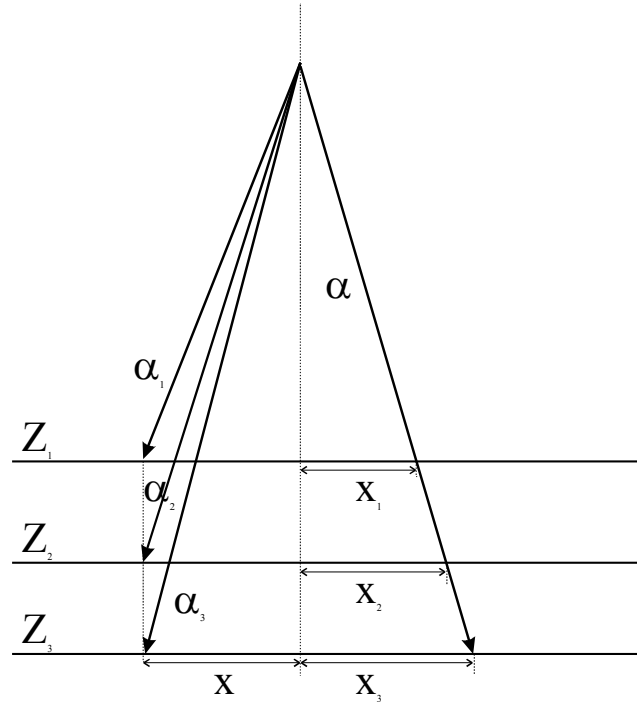


Figure 2.13 Calibration of deflection as a function of z position (vertical axis).

The calibration establishes the relation of the voltage applied to the coils with the lateral dimension equivalence. In Figure 2.13 representation of this concept is schematized. For different positions z_i of the sample, the deflection angles (α_i) for the same point (x) are different (Figure 2.13, left). Since deflection angle is proportional to the applied voltage, the conversion factor is determined in the control PC. The same concept can be illustrated as seen in Figure 2.13, right. For a constant deflection angle (α), i.e. constant potential applied to the coils, the distances respect to the origin (x_i) are different at varying substrate level (z_i). In addition, SEM is internally calibrated to correlate the magnification and working distance (WD). The WD is the distance to the focused point on the sample surface.

In consequence, the parameters involved in the calibration are substrate position (z), related to the WD and magnification. The determination of magnification determines the exposure area (WF) that can be irradiated. The beam deflection is obviously restricted and limited by the aberrations caused by deflection by angular control. This is, non linearity to scan flat surfaces.

Since the number of positions that resolves the deflection system is finite and constant, the WF (i.e. magnification) used influences the resolution. Due to this, higher magnification (smaller WF) is required for maximum resolution. The execution of calibration also depends on the existence of a prestructure in the substrate, but the principle is equivalent.

From a reference sample that is formed by features of predefined dimensions and coordinates, calibration communicates to the control PC which are these values and where they are located. Marks are positioned on determined coordinates of an image by means of the control interface (Figure 2.14, right).

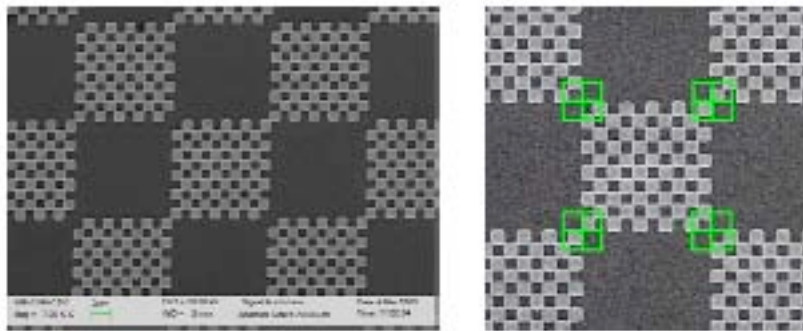


Figure 2.14 (Left) SEM image of Chess WF calibration sample and (right) deflection calibration through the lithographic interface.

2.3.4 Positioning

The positioning on bare substrates and the alignment with prestructures existing on the sample is another important step of EBL process. It comprises the definition of reference systems (SR) and the hardware transformations to accomplish a correct exposure execution. There are four levels of coordinate systems that have to be correlated:

- the SR of the sample support (stage),
- the SR correlated to the sample,
- the coordinates defined within the design,
- the SR established by the beam.

The last level corresponds to the coordinate system that determines the beam deflection defined in previous section as calibration (Figure 2.15, right).

The samples are placed into the SEM chamber mounted in the sample holder. The coordinate system (xyzr) is determined by the SEM hardware and it references the origin in the central point of the moving support. The sample is located at some point of the sample holder (x, y), it has certain thickness (z) and it is oriented (r) (Figure 2.15, left).

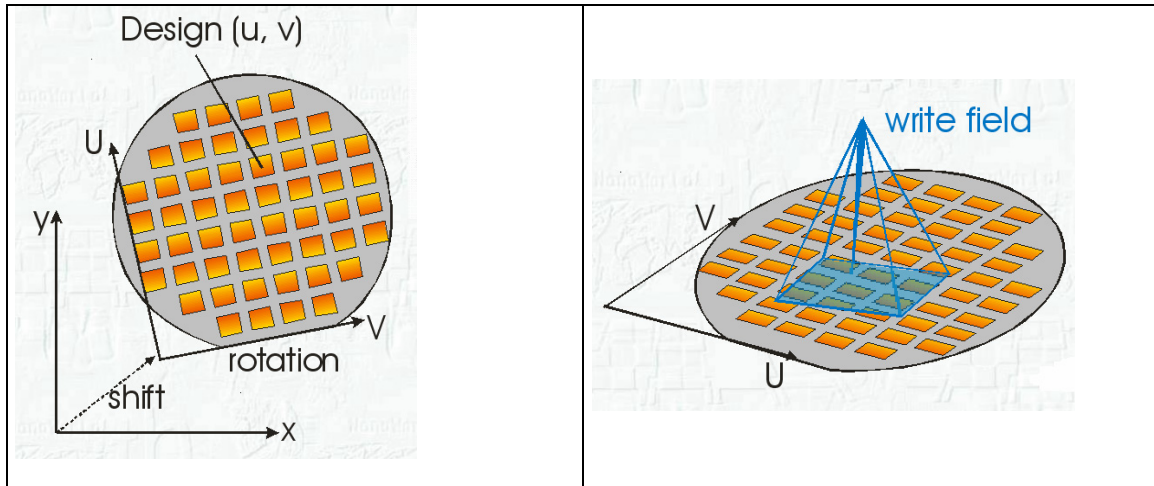


Figure 2.15 Reference systems of EBL configuration.

The sample defines itself the limiting area and positioning range. Nonstructured samples determine with their dimensions the accessibility for the exposure process. Preprocessed samples explicitly tighten the alignment: their designs have determined position, orientation and dimensions on the sample. In consequence, a second reference system (U, V) is defined respect to the wafer (for example, using the flat) or with a specific point or feature of the substrate (corner, edge, etc).

The design features present their own coordinates established in the design program, which introduces a new coordinate system (u, v). The beam displacements have defined a specific reference system. The field calibration on the substrate for determined magnification, z position of the stage (WD) and emission parameters (beam energy) attributes the beam deflection to determine the values of magnification, translation and rotation in the reference system (U, V), (Figure 2.16, left).

Hence, only the correlation of equivalence between support and sample coordinates and between sample and design has to be established.

In bare samples, the corner and the edge of the sample are typically used to define the relation of origin and orientation for both reference systems, and translations are considered then equivalent. For prestructured samples, the correlation is usually taken from the preexisting coordinate system, i.e. from marks or positions defined in the substrate. The equivalence is defined allocating three points of known coordinates from the sample to three points of the coordinate system of the sample support (Figure 2.16, right).

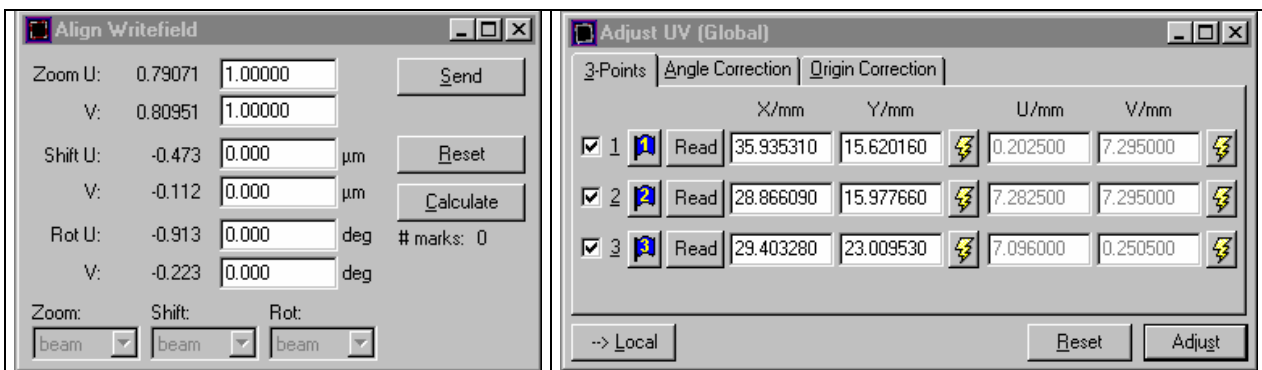


Figure 2.16 Windows for WF (left) and SR UV (right) adjustment within Elphy Plus program.

In the second coordinate transformation, the translation to be correctly placed before the exposure is defined. By defect, the axis between Uu and Vv are considered parallels. For automated multiple irradiations, the translations correspond to the coordinates established in the so-called Positionlist. If driven manually, the exposure positions are the displacements executed before the irradiation (Figure 2.17)

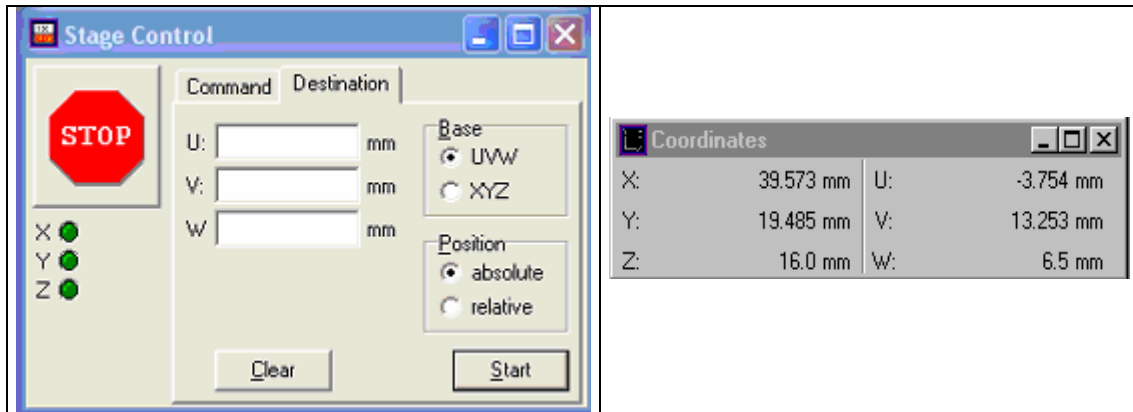


Figure 2.17 Windows for positioning (left) and coordinates control (right) of Elphy Plus program.

The Positionlist is the file that allows to automate the exposure. In general, it is used to manage several designs in determined positions and varying conditions (layers, doses, etc), but also enables to control other SEM actions, as for example, magnification, beam energy, etc (Figure 2.18).

ID	U	V	Attribute	Template	Comment	Type	Size-U	Size-V	Pos1	Pos2	File	Layer	Are	DoseFactor	Dot
0	7.000	4.700	XN	UV	marca	EXPOSURE	50.000	50.000	25.000	25.000	C:\Elphy32\G 0	1.0	...
1	7.100	4.600	XN	UV	array100vertical	EXPOSURE	99.000	100.000	49.500	50.000	C:\Elphy32\G 0	1.0	...
2	7.300	4.400	XN	UV	array100vertical	EXPOSURE	99.000	100.000	49.500	50.000	C:\Elphy32\G 0	2	...
3	7.500	4.200	XN	UV	array50vertical	EXPOSURE	98.000	100.000	49.000	50.000	C:\Elphy32\G 0	1.0	...
4	7.700	4.000	XN	UV	array50vertical	EXPOSURE	98.000	100.000	49.000	50.000	C:\Elphy32\G 0	2	...
5	7.000	3.000	XN	UV	marca	EXPOSURE	50.000	50.000	25.000	25.000	C:\Elphy32\G 0	1.0	...
6	7.100	3.700	XN	UV	array100vertical	EXPOSURE	99.000	100.000	49.500	50.000	C:\Elphy32\G 0	1.0	...
7	7.300	3.500	XN	UV	array100vertical	EXPOSURE	99.000	100.000	49.500	50.000	C:\Elphy32\G 0	2	...
8	7.500	3.300	XN	UV	array50vertical	EXPOSURE	98.000	100.000	49.000	50.000	C:\Elphy32\G 0	1.0	...
9	7.700	3.100	XN	UV	array50vertical	EXPOSURE	98.000	100.000	49.000	50.000	C:\Elphy32\G 0	2	...
10	8.700	4.700	XN	UV	marca	EXPOSURE	50.000	50.000	25.000	25.000	C:\Elphy32\G 0	1.0	...
11	8.000	4.600	XN	UV	array100vertical	EXPOSURE	99.000	100.000	49.500	50.000	C:\Elphy32\G 0	1.0	...
12	8.200	4.400	XN	UV	array100vertical	EXPOSURE	99.000	100.000	49.500	50.000	C:\Elphy32\G 0	2	...
13	8.400	4.200	XN	UV	array50vertical	EXPOSURE	98.000	100.000	49.000	50.000	C:\Elphy32\G 0	1.0	...
14	8.600	4.000	XN	UV	array50vertical	EXPOSURE	98.000	100.000	49.000	50.000	C:\Elphy32\G 0	2	...
15	7.900	3.900	XN	UV	marca	EXPOSURE	50.000	50.000	25.000	25.000	C:\Elphy32\G 0	1.0	...
16	8.000	3.700	XN	UV	array100vertical	EXPOSURE	99.000	100.000	49.500	50.000	C:\Elphy32\G 0	1.0	...
17	8.200	3.500	XN	UV	array100vertical	EXPOSURE	99.000	100.000	49.500	50.000	C:\Elphy32\G 0	2	...
18	8.400	3.300	XN	UV	array50vertical	EXPOSURE	98.000	100.000	49.000	50.000	C:\Elphy32\G 0	1.0	...
19	8.600	3.100	XN	UV	array50vertical	EXPOSURE	98.000	100.000	49.000	50.000	C:\Elphy32\G 0	2	...
20	8.700	3.000	XN	UV	marca	EXPOSURE	50.000	50.000	25.000	25.000	C:\Elphy32\G 0	1.0	...

Figure 2.18 Example of Positionlist file for automation of EBL exposure.

The working area (WA) is the part of the WF that is used during each exposure. For big designs, the pattern is usually divided into smaller parts that are exposed separately. If WA=WF, the center of both fields is coincidental. If WA is smaller or bigger than the WF, the central position of the design or the positions of the different exposures have to be determined, respectively (Figure 2.19, left and right).

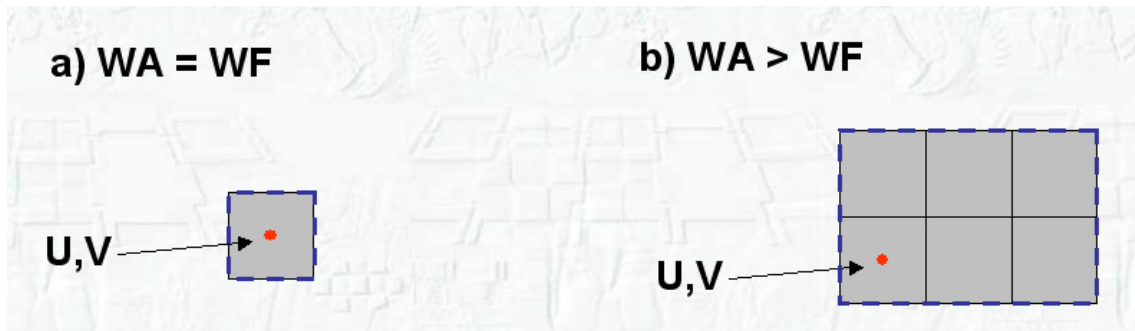


Figure 2.19 Relation between WA and WF as a function of their relative dimensions.

2.3.5 Focusing

The optimization of beam focus comprises three main actions that are next described.

Together with the sample that will be processed, the focus calibration sample is simultaneously introduced in the SEM chamber. It is formed by small grains of gold of variable size on a carbon substrate (Figure 2.20).

The Au grains are characterized by their round or spheric shape and high atomic weight, overall compared to C. These two properties imply that this kind of sample is ideal to finely focus the beam at certain WD, beam energy and aperture, thanks to the high contrast signal and possibility to correct the astigmatism.

The focusing process comprises, typically, the adjustment of aperture position respect to the beam axis, the elimination of astigmatism (sharpness), WD adjustment and balance of brightness and contrast.

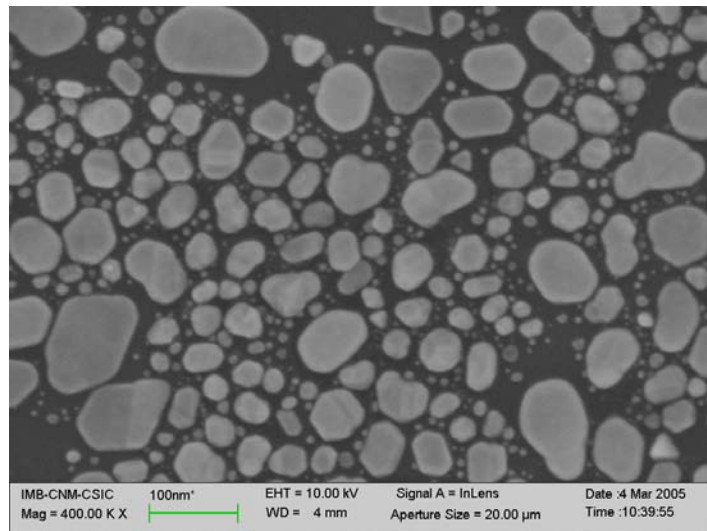


Figure 2.20 SEM image of gold sample for focusing optimization.

This prefocusing optimization serves to establish the starting point for focusing on the sample to be exposed, mainly if the z position of both substrates is approximately the same. On the exposure sample, focusing is performed in a defect or a scratch on the resist, some particle or preexisting structures placed in an area that will not be used for

lithography. If the different exposure positions are not much separated, same focus conditions can be shared.

However, the final verification of proper focusing is recommended (and essential for high resolution lithography) by means of what is called the contamination dot. It consists of stopping the beam in a specific position during a few seconds. If the beam is perfectly focused in the top of the surface, the concentration may cause the creation of a white circular spot of less than 100 nm in diameter

2.3.6 Pattern design

There exist various commercial systems to adapt SEMs for lithography. They allow the design, simulation, parametrization, calibration, positioning and exposure execution. The vector scan mode, which conducts the beam directly and only in the areas to be irradiated, requires a dedicated software. The most commonly used systems are Nanometer Pattern Generation System (NPGS) from JC Nability Systems and the program of Raith GmbH company.

Elphy Plus, Raith GmbH

The support package for SEM based lithography at the Nanofabrication Laboratory is Elphy Plus from Raith GmbH. It is a PC based controller including software and hardware. It allows the creation of the designs, the remote control of electron beam system, the automation of some actions and, optional, the proximity effect correction or metrology. The specifications of the lithographic capabilities include a DAC of 16 bits, data transmission at 2.6 MHz, control of exposure time for each pixel lower than 10 ns, digital acquisition of images, alignment and mark recognition, automation of different tasks through macros, etc. The software works in Windows 98 or NT, graphically oriented and it integrates all the modules in a single package. The other specifications involved in lithography, such as resolution, detectors, electron source, stage movement and precision, etc depend essentially on the SEM characteristics.

Design files

The design files are organized by jerarquic structures in databases of extended GDSII format. This format enables to determine dose information and includes special structures, such as single pixel lines (SPL), text or bitmaps. In addition, it is CAD file compatible with GDSII, DXF and CIF formats, or ASCII database. In both cases, the use of external files is based on the conversion to the internal GDSII.

The visualization and edition is completely graphic and it allows flexible and fast data manipulation. In particular, the program allows to draw as basic structures, rectangles, polygons, circles, ellipsoids, lines, dots, etc in separated layers for multilevel exposure. Text can be included, together with practical information for documentation (date and time of exposure). It includes a generator of mathematical functions to create curves matrices or many actions to modify the basic structures: translation, scaling, iteration, deleting, merging, etc (Figure 2.21).

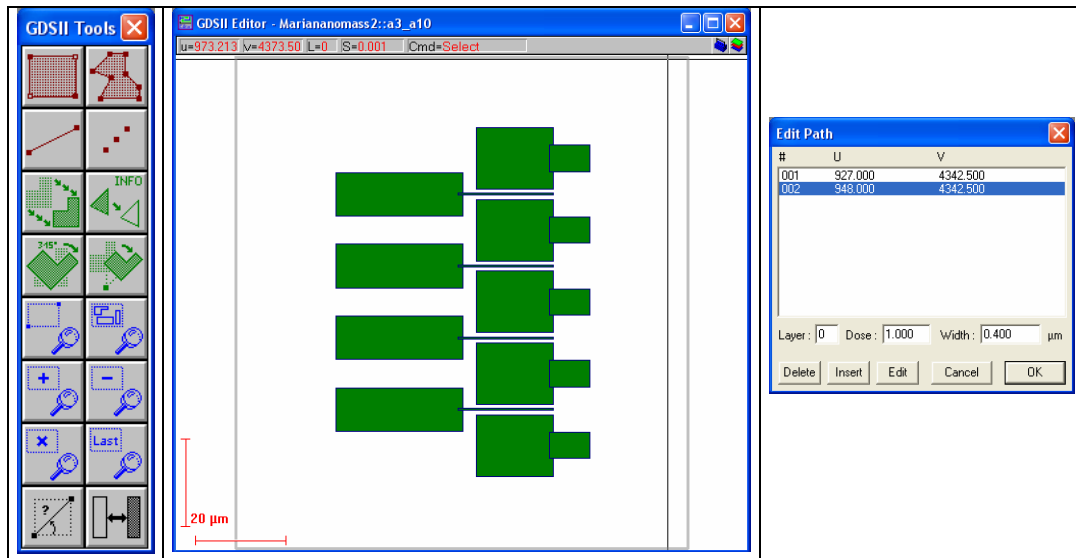


Figure 2.21 Edition windows for designs in the Elphy Plus program.

Design vs exposure result. Proximity effect

As mentioned in the introduction of this chapter, one of the limiting factors of EBL is the divergence between the design and the result of the exposure after development. The electron-solid interactions cause that absorbed dose is not confined to the zone where beam has been driven. This fact causes dimensional imprecisions and design distortions, that are called proximity effect in its more extended version (more details in Chapter 3).

There exist several techniques to compensate these phenomena. The choice of system configuration or exposure conditions can minimize them, for example, the use of very thin layers or beam energy selection. In addition, the design program allows to introduce corrections to reduce the proximity effect. Basically, feature fragmentation and determination of the optimal scan direction, dimensional and shape adjustment, or compensation of the absorbed dose inhomogeneity by dose balance in the design.

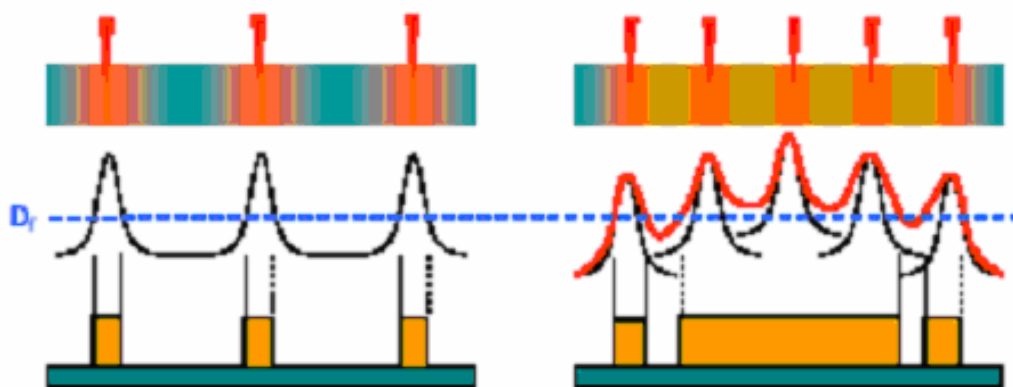


Figure 2.22 Representation of electron dose absorbed in the case of isolated (left) or areal (right) features.

Due to proximity effect, areas receive additional dose in the central zones of the features. Proper fragmentation could help to reduce this effect, for example, when gap

distances between areas are intended to be of a few tens of nanometers. It is possible even to determine the order and the scan direction of the different exposure elements.

Dimensional adjustment is usually determined from experimental results, by iterated tests, which implies that it is only a useful correction technique for reproducible designs and not very complex.

The last option, dose adjustment, is the more robust method and it has generated the development of simulation programs for absorbed dose and algorithms of proximity effect correction. An exhaustive presentation of the proximity effect correction is included in Chapter 3.

2.3.7 Exposure conditions

The writing strategy of present EBL system is based on the vectorial scanning technique. The beam of ideal circular section and gaussian intensity profile is driven, in general, along straight lines. In order to reproduce the design features, exposure consists of filling the areas using a finite number of scan lines. The determination of the conditions and the different parameters involved in the irradiation are next presented.

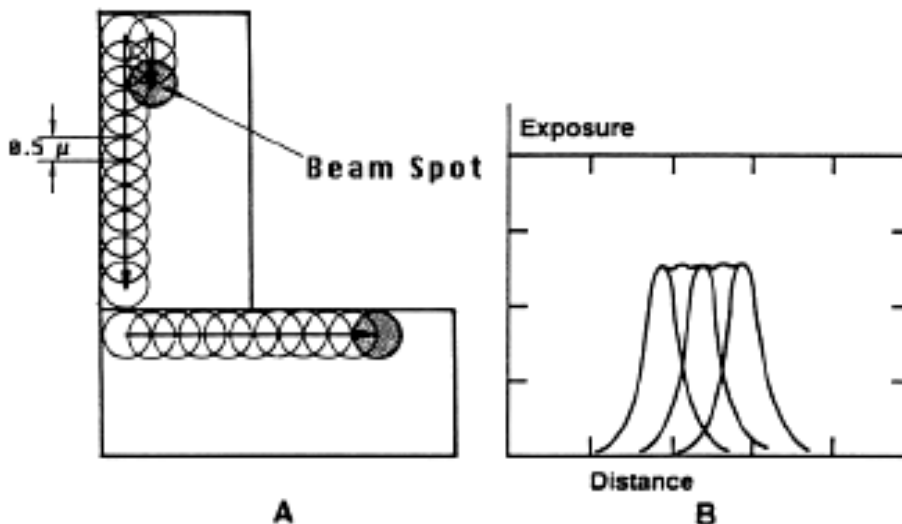


Figure 2.23 Exposure strategy of direct write EBL (16).

Exposure dose

All the procedure and exposure parameters are partially defined by the operation technique, but also by the concept that determines the delivery and quantification of the dose. The concept of dose is established as the number of incoming electrons that are needed to fully develop the resist thickness, whatever its shape, area, lines defined as SPL or a dot. The expression for each case is slightly different (Figure 2.24):

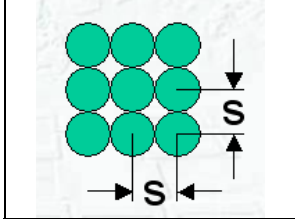
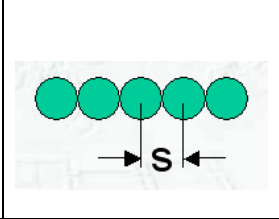
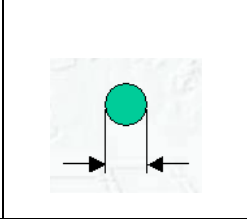
Area dose (AD)	SPL dose (LD)	Dot dose (DD)
$AD = I_{\text{beam}} \cdot T_{\text{dwell}} / s^2$ ($\mu\text{As}/\text{cm}^2$)	$LD = I_{\text{beam}} \cdot T_{\text{dwell}} / s$ (pAs/cm)	$DD = I_{\text{beam}} \cdot T_{\text{dwell}}$ (pAs)
		

Figure 2.24 Expressions for the different concepts of dose for, areas, lines or dots.

It is considered that punctual beam delivery deposits a certain amount of electronic charge determined by beam current intensity. The beam is non zero dimensional, but it affects an effective radius (s , stepsize). Hence, the scanning speed during exposure is performed based on this assumption and the definition of the dwelltime (T_{dwell} , the time that beam remains in each exel to deliver the correct dose). Stepsize and dweltime determine the beam deflection speed during the exposure.

The proper dose is determined during the exposure process and depends on many interelated parameters: resist, developer, temperature, beam energy, etc.

Beam energy

The term electron energy is used to refer to the kinetic energy of the charges. It is directly related to the acceleration voltage applied to the beam in the SEM column. The penetration depth of electrons in the matter depends on this parameter and it also conditions the focusing depth, among other phenomena.

At low energy, the penetration range is short, what causes that the interaction occurs mainly in the surface. In addition, damage and charging are reduced, but resolution is lower. At higher acceleration voltages, resolution is higher, but also substrate heating and damage in the crystalline structure increases.

For lithography, the dependence of resist sensitivity with incoming beam energy is registered. The electron efficiency is inversely proportional to the acceleration voltage, i.e. increasing incoming energy implies that dose should be higher.

Aperture. Beam intensity

The electron source parameters (intensity and extraction voltage) and acceleration voltage applied to the beam determine the intensity of the beam current. However, often the selection of beam current to be used during exposure is determined by means of the different apertures.

Since apertures are circular, the beam intensity is proportional to the squared radius of the hole. In order to determine the current, the measurement is performed with the probe based on a Faraday cup (Figure 2.25, left). It consists of a retractable arm coupled to the SEM chamber, which is introduced laterally until it reaches the beam

axis. Manually, the aperture of the probe is finely adjusted with two screws (one for each axis, X and Y) (Figure 2.25, right). The positioning is assessed using the SEM and the intensity value is registered at high magnification. The measurement is introduced in the window where calculation and exposure parameters determination is executed.

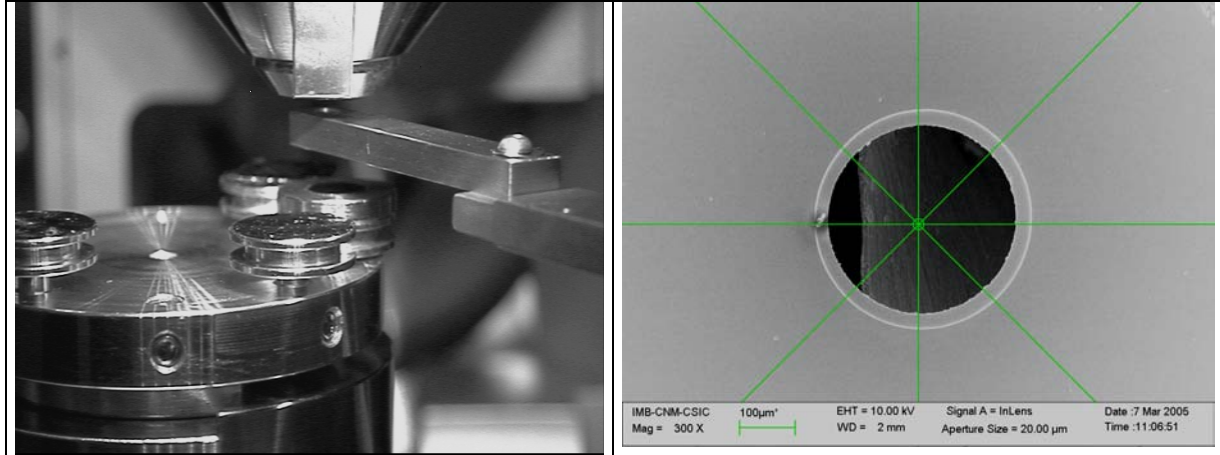


Figure 2.25 CCD image of measurement of beam intensity. (Left) Arm of the Faraday cup introduced to the SEM chamber and (right) aperture of the Faraday cup aligned with the electron beam axis direction.

The magnitude of the beam current determines two characteristics of the accomplishment of the exposure: the throughput and the resolution. The present SEM is provided with six different apertures of 7.5, 10, 20, 30, 60 and 120 μm in diameter. Bigger apertures imply larger currents, which enables faster delivery of the electron dose. The smaller apertures limit beam intensity and reduce the effective beam diameter. In addition, the intensity profile is confined more abruptly. As a result, it is possible to control more precisely the quantity and position of delivered dose, but at the same time, the exposure time increases and focusing is more difficult.

In summary, apertures of larger diameter are used to expose big areas that do not require high patterning resolution, i.e. when high yield is desired. Reduced apertures are useful for delicate applications, where maximum resolution is pursued.

Field parameters

The deflection calibration for the exposure control by means of the lithographic system establishes the relation between WD, magnification and WF.

The position in z of the substrate determines the distance of focusing, which is slightly dependent on the acceleration voltage. Since deflection is confined and limited by the aberrations that occur at large deflection angles, the WD conditions the magnification to be used for each WF. The z position together with the deflection limits establish the scanning area accessible for a determined magnification.

Since the number of pixels that can be resolved during lithographic irradiation is finite, the resolution is also constraint to the calibration for each WF/magnification pair. High magnification means that the beam deflection respect to the optical axis is small. Hence, the aberrations related to the WD are minimized and but, also, WF is limited. Due to this, the WA is reduced, but lithographic resolution can be increased. To pattern

large areas in a single exposure step, it is necessary to use low magnification, and large WD, but the loss of resolution can be significant.

Experimentally, the determination of the set of proper conditions is the compromise of all the variables and is adjusted for each specific application. As an example, for a WD of ~8 mm the magnification of 1500x is used for a WF of 100 x 100 μm^2 .

Deflection speed

The scanning operation is executed during the beam exposure as a function of several variables. The concept of dose depends on three parameters: beam intensity, distance between exposure points (stepsize) and the time that the beam remains in each exposure point (dwelltime). The dose value depends on the exact resist sensitivity at certain exposure and development conditions. It is established experimentally. The beam intensity is defined by SEM column parameters (including acceleration voltage and aperture) and it is measured with the Faraday cup. The two remaining parameters, area stepsize and dwelltime might be established and correspond to the beam speed during the scanning. Fixing one of the variables (usually stepsize), the third (dwelltime) is calculated using the experimental sensitivity value and the expression for dose.

It is obvious that proper beam velocity is limited. As a matter of fact, it is considered that reasonable scan speed is around 2-4 $\mu\text{m}/\mu\text{s}$. The program establishes the minimum dwelltime in 0.385 μs and WF size determines the minimum stepsize resulting from the finite pixel number (65536). Similarly to the field parameters, the relation of these parameters is a compromise and the optimal ones are those that adjust the desired exposure result. Some determining factors are the design, exposure yield, precision, etc.

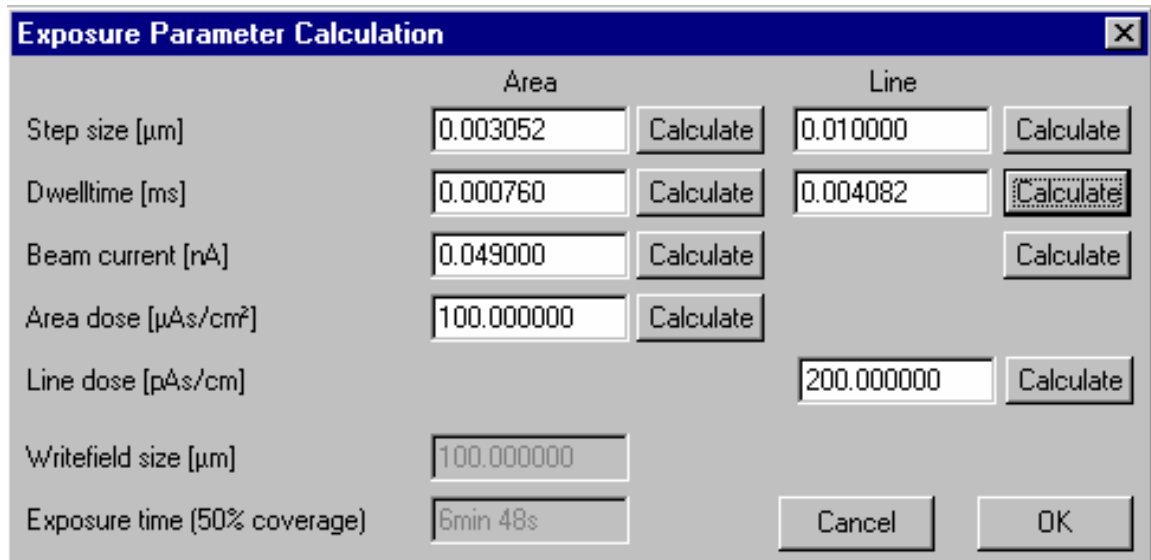


Figure 2.26 Window for calculation and determination of exposure parameters.

SPL, dots

Lines defined as SPL and dots are considered as special elements in terms of the determination of the exposure parameters.

Lines can be designed with determined width, which will be more or less reliably reproduced once exposed and developed. The alternative to control linewidth is to attribute them “zero” linewidth and to adjust the result by means of the deflection speed. Slower velocity, i.e. small line stepsize (large dwelltime) implies higher delivered dose. In consequence, the linewidth after development is larger (and viceversa).

Similarly for dots, exposure is performed stopping the beam for determined time period. Depending on beam intensity the exposure dose is then defined. Since charge distribution around the exposure site is radial, the result is a circular feature. Adjustment of dwelltime enables to modulate the size of the resulting dots, but it is essential that there is no drift, astigmatism or defocusing, in order to achieve optimum results, i.e. absolutely circular dots.

Other parameters

The program for lithography assistance provides other additional parameters that, not being indispensable, can be useful or convenient for specific cases. As some examples, it is possible to determine the number of times that a same irradiation is executed in a same coordinate (loop). Besides this, the waiting time once the beam is located in the initial position of each exposure element (settling time) or the waiting time between different lines of a same element (flyback time) can be established. In general, these variables are not critical, but can be influential in high resolution exposures. New versions of the program even introduce the choice of different scan modes: line, meander and circular mode, which correspond, respectively, to scan in lines of constant orientation, opposite direction or concentric trajectories.

In summary, within this chapter, the elements and operation of a direct write electron beam lithography system has been described. In particular, the equipment that has been used during the development of this thesis. Electron beam constitutes the common aspect for all the results that are included in the following chapters. The specifications, limitations and characteristics of the electron beam lithography technique and the instrumental that is used, determine the design, execution and results obtained when applied to nanofabrication.

References

- (1) Encyclopedia Britannica
- (2) A. A. Tseng, K. Chen, C. D. Chen, and K. J. Ma
Electron beam lithography in nanoscale fabrication: recent development
Ieee Transactions on Electronics Packaging Manufacturing **26** (2), 141-149 (2003)
- (3) D.J. Grant
Electron Beam Lithography: From Past to Present
University of Waterloo (2003)
- (4) D. K. Ferry, M. Khoury, D. P. Pivin, K. M. Connolly, T. K. Whidden, M. N. Kozicki, and D. R. Allee
Nanolithography
Semiconductor Science and Technology **11** (11), 1552-1557 (1996)
- (5) D. M. Tennant
Nanotechnology
Springer NY (1999)
- (6) A. N. Broers
Fabrication limits of electron beam lithography and of UV, X-ray and ion-beam lithographies
Philosophical Transactions of the Royal Society of London Series a-
Mathematical Physical and Engineering Sciences **353** (1703), 291-311 (1995)
- (7) A. N. Broers, A. C. F. Hoole, and J. M. Ryan
Electron beam lithography - Resolution limits
Microelectronic Engineering **32** (1-4), 131-142 (1996)
- (8) J. L. Mauer, H. C. Pfeiffer, and W. Stickel
Electron Optics of an Electron-Beam Lithographic System
Ibm Journal of Research and Development **21** (6), 514-521 (1977)
- (9) T. H. P. Chang, M. G. R. Thomson, M. L. Yu, E. Kratschmer, H. S. Kim, K. Y. Lee, S. A. Rishton, and S. Zolgharnain
Electron beam technology - SEM to microcolumn
Microelectronic Engineering **32** (1-4), 113-130 (1996)
- (10) M.A. McCord
Handbook of Microlithography, micromachining and microfabrication. Volume 1: Microlithography. Chapter 2: Introduction to Electron Beam Lithography
SPIE (1999)
- (11) P.W. Hawkes
Electron optics and electron microscopy
Taylor & Francis, London (1972)

- (12) Herriot and Brewer
Electron beam technology in microelectronic fabrication
Academic Press NY (1980)
- (13) E. Chen
Introduction to Nanofabrication
Applied Physics **294r** (Harvard University) (2004)
- (14) A. J. Speth, A. D. Wilson, A. Kern, and T. H. P. Chang
Electron-Beam Lithography Using Vector-Scan Techniques
Journal of Vacuum Science & Technology **12** (6), 1235-1239 (1975)
- (15) R. Bojko
EBFM manual
Cornell University
- (16) W. Moreau
Semiconductor Lithography
Plenum NY (1988)

Resists materials are crucial elements in most of the lithographic processes and their performance determines the final result of the process. A detailed study of the irradiation as a function of beam energy, substrate, dose, etc is presented. A Monte Carlo simulator is used to quantify the scattering processes and, therefore, to depict the electron trajectories during exposure. Experimental results on conventional methacrylic resists (PMMA) are presented. Submicronic features are defined on thick layers of an experimental negative resist. The performance of a new electron beam negative resist is characterized and the post processing by etching methods is tested. The complete methodology for proximity effect correction is established and accomplished for both PMMA and the new negative resist.

3 Electron beam irradiation of resists

3.1 Exposure effect

Lithography has been used for ages as the technique for transferring patterns to a material. In silicon-based technologies, the most common method is photolithography which is based on light source exposure onto a resist layer. The resist is the material that supports the recording of the latent image and acts as the transfer media for subsequent processes. In photolithography, some limitations may be encountered in terms of resolution or flexibility, instead of having high throughput and simple and well-developed technology. The minimum feature size is limited by the wavelength of the light and, even when development of light sources is still on going, these sources are substantially more expensive. Fabrication of the mask for selective exposure in photolithography requires the use of a higher resolution technique (1).

EBL is a direct writing method. It modifies the resist composition of the exposed areas and hence pattern features materialize with the development process. The EBL mechanism involves many physical and chemical effects that need to be understood for its proper and optimal performance. The ultimate resolution depends on both physics and chemistry processes and the quantification of each contribution is not modeled. In addition to the electron scattering and proximity effects, the chemical phenomena in the resist include the resist collision, resist development and, in some cases, post exposure bake (PEB) and acid diffusion (2).

Resist performance is defined mainly by four characteristics: tone, sensitivity, resolution and etching resistance.

- Tone determines the areas that will be removed in the development. For positive tone resists, patterned areas are removed with the developer, whereas for the negative ones, the result is the inverse of exposed features, resist is not dissolved where irradiated.
- Sensitivity quantifies the minimum amount of delivered dose that is required to achieve the selective development, where dose is the number of electrons per unit area.
- Resolution defines the minimum feature size or the smallest distance between two patterns that can be resolved.
- Contrast (γ) describes how abrupt is the dependence of thickness on dose, which also has implications upon resolution. It is determined from the linear slope of the sensitivity curves (3.1).

$$\gamma = \frac{1}{(\log D - \log D^0)} = \left[\log \frac{D}{D^0} \right]^{-1} \quad (3.1)$$

where D is the dose of full thickness exposure or complete development and D_0 is the dose that causes no remaining thickness or no resist dissolution on developer (for negative or positive resists, respectively).

- Etch resistance parametrises the resist integrity under chemical (wet) and physical (dry) etching processes. Other resist variables are adhesion to the different substrates, compatibility with conventional techniques or shelf life.

From their composition, resists can be classified basically in two types: inorganic and organic. The main difference concerning to EBL is that inorganic resists are only affected by the primary beam, high energy electrons, whereas organic resists are chemically modified by the secondary electrons, that is, the low energy electrons.

Inorganic resists have demonstrated a high resolution performance, but lower sensitivity and difficulties to combine them with subsequent fabrication processes restrict their actual use (3). Organic resists certainly offer many more advantages and due to this a more detailed general description is presented in the next section. In addition, experimental use of different organic resists is evaluated.

3.1.1 Organic resists

As mentioned, organic resists are widely used in lithography as the pattern transfer media. Resists can be synthesised with a great diversity of polymeric materials and almost all types can be patterned by EBL. Also important, it is often possible to vary their properties modifying the polymer structure and molecular properties. Therefore, tone, sensitivity, thickness, etc, can be adjusted for an optimal performance or tailored for specific applications (4, 5, 6).

The effect of electron beam on the organic resists determines the tone. The interaction of the resist with the charges induces a different mechanism for positive or negative resists that is determined by their particular composition.

Positive tone resists are based on the degradation of exposed resist material. Secondary electrons from inelastic collisions modify chemical composition by chain scission. The break of backbone bonds causes polymer fragmentation. In fact, it is considered that the creation of radicals may result in additional decomposition processes (4). As a result, patterned features present an increased solubility when immersed in the

developer and even it can be seen as enhanced by pores that facilitate developer swelling.

Negative resists are based on the cross-linking of the polymer chains due to the beam charges. Secondary electrons cause a further solid-state polymerization by intermixture of polymer chains. The consequence of intermolecular or intramolecular crosslink is a decrease in the solubility of the patterned areas. Often the limitation comes from a certain tendency to scum, feature bridging and swelling. In this case, sensitivity is defined in close relation with the remaining thickness (Figure 3.1, right).

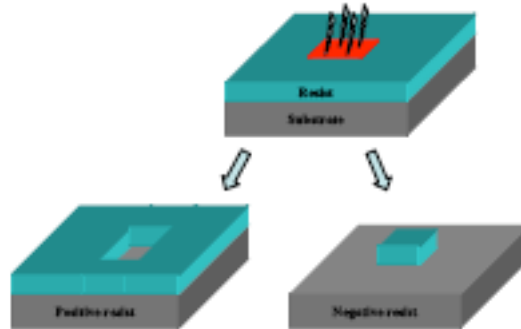


Figure 3.1 Electron beam exposure causes molecular changes in the resist layer. (Left) Positive tone resists suffer chain scission. (Right) Negative tone resists experience cross-linking.

An special type of negative resist is based on the enhancement of resist sensitivity by chemical amplification, this concept is based on acid catalyzed reactions. Chemically amplified resists consist of a matrix polymer (resin) and a polymeric binder that are mixed with a certain amount of a photoacid generator (PAG). PAG catalyzes the number of chemical events that cause polymer cross-linking, by means of an acid. Although the resist is modified as an effect of the beam delivery, the formation of the latent image takes place during PEB. PAG either activates the reaction for polymer cross-linking or could also be itself which reacts (7) (Figure 3.2).

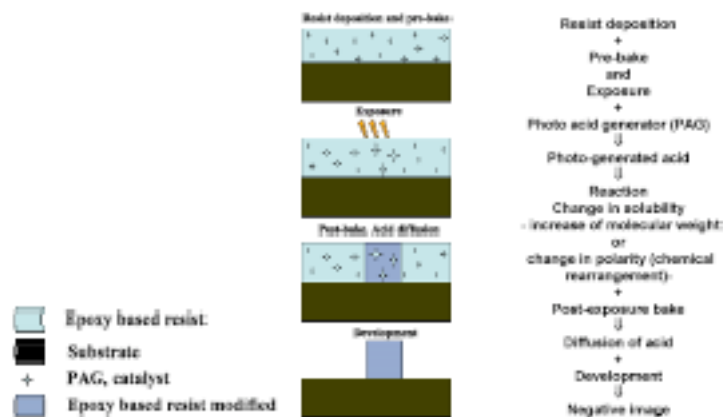


Figure 3.2 Complete sequence of photolithography on chemically amplified resists. Pre- and post exposure bake are critical steps of the process. PAG initiates the acid generation for the cross-linking reaction.

The reaction mechanism that induces the acid generation in lithography is reported to be different in the case of photolithography or EBL (8). There are two main processes that start the actual exposure reaction. Excitation channel acts either on the acid generator or the base polymer and it is attributed to describe photolithography exposure. In the case of electron beam irradiation, EBL, and also X-ray and EUV, ionization channel is the dominating process. PAG captures low energy electrons from resist ionization to produce counter anions of acids (9). The beam energy is extremely higher than resist ionization energy, so it is considered that protons used during crosslinking process are originated from base polymer ionization. The acid diffusion plays an important role in the latent image formation and depends on process conditions and structure of base polymer and acids.

More generally, the energies involved in both chain scission and crosslinking, i.e. those which are responsible of electron-chemical bond interaction, are much lower than the actual energies of the electron beam. Due to this the radiation chemistry involved is much more complicate than the analogous for photolithography.

An approach to study radiation chemistry that is independent of the mechanism is proposed in (10). It quantifies the irradiation induced events by the parameter G , defined as the scission, $G(s)$, or cross-linking, $G(x)$, efficiency of the radiation. In particular, it is defined as the number of chains broken or crosslinked that occur per 100 eV of absorbed energy, when the quantum efficiency is 1 (11). As a matter of fact, both scission and cross linking occur simultaneously, but, the predominant electron-induced reaction determines the tone of the resist material (12). For negative resists, a high $G(x)$ is encountered on certain chemical groups, as epoxy, vinyl or allyls. Positive resists are less efficient, hence, it is interesting to get resists with large $G(s)$ values in order to increase the sensitivity. Again, Charlesby (10) derived an expression where high molecular weights are related to high scission radiation values. With this method it is possible to evaluate the effect of the electron beam exposure in terms of the original and resulting molecular weight, beam energy, etc by molecular weight techniques, e.g. gel permeation chromatography, infrared spectroscopy, etc. Modification of the resist composition for achieving larger irradiation effect or comparison of cross-linking rates are contrasted, then, with the predicted behaviour (5). However, as another example, the work of E.Gipstein et al (6) on PMMA (13) concludes that the size of the molecular solvent is more important than the molecular weight of the resist in the solubility rate. The analytical description of the radiation chemistry has not been determined yet.

In addition to the events that effectively expose the resist, other effects may occur as a result of electron-substrate interaction. Charging, resist heating or etching could contribute importantly to the exposure process.

Charging occurs on insulating substrates when the absorbed charge from the beam cannot be dissipated. Pattern deformations occur as a result of beam deflections induced by the confined charge. A way to reduce its consequences relies on the exposure strategy, where smaller features and critical zones are firstly exposed and bigger areas and features are left to be irradiated at the end. Conductive pins are also used to discharge the resist, but one of the most common method is the deposition of a thin metal layer. The metal layer is stripped before development and, while avoiding charging effects, does not affect resist exposure (14).

Resist heating is inherent to the lithographic process and it may cause pattern distortion. For an incident beam energy of 20 keV on Si, about 85 % of beam power is

dissipated as heat in the substrate, whereas the rest is divided between forward or backscattered electrons in the resist and backscattered electrons from the resist surface (15). The increase of resist temperature has been reported as a function of increasing beam current density (16). As temperature rises, the resist sensitivity becomes higher and, thus, pattern distortion may appear. If dose corrections are not applied or glass transition temperature is reached, distorted exposure images are found. It is even possible that the crosslinking effect of high electron dose in PMMA (~ 10 times the clearing dose) is intimately related to heating effect.

Resist etching is often seen during imaging polymers with the SEM and, as thermal effects, it is irreversible (17). Electron beam may cause localized mass loss that can appear as areas, lines, holes, cracks or bubbles depending on the material and the exposure. Crystalline solid materials are less sensitive than amorphous. Direct sublimation can be used as a method of patterning and indeed extremely high resolution is achieved. However, some inconvenients limit their use: very low sensitivity, poor etching resistance, etc (18).

3.1.2 Resist processing

Along this chapter, two kinds of resists are studied in detail: positive tone PMMA (and its derivatives), which is the most widely used for EBL, and epoxy based resists, as negative tone chemically amplified polymers.

One of the outstanding characteristic of polymers is the possibility to dilute their molecules in different solvents. Hence, the preparation of resist layers is achieved simply by spin coating and the solution concentration can be adjusted to control the layer thickness. Most of the resists are compound of several materials and even they can be precisely modified for polymer performance enhancement.

The resist deposition process is slightly different for PMMA and epoxy based resists. PMMA is just spin coated and shortly softbaked in a hot plate, whereas negative resists softbake is more critical. The details for standard deposition of each kind of resist are found in Figure 3.3.

Methacrylic resist type	Spin speed (rpm)	Soft bake (time (s) / T(°C))	Thickness (nm)
950k MW	1500	60 / 180	100
495k MW	1500	60 / 180	100
35k MW	1500	60 / 180	350
MMA-MAA EL6	1000	60 / 150	325

Figure 3.3 Standard deposition conditions for different methacrylic resists and resulting thickness.

Another characteristic of polymers relies in the combination of deposited layers. Usually, single layers of thin thicknesses are used to achieve high resolution patterns, whereas multiple layers allow a great diversity of specific applications or improvement of post-lithography processes. The multiple layer configurations are based on the difference of sensitivity, concentration, etc that will determine, dose, resist thickness or development rate of each layer. Hence, double layers are often used to facilitate the lift off process, trilayers for T-gate transistors, etc.

Development process is, together with electron irradiation, a crucial part of resist lithography. Unlike electron scattering, development process is difficult to be theoretically predicted and only experimental expressions are determined (15). In general, development consists of the immersion of the sample in a solution for a certain time. The solution is formed by the real solvent of the resist and a resist-non solvent part. The ratio determines the solubility rate and it can be adjusted as needed. The ideal developer is the one that does not dissolve at all the part that has not been exposed (positive) or, contrarily, in the irradiated one (negative). In practice, different solubility rates are found for exposed/unexposed areas, so often thinner layers are more convenient to optimize development performance. Resist swelling may also occur for certain resists and developers, specially for long time developments or thick layers. The effect is often irreversible for pattern distortion and may even induce additional stresses when resist contracts. In consequence, loss of adhesion or shape deformations are found.

As presented, chemically amplified resists require PEB to activate the effect of electron irradiation. Then, time delay for development and controlled temperature ramps are established for an optimal resist performance. Its critical contribution to the final result makes the processing more complicate and restricts the use of this kind of resists. The table in Figure 3.4 summarises the deposition and development processes used for each specific case. More details are included in the section 3.4.

Negative resist	Spin speed (rpm)	Soft bake (time (min)/T(°C))	PEB (time (min)/T(°C))	Thickness (nm)	Developer
mr-EBL 6000.1 XP	2500	20 / ramp 65-95	20 / ramp 65-95	100	PGMEA
mr-L 5005 XP	3000	20 / ramp 65-95	20 / ramp 65-95	5000	PGMEA
ma-N 2401	3000	1 / 90	---	100	ma-D 532

Figure 3.4 Pre- and post-exposure processing for negative resists.

3.1.3 Modeling the effect of exposure

The mechanism and resolution of EBL is determined by chemical and physical effects. Radiation chemistry and development have been presented in the previous section (3.1). Physical phenomena include EBL system optics (Chapter 2) and electron scattering. Electron collisions are next described from a theoretical point of view.

Electron beam technology allows to obtain beam diameters below the nanometer range. However, in EBL such resolution is not experimentally obtained and that is not exclusively caused by resist limitations. Electrons are massive charged particles, which implies that electron-solid interactions have to be taken into account.

The studies of the effect of electron beam scattering when entering a solid substrate have been deeply developed to assess SEM imaging. The comprehension of the nature of collected signal (e.g. backscattered electrons) is not only basic for reconstructing the sampled image, but also helps to deduce sample surface information and to optimize the conditions for the acquisition of the image.

During EBL, the energetic electron beam suffers collisions when interacting with the resist and substrate atoms and molecules. Both elastic and inelastic processes occur, resulting in the creation of backward and forward scattered electrons, respectively. The energetic transfer in the resist mainly causes the resist exposure, whereas interaction with the substrate underneath is manifested as heating and origins more backscattered electrons.

Usually, elastic collisions are expressed in terms of the unscreened single electron scattering of Rutherford. It evaluates the process as a probability of interaction that strongly depends on the solid atomic number and the electron energy. The probability (Q) of elastic scattering for angles greater than a specific ϕ_0 can be expressed as,

$$Q(> \phi_0) = 1.62 \cdot 10^{-20} \left(\frac{Z^2}{E^2} \right) \cot^2 \left(\frac{\phi_0}{2} \right)$$

events $> \phi_0$ (3.2)

[units : electron(atom / cm²)]

where Q is called the cross section of elastic scattering, Z is the atomic number of the solid and E is the electron energy.

Inelastic collisions are the cause of the loss of electron energy and it is typically described by the Bethe's continuous slowing down model.

$$\frac{dE}{ds} \left(\frac{\text{keV}}{\text{cm}} \right) = -2\pi e^4 N_0 \frac{Z\rho}{AE_i} \ln \left(\frac{1.166E_i}{J} \right)$$

(3.3)

$$J(\text{keV}) = (9.76Z + 58.5Z^{-0.19}) \cdot 10^{-3}$$

where $2\pi e^4 = 1.304 \cdot 10^{-19}$ expressing E in keV, N_0 is Avogadro's number, ρ is the solid density (g/cm³), A is the atomic weight (g/mole), E_i is the electron energy (keV) and J is the average loss in energy per scattering event.

As a result, electron trajectories are mostly dependent of electron energy and the substrate composition. In the resist, forward scattering is the more probable process, i.e. main parameter is the energy, while the interaction with the substrate comes from backscattering, which is highly dependent on both charge energy and substrate nature. Thus, electron trajectories are typically distributed in a certain 3D interaction volume that reaches few microns in range for an incoming electron energy of 10-20 keV. The usual pearl shape of electron distribution in the resists can be easily explained from the low atomic number and density of the resists. High energy electrons initially are just slightly deviated from the incoming direction, since elastic contribution is weak ($\sim Z^2$), but once they are slow down, lateral scattering dominates ($1/E^2$) (Figure 3.5).

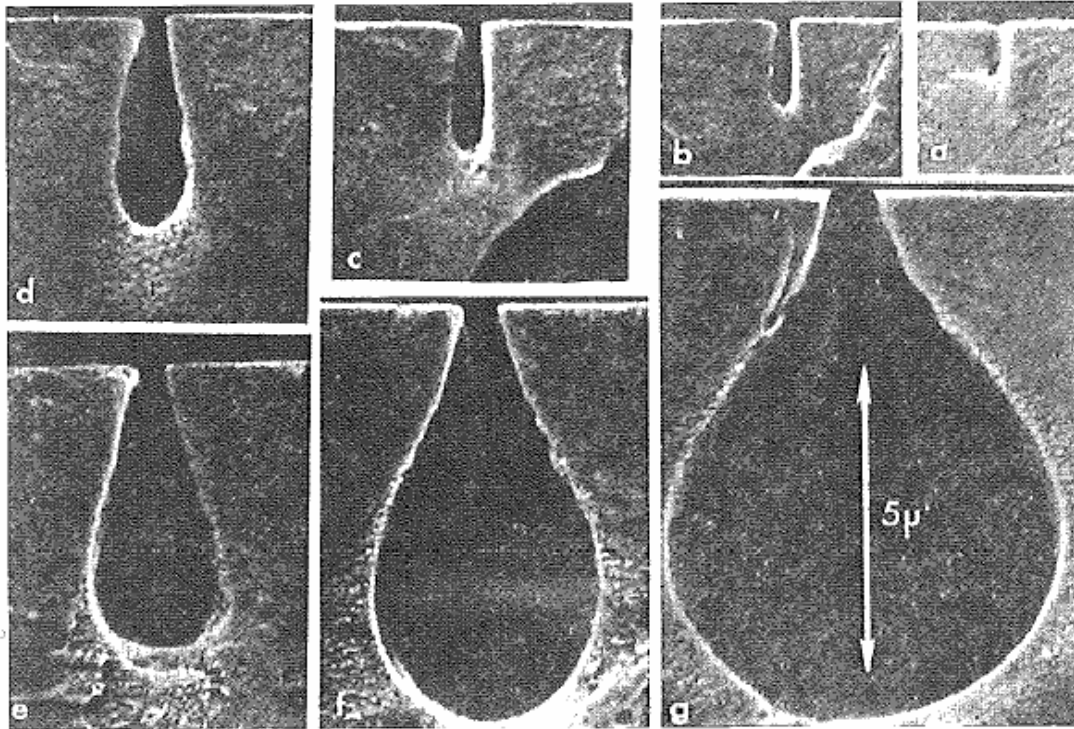


Figure 3.5 Experimental evidence of pearl-shape electron trajectories caused by electron-resist scattering. A 5 μm thick layer of PMMA is developed with increasing times from a to g, (17).

Electron trajectories simulator

The simulation of physical events based on theoretical considerations and the consequent contrasting with experimental results usually enables to establish the key parameters of the process performance (19).

Monte Carlo method is used to simulate a significant number of electron trajectories, but it does not explain the energy deposition process that describes the resist exposure nor the development rates. However, it may help to optimize the lithographic process by estimating the effect of proximity and predicting the maximum achievable resolution. In consequence, the number of experimental tests could be reduced, together with a better comprehension of the EBL process or corroboration of theoretical considerations.

Monte Carlo technique is a computing method that relies on random and probabilistic processes. Applied to the interaction of electrons with the solids it does not solve the scattering equations, instead it expresses the random nature of the electron scattering. Indeed, the collisions between electrons and atoms occur randomly and it is measured in terms of probability in the simulation. The direction after each scattering process and the electron range until the next collision event are also random, so probability is again applied for the numeric solution. Due to this, a good number of trajectories should be represented in order to reflect correctly the whole interaction process.

The simulation program that is used has been developed by Prof. Joan Bausells. Based on Monte Carlo method, it represents the cylindrically symmetric electron trajectories as a consequence of their interactions with the solid substrate in a 2D graphic (planar projection). For each electron with an incoming energy determined by the EBL system, electrons experience elastic collisions that change their direction and,

between two elastic events, are slow down and little deviated due to the inelastic interactions. These processes repeatedly occur until a certain threshold value of few eV is reached. Then, the cycle calculation starts for the next incoming electron. The program structure is based on (20).

In this program, the main difference from the usual computing method is the introduction of the Mott equation (21), instead of the classical Rutherford expression for the elastic collisions. When calculating the mean free path of electrons, this quantum relativistic model introduces a different equation that depends on electron energy and atomic number in the cross section function. This consideration is only important at low electron energies and for heavy elements.

The Rutherford cross section for elastic scattering is calculated using classical mechanics. Two charged particles are assumed, interacting through a Coulomb electrostatic potential. The original Rutherford calculation (3.2) used an unscreened potential, but electron trajectory simulators use a screened interaction, which accounts for the fact that the incident electron does not see all of the charge of the nucleus due to the cloud of electrons surrounding it. The screened total cross section is given by (20),

$$\sigma_R = 5.21 \times 10^{-21} \frac{Z^2}{E^2} \frac{\pi}{\alpha(1+\alpha)} \quad \text{cm}^2 / \text{atom} \quad (3.4)$$

with E in keV, where α is the screening parameter, defined as $\alpha = 3.4 \times 10^{-3} \frac{Z^{0.67}}{E}$.

The Rutherford cross section losses accuracy for high-atomic-number target elements ($Z > 30$) when the electrons have a low energy (< 10 - 20 keV). In this case the scattering angles are large, and the strong atomic potential accelerates the electron to very high velocities while it passes close to the nucleus. A correct scattering calculation must use relativistic quantum mechanics. Mott (22) used the Dirac equation to calculate the scattering of a fast electron by an (unscreened) atomic nucleus. The effect of the Dirac equation is to introduce corrections to the $1/r$ Coulomb potential: a relativistic $1/r^2$ term which is only important for heavy nuclei, and a spin term (roughly $1/r^3$) which is important for high electron velocities. The Mott scattering solution is given in the form of a partial-wave series expansion, which means that it has not an analytical formula and it has been normally used in a tabular form. However, Browning (23) calculated an approximate analytical equation by fitting the results for target materials between C and U and for energies between 1 and 100 keV, which has been used in our simulation software,

$$\sigma_M = 4.7 \times 10^{-18} \frac{Z^{1.33} + 0.032 Z^2}{(E + 0.0155 Z^{1.33} E^{0.5})(1 - 0.02 Z^{0.5} e^{-u^2})} \quad \text{cm}^2 \quad (3.5)$$

where $u = \log(8 E Z^{-1.33})$.

The program allows to select the values of the main variables involved in the process (Figure 3.6). For the beam, both acceleration voltage (>1 keV) and beam diameter are to be fixed. Concerning to the substrate, up to three different layers can be

modeled with specific thicknesses and for seven different elements or materials (Aluminum, PMMA, Silicon, Silicon Dioxide, Silicon Nitride, Gold and SU8, which are among the more usual for fabrication). Plotting options enable to determine the number of electrons to be simulated and even it is possible to visualize only the final electron position or not to generate of secondary electrons.

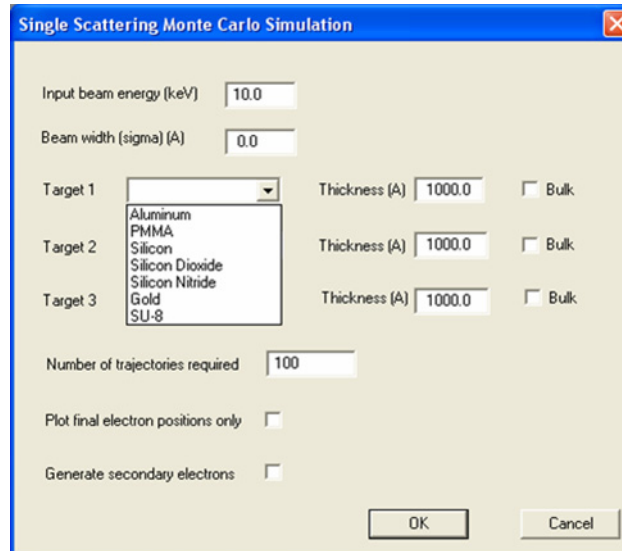


Figure 3.6 Simulation program interface for the electron-solid interaction. Variables for the Monte Carlo simulation of the electron trajectories.

The program is used in 3.2.2 and 3.2.3 to acquire an estimation of the EBL performance on resists for relevant configurations, which can later be compared with the experimental results (sections 3.3 and 3.4). Mainly, the effect of electron energy and substrate are evaluated in terms of interaction volume, backscattering and secondary electrons, paying attention to the electron range in depth and lateral dimension, number and range of backscattered electrons and number and distribution of generated secondary electrons.

The dependence of beam energy on the electron trajectories is clearly seen in Figure 3.7. Final electron positions are depicted as blue points, whereas red lines represent the generation of secondary electrons. The same number of electrons (100) are plotted for all the simulations at 3 or 10 keV electron. As can be observed, the interaction volume is directly related with the beam energy, so it is the total penetration depth and lateral distribution. The resulting charge distribution is, then, much more confined for the low energy and only a slight difference in the shape is encountered for the different interacting substrates, Si vs SiO₂, due to the relatively similar atomic number and calculated density ($\rho_{\text{Si}}=2.328\text{g/cm}^3$, $\rho_{\text{SiO}_2}=2.2\text{g/cm}^3$).

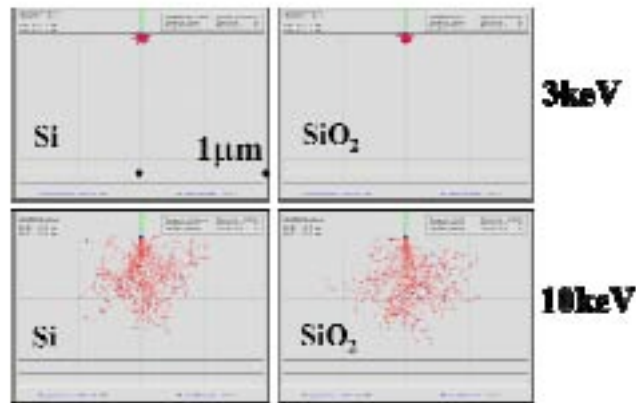


Figure 3.7 Simulator results for 3 and 10 keV on Si or SiO₂ bulk substrate. Beam energy strongly determines the electron stopping power. The electron penetration ranges are similar for Si and SiO₂, but lateral backscattering is slightly higher for Si.

Analyzing the substrate contribution to the electron-solid interactions, three behaviours are distinguished in Figure 3.8. For 10 keV beam energy on Si, SiO₂ and Al similar distributions are obtained, whereas higher atomic number elements had a higher stopping power that results in a large charge density. In the case of the resists, the effect of a lower material density allows a higher penetration depth and considerably lower number of backscattered electrons re-ejected from the surface.

Further consequences from the different substrates will be detailed in the next sections, but these phenomena are well known in SEM imaging. Coverage of samples with a thin gold layer is currently used to increase image contrast, since higher number of backscattered electrons can be, thus, collected. In addition, the use of low energies also increases the quantity of re-emerging electrons and mainly informs about the characteristics of the sample surface.

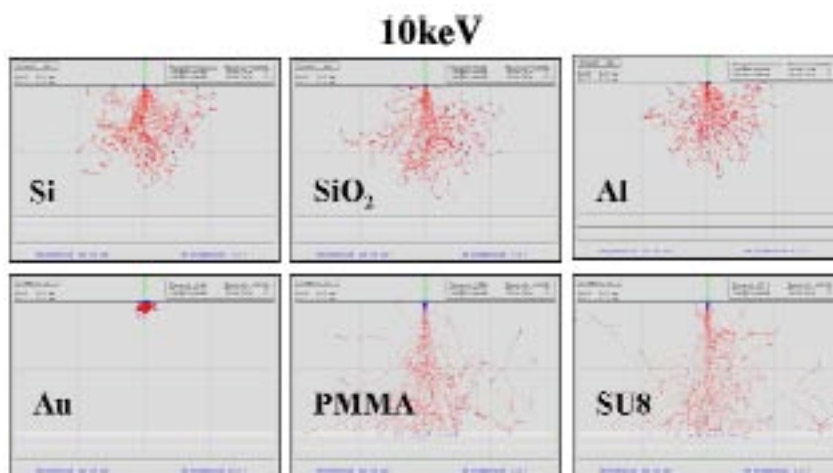


Figure 3.8 Effect of substrate on electron trajectories. For 10 keV, similar Z substrates lead to similar results (Si, SiO₂, Al), whereas high Z (Au) limits electron penetration and resists (low Z) have low stopping power.

From plotting options, the contribution of the energy loss by the creation of secondary electrons can be visualised in Figure 3.9. In the left and center image, blue lines delineate the electron trajectories. When secondary electrons are considered (in the center and right plots) the electron range is about 2 μm shorter for the beam entering in Si at 10 keV.

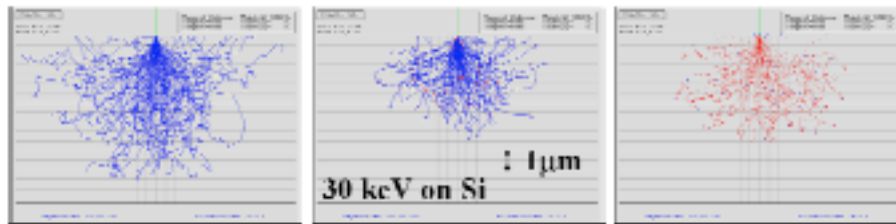


Figure 3.9 Plotting options for the simulator. 100 electron trajectories are depicted for a 30 keV electron beam energy on bulk Si substrate. (Left) Representation of primary electron trajectories. (Center) Representation of primary electron trajectories including the generation of secondary electrons. (Right) Representation of secondary electron trajectories and final electron position.

A rough idea of the contour distribution of charges for an area exposure by EBL can be extrapolated from the simulation of the process with different relatively wide beam diameter (incoming green lines). In the Figure 3.10, 10 keV beam energy is used to penetrate a 100 nm PMMA layer upon Si for two “beam widths” of 2 μm and 250 nm, respectively for bottom and top plots. In consequence, seems reasonable to infer how the high number of backscattered electrons that are accumulated in the sides may widen the original pattern sizes after development.

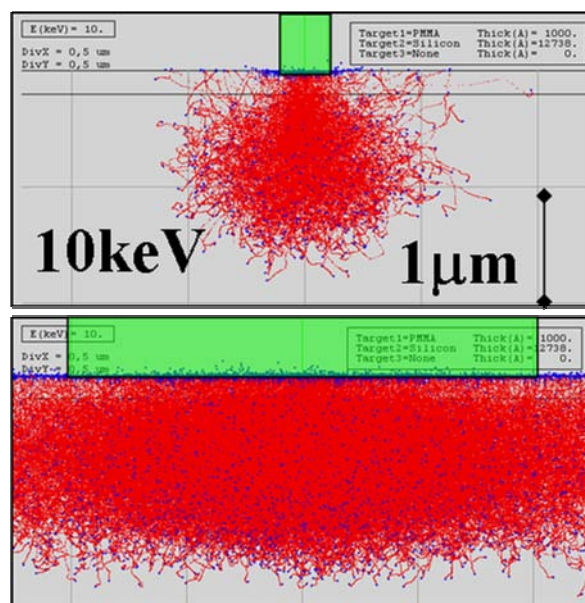


Figure 3.10 Simulations for 100 nm of PMMA on Si at 10 keV with different incident beam widths (green) : 250 nm (top) and 2 μm (bottom).

Similarly, when using different substrates underneath the resist, the contribution of a heavier element substrate causes a stronger design edge effect that will have implications on deposited energy and, hence, EBL result (Figure 3.11). Taking advantage of this, the recognition of marks for alignment is strongly benefited when using gold as the metal for the fabrication. But, also resist heating might be more important.

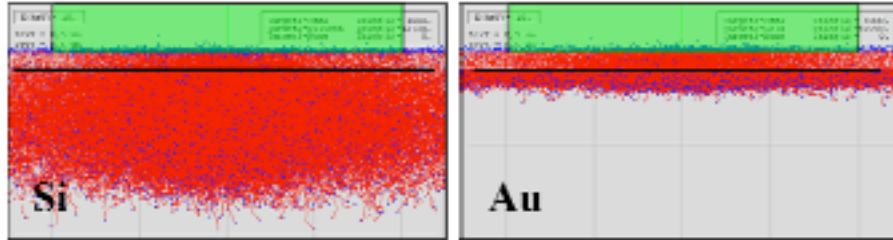


Figure 3.11 Simulations for 10 keV extended exposure (green) of 100 nm PMMA on Si (left) and Au (right). Substrate heating will be important for high Z substrates.

3.2 Poly(methyl methacrylate). A positive resist

General description

Poly(methyl methacrylate) (PMMA) was the first polymer tested as a resist for EBL (24) and still continues to be the most widely used. It performs as a positive tone resist under EBL, X-rays and Deep UV radiation. The exposure induces the scission of the chain of methacrylic monomers that constitute the resist material (25). It is generally accepted that the main process consist of the break of the main chain, but other scission possibilities may also occur (Figure 3.12).

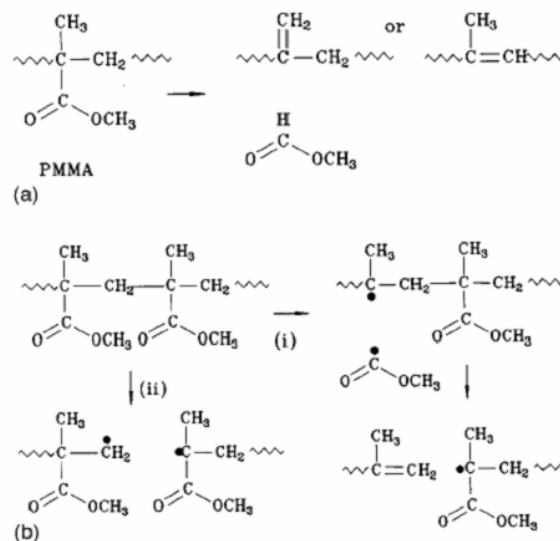


Figure 3.12 Schematic diagrams for the generic reaction paths caused by EBL on PMMA, from (11).

Used as a resist for EBL, PMMA demonstrates good properties that make it a convenient choice for a great number of applications. It is particularly suitable for defining very small features due to its high resolution (less than 20 nm) (Figure 3.13) and shows minimal swelling during wet development. Different from other polymers, wettability on, for example, methyl isobutyl ketone (MIBK), methyl ethyl ketone and chloroform is controlled by the mixture with a weaker developer. In particular, MIBK mixed with isopropanol (IPA) in 1:3 ratio shows low sensitivity, but high contrast, whereas 1:1 ratio enhances sensitivity (lower doses are needed) without a significant loss of contrast. The improvement of its medium-low sensitivity has been tested with the introduction of substituents, copolymers and terpolymers. They should increase the scission radiation efficiency $G(s)$ with no effect on $G(x)$ (26). However, it often implies a substantial loss of resolution. Terpolymers are also proposed to increase thermal stability and, hence, also optimize the etch resistance. Glass transition temperature is moderate, 114 °C. PMMA can be used as a mask for acid, base and ion etching, but its performance in plasma is poorer compared to novolac-based resists, the photoresists. Also, it is not a good mask for dry etching, since selectivity to silicon oxide/nitride is around 1:1 (27).

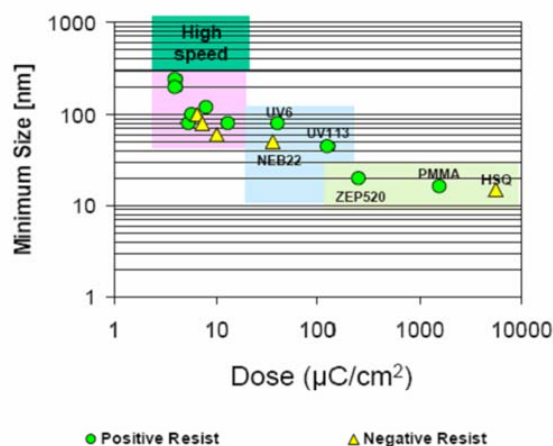


Figure 3.13 Comparison of performance for different positive and negative electron beam resists (25) exposed at 100 keV. Representation of sensitivity in function of resolution. PMMA has high resolution, but requires higher doses than ZEP520.

In Figure 3.13, PMMA is compared to other existing resists in function of dose and resolution. As can be seen, fast resists (low clearing dose) present low resolution, whereas the highest resolution tends to medium-low sensitivity.

As mentioned, the EB system optics, which determines the final beam width, is not the single factor that limits the resolution of the EBL technique. It should be more correct to attribute it to the exposure event combined with the resist characteristics. For PMMA, the range of electrons at energies in the exposure range are found to be between 4 and 20 nm (Figure 3.14). Therefore, even if the chain resist could sustain it breaking in smaller chain scission products, the effect of very low energy electrons leads to think that further resolution than few nanometers is not feasible.

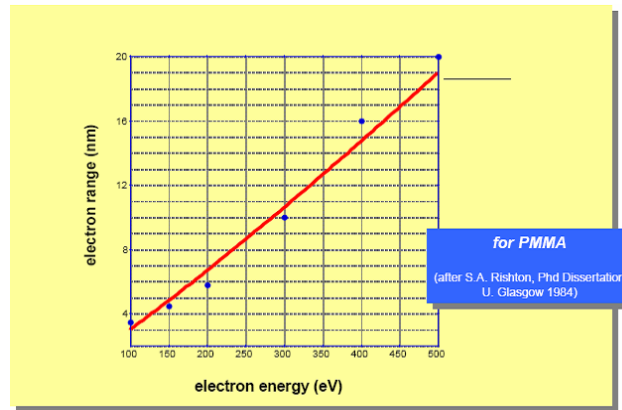


Figure 3.14 Electron range at resist exposure energies, 100-500 eV, is 4 to 20 nm. Hence, the controllable resolution of PMMA will not exceed these values (28).

PMMA is commercialised in solution to be deposited as thin layers (down to 100 nm) by spin coating. Casting solvents are chlorobenzene or (safer) anisole and the control of the deposited thickness layer is achieved by the solution viscosity and the spin speed. There are different types of PMMA depending on the average weight of the molecular chains. The most used are 950k MW and 495k MW, but others exist, specially used for imprinting, e.g. PMMA 50k or 35k MW. It is considered that resolution scales proportionally with molecular weight, so higher molecular weights will allow higher resolution. This is due to the smaller size of the chain scission products in high MW polymers and, in consequence, higher resolution in the resist removal after development. On the other hand, sensitivity, and contrast, is inversely proportional to the molecular weight. This is attributed to a lower solubility in the developer for increasing relative molecular mass.

In the next sections, some of these reported properties or theoretical considerations will be tested experimentally, in order to establish the current EBL system and methodology performance and to evaluate the precision of theoretical and fundamental approximations.

3.2.1 Simulations on PMMA

Once seen the general performance of the simulator in section 3.1.2, some simulation examples on the PMMA can be studied. As mentioned, PMMA is the most widely used resist for EBL and typical thicknesses are in the submicron range. In figure 3.15, a 100 nm thick layer of PMMA on a Si substrate is irradiated at 3, 10 and 20 keV beam energy.

The effect of the thin resist layer does not modify significantly the dependence of the interaction volume on beam energy (Figure 3.15). At 3 keV, electrons only can shortly penetrate in the Si material, meanwhile, at 20 keV, they even reach $\sim 2.5 \mu\text{m}$ depth in the Si substrate. The probability of electron-resist interaction is not only higher for lower energy electrons, but, also, will lose their energy more rapidly. As a result, knowing that resist exposure occurs at few eV, it is easy to infer the dose scaling in clearing dose in function of the energy and the loss of minimum line width resolution for lower energies.

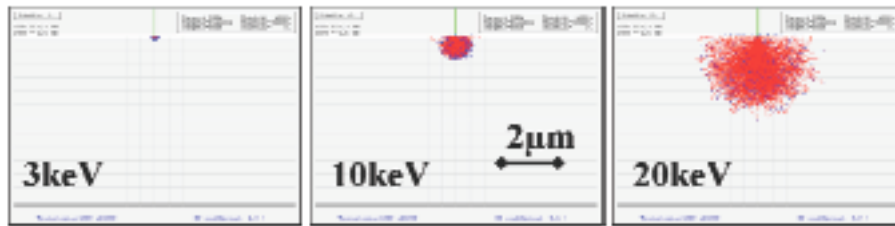


Figure 3.15 Effect of beam energy for exposure of 100 nm of PMMA on bulk Si.

Regarding the contribution of the substrates on the electron trajectories and its consequences in the backscattered charges and generation of secondary electrons, some examples are shown in figure 3.16. On left, the 20 keV electron beam is similarly spread for Si and SiO₂ (300 nm thickness on Si), but shows a strong confinement for the 300 nm thick layer of Au. More secondary electrons on the resist should induce a lower clearing dose. However it is possible that this advantage in terms of resist efficiency will also limit the minimum achievable feature size.

On the right side of figure 3.16, EBL on PMMA are modeled for some usual multilayer configurations. The contribution of a thin layer between PMMA and Si diminishes the quantity of backscattered electron that re-enter the resist matrix. In the case of 35 nm Au layer (3rd plot), the lateral range in Si at this energy is not modified, while the accumulation of charge in the resist in the beam axis, seen in the left side figure, disappears. For SiO₂, even seems that backscattering contribution can be avoided or minimized with the use of a thickness determined insulating layer.

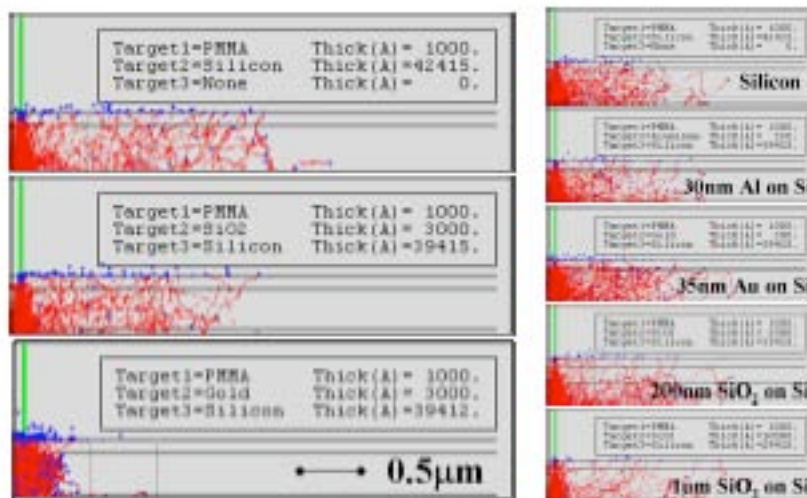


Figure 3.16 Simulations of 20 keV exposure on different multilayer substrate systems. The layer between (100 nm thick) PMMA and bulk Si diminishes the lateral spread of the electron trajectories.

For thicker PMMA layers (1 µm) on Si, the effect of forward scattering on the electron trajectories arises. Hence, a similar result to the one shown in Figure 3.5 (d, e) should be expected (Figure 3.17). This performance may be interesting for some applications where high undercut is desired after development. On the other hand, the

increase of required dose (and beam energy) to fully exposure the resist layer, together with real difficulties to obtain dense patterns may dissuade to experiment with it.

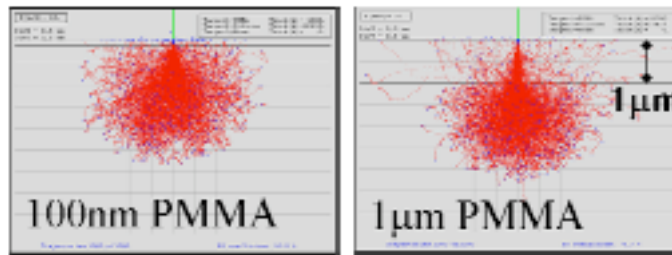


Figure 3.17 Simulation of electron trajectories for different PMMA layer thicknesses at 20 keV. Thin layer of 100 nm (left) does not account for forward scattering within the resist, whereas thicker layer shows a significant beam spreading (right).

A complete overview of electron trajectories in terms of beam energy and substrate materials can help to predict some EBL phenomena, although current simulations do not inform about the final result. It is not easy to infer similar conclusions in terms of expected resolution. If few trajectories are represented repeatedly on different substrates (Figure 3.18, left), results may be very variable and, thus, not reliable (e.g. Si, Al), but certain tendency to wider results is seen for Au (heavier substrates). Similar to this, the contribution of beam width is not conclusive. In the Figure 3.18, right, the electron trajectories for “0”, 10 and 50 nm width beams do not seem to differ importantly, so neither resolution would be expected to change. However, this inference is completely against the general consideration of beam focus and diameter contribution to obtain fine patterns.

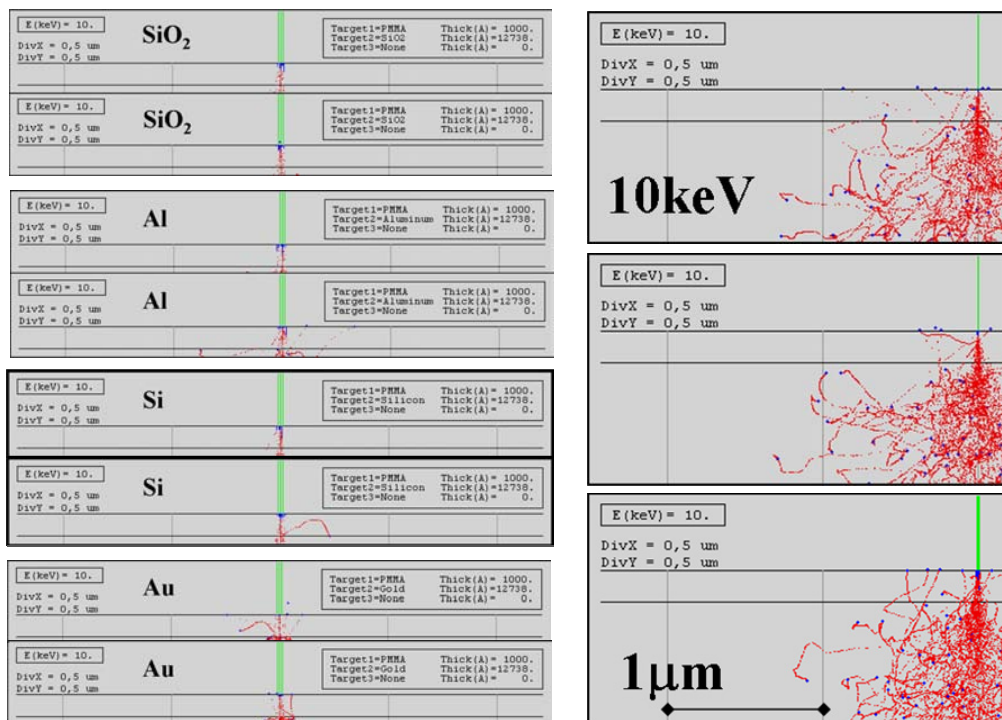


Figure 3.18 Simulations of electron trajectories at 10 keV on 100 nm PMMA for different substrates (left) and beam widths (right). It is difficult to predict results in terms of resolution.

It is often said that a thin layer of conductive metal can be used to avoid charging effects on thick insulating materials. However, as can be seen in Figure 3.19, the use of a 30 nm thick layer of Au on PMMA does not seem to allow high resolution results, due to the resulting high beam spreading and, at least, higher energies (>10 keV) should be used to minimize this effect or thinner metal layers.



Figure 3.19 At 10 keV beam energy on 1µm thick PMMA, the inclusion of a 30 nm Au layer on the resist to avoid charging causes higher beam spread. Thinner metal layer and higher beam energies will improve the resolution.

3.2.2 Exposure results in PMMA

A set of irradiation tests is performed on different substrates and PMMA types under a variety of exposure conditions. A dose test design (Figure 3.20) is common for all the cases, but the specific dose value for each feature is modulated by the selected exposure dose (D_0) in the lithography control window (see details about effective exposure dose in Chapter 2). The pattern consists of an array of $5 \times 5 \mu\text{m}^2$ squares that are scaled by the design internal dose factor, from 1 to 10 in steps of 0.5. The same development process is used throughout this work: 30 s of immersion in MIBK:IPA (1:3), 30 s rinse in IPA and drying with N_2 .

In Figure 3.24, the results of the dose test on PMMA 495k MW (standard deposition, 1500 rpm) are shown. Exposures are performed at 3, 10 and 20 keV beam energy and the decrease of resist sensitivity with increasing beam energy is corroborated.

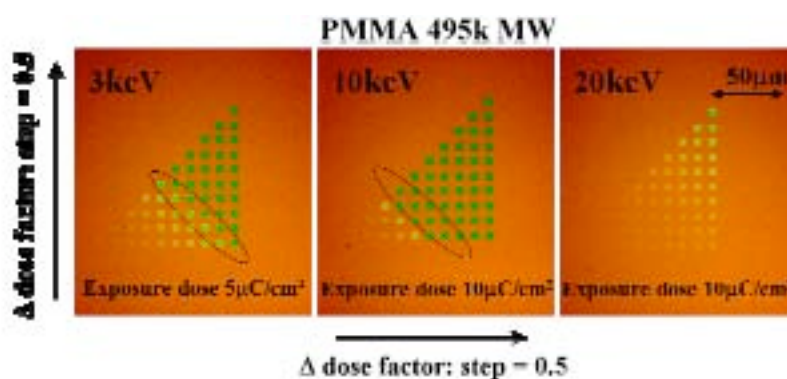


Figure 3.20 Results for dose test design on 100nm of PMMA 495k MW on Si at different beam energies.

The delivered dose in each feature is determined by multiplying dose factor and exposure dose (D_0) (variable of exposure window parameter, chapter 2). Dose factor range is 1-10. Image contrast has been enhanced to explain the pattern design and clearing dose determination from optical images.

Comparison between the two higher resolution PMMAs is also established for these three beam energies on Si. For PMMA 950k, clearing dose determined from optical inspection is about 20, 50-60 and 100 $\mu\text{C}/\text{cm}^2$ for 3, 10 and 20 keV, respectively. The results almost coincide with the ones of PMMA 495k (17.5, 40, >100 $\mu\text{C}/\text{cm}^2$) (Figure 3.21).

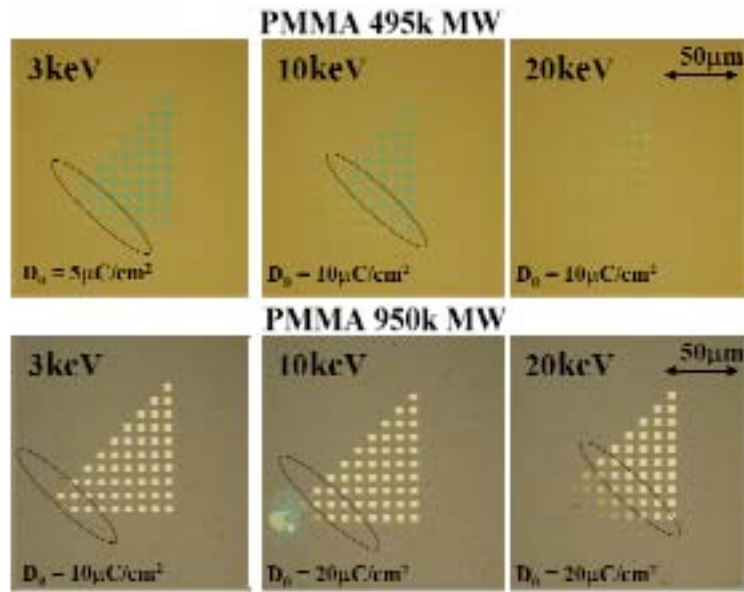


Figure 3.21 Sensitivity comparison of 495k and 950k PMMA for 100 nm thick resist on Si and different beam energies. Clearing dose results are similar for both resists and almost linear with beam energy.

The dose dependence with the substrate material underneath the resist film is summarized in Figure 3.22. As an example, standard deposition of PMMA 950k on four different substrates is shown: bulk Si, 200 nm layer of SiO_2 on Si, (100+180) nm of ($\text{SiO}_2 + \text{Si}_2\text{N}_3$) (here, termed as SiON) on Si and a 30 nm layer of Au on Si. Clearing dose at 20 keV beam energy, optically determined, is respectively 100, 110, 120 and 100 $\mu\text{C}/\text{cm}^2$ (Figure 3.22).

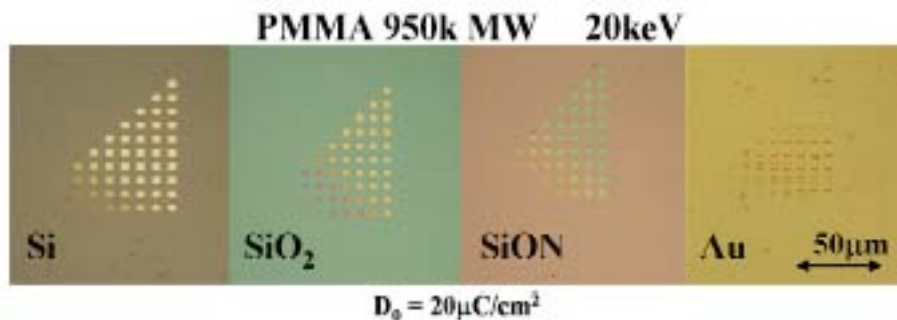


Figure 3.22 Dose test exposure at 20 keV on different substrates for ~100nm of 950k PMMA. Clearing doses do not depend significantly for these substrates.

In fact, the observed little differences can not be directly compared since resulting deposited layer thickness is not the same. For bulk Si, it is a 100 nm thickness layer, whereas on SiO₂, SiON and Au, they are 140, 130 and 130 nm, respectively. It is possible that dose variations also account for this. Perhaps thickness difference is due to a better adhesion of PMMA to these substrates, caused by certain surface porosity, microroughness, etc.

The optical dose determination is not the more accurate method, even if qualitatively is valid to evaluate and compare resist performance. As can be seen in Figure 3.23, AFM characterization at the locations where clearing dose is attributed to be complete (100 $\mu\text{C}/\text{cm}^2$) shows that some residual resist still remains at the center and specially in the edges for 950k on Si at 20 keV (Figure 3.23, bottom). Since about double of this value complete development is not achieved (Figure 3.23, top). Precise topographic imaging suggests a spatial non uniform dose deposition, being lower the dose absorption at the square edges.

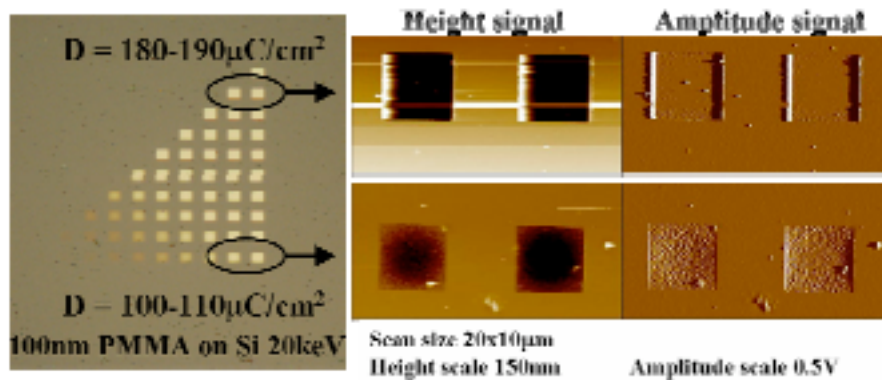


Figure 3.23 (Left) Optical images do not resolve the nonuniformities or very thin residuals after resist development. (Right) For accurate results AFM inspection is needed.

The effect of surface material on resolution can not be unambiguously determined from the AFM images of PMMA 950k exposure at 10 keV, neither for Si or Au (Figure 3.24). Au layer on the Si substrate induces sharper edges, that is eventually be explained from the limited lateral confinement of electrons, observed in the electron scattering simulations. However, for the same exposure dose a better cleared pattern is found in Au covered surface (higher sensitivity), which may be coherent with the last statement. It would be interesting to determine the sign of resist slope in the developed profile to understand more precisely the exposure mechanisms and determine the influence of heavier substrates. At 20 keV, slightly higher sensitivity is found, but higher beam energy does not seem to lead to sharper edges. As a matter of fact, at this electron energy for this Au layer thickness, the effect of backscattered electrons is not so constraint, so it seems reasonable than the behaviour seen for 10 keV is not repeated at 20 keV. Contrast can be determined from the plot of remaining thickness in function of delivered dose, $\gamma = (4.5, 4)$ (Figure 3.24, right).

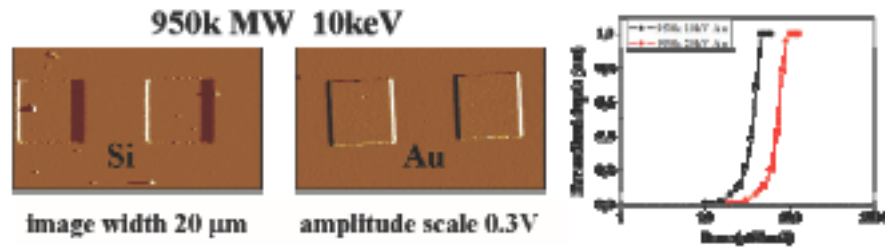


Figure 3.24 (Left) AFM images (amplitude signal) for 10 keV on PMMA comparing Si and Au substrates. Edge definition seems better for the Au substrate. (Right) Contrast curves for 10 and 20 keV beam energy on Au substrate. Contrast is about 4.5.

Lower molecular weights are usually supplied to achieve thicker resists films. With the standard deposition, at 1500 rpm, PMMA 35k on Si film is 325 nm thick. Comparison of sensitivity with the high MW PMMA is done depositing three layers of both 950k and 495k, resulting in 400 and 350 nm, respectively. As it is shown in Figure 3.25, exposure at 20 keV beam energy highlights the increase of resist sensitivity for lower MW. About $45 \mu\text{C}/\text{cm}^2$ is enough dose for PMMA 35k, while $135 \mu\text{C}/\text{cm}^2$ is needed for 950k and 495k. In addition, the dependence of clearing dose with resist thickness is manifest, since it was about $100 \mu\text{C}/\text{cm}^2$ for the 100 nm films of 950k and 495k PMMA. Another interesting behaviour is obviously remarked. As a consequence of resist thickness, the inhomogeneous dose deposition is clearly seen yet from the optical images and much more important for high MW (Figure 3.25, left and center). A high shape distortion of the pattern, intraproximity effect, is seen. This specific behaviour will be treated more in detail in section 3.5. In consequence, thicker resists require higher exposure doses and magnify proximity effect and lower MW are exposed at lower doses to the detriment of resolution.

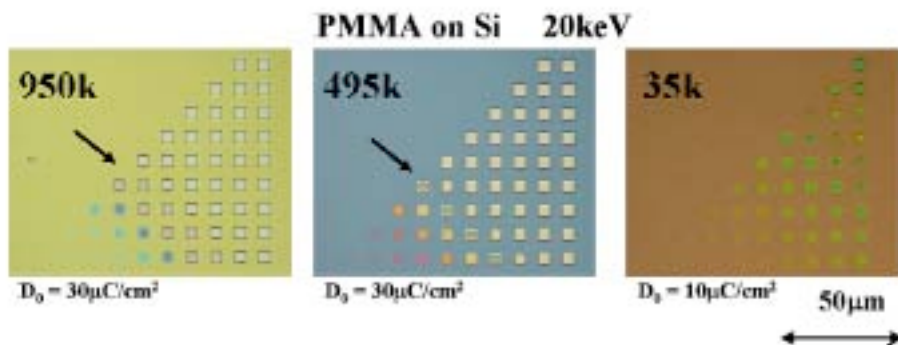


Figure 3.25 Comparison of sensitivity at 20 keV for different types of PMMA and layer thicknesses between 300-400 nm. Clearing dose is significantly lower for low MW resist (35k MW). Intraproximity effect arises (arrows).

For the same thick layers, but at lower beam energy, 10 keV, the non uniform electron dose deposition is not so important. Both, the change of clearing dose with the

resist thickness and the feature shape are less thickness dependent (Figure 3.26). For PMMA 495k, dose shifts from 55 to 90 $\mu\text{C}/\text{cm}^2$ when layer varies from 100 nm to 350 nm and the interproximity effect, although present, respects more the squared shape of the pattern. It can be explained from the results of the electron trajectories simulations, in the previous section, where charge confinement is shown to strongly depend on beam energy.

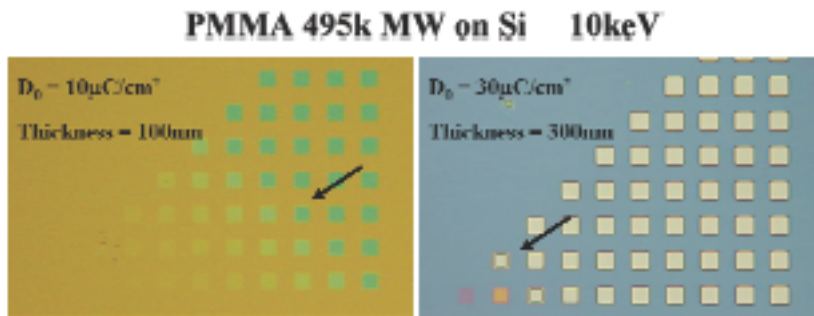


Figure 3.26 Dose test on 100 nm (left) and 300 nm (right) thick PMMA 495k on Si at 10 keV. Clearing dose and interproximity effect are slightly higher for the thicker layer.

In the case of thick layer exposure at lower energy (3 keV), this proximity effect behaviour is not found at all, but other interesting questions are observed. The lower definition of pattern edges is clear in Figure 3.27, both at low and high exposure doses, which confirms the tendency of using higher beam energies in order to reduce beam-resist interaction (forward scattering) and, thus, to enhance feature resolution. Also the colour of developed areas does not reach a uniform tone that suggests the complete development is reached, as seen in 3.21, left, or 3.25 left and center. From scattering simulations, it is shown (Figure 3.15) that electrons are not supposed to be able to penetrate 400 nm depth in the PMMA. Certainly, it is not a matter of dose, where in Figure 3.27, left, dose should be large enough to fully expose the resist, but it should be explained from the limited penetration range of 3 keV electrons. However, the delivery of very high doses gives rise to a non linear behaviour (Figure 3.27, right).

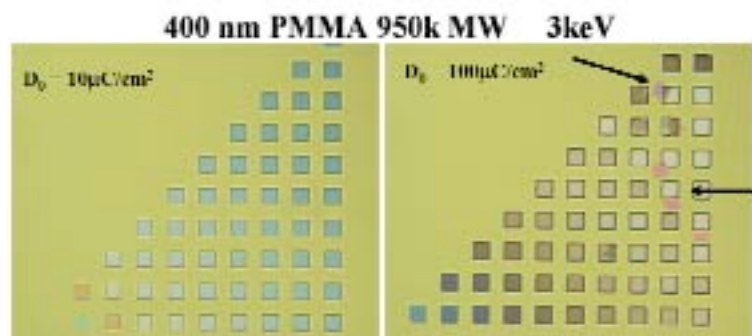


Figure 3.27 Low energy (3 keV) exposure of thick resist layer (400 nm) might not fully expose the whole resist thickness due to limited electron penetration range. Non linear behaviour is found at very high delivered doses.

This unusual behaviour can be explained by AFM imaging. In Figure 3.28, it is shown that it consists of the peel off of part of the PMMA layer in some selected sites. Squared shapes are not only not fully developed, but they are detached from the rest of resist layer and a thickness of 80 nm is measured (Figure 3.28, bottom). As mentioned, PMMA performs as a negative resist when it is irradiated with about 10 times the clearing dose. Therefore, this may be the cause of these results. Since it does not reach the 400 nm thickness measured, limited electron range seems reinforced and crosslinking may be consequence of the resist heating effect.

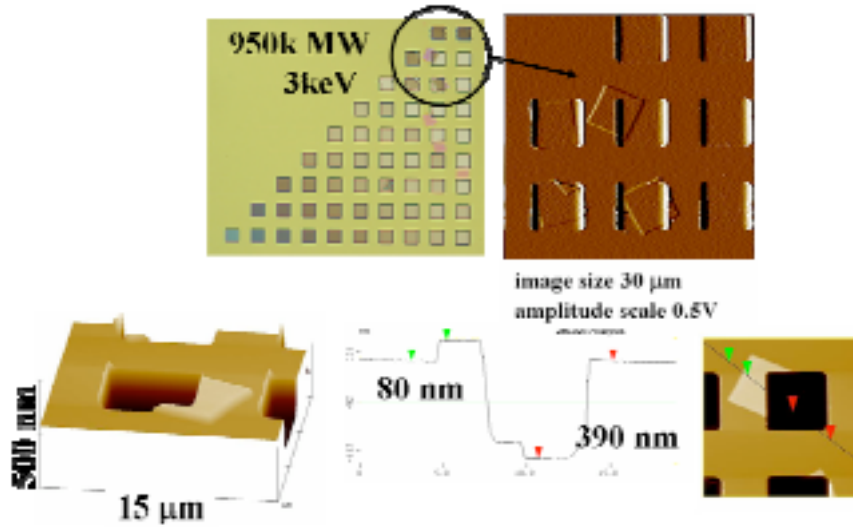


Figure 3.28 Non linear behaviour in thick PMMA layer at low beam energy (3 keV) is attributed to cross-linking phenomena caused by very high exposure doses and heating effect. AFM images confirm this supposition.

The following table resumes dose sensitivities obtained in the experiments presented above on Si substrate, by optical image determination.

PMMA MW	Beam energy (keV)	Dose ($\mu\text{C}/\text{cm}^2$)	Thickness (nm)
950 k	3	25 / ---	100 / 400
	10	55 / 85	
	20	100 / 180	
495 k	3	20 / ---	100 / 350
	10	40 / 90	
	20	105 / 200	
35 k	3	---	350
	10	50	
	20	100	

3.2.3 Methacrylic resists

Copolymer resists is the term used to refer to the resists that are formed by a mixture of several polymers. The mixture of methyl methacrylate with methacrylic acid (MMA-MAA) is intended to significantly improve the throughput of EBL technique by means of resist sensitivity. MMA-MAA is reported to have clearing doses one order of magnitude below PMMA: dose of PMMA is $50\text{-}100\ \mu\text{C}/\text{cm}^2$, whereas for P(MMA-MAA) is $2\text{-}10\ \mu\text{C}/\text{cm}^2$ (26). Like PMMA, they are commercialised in different viscosities, which enables to deposit from $100\ \text{nm}$ to $1\ \mu\text{m}$ thick films. In this case, the solvent is ethyl lactate. Both the vendor-supplied and the experimental spin curves are included in Figure 3.29 and relative agreement for the copolymer thickness (MMA-MAA EL6) on Si is found.

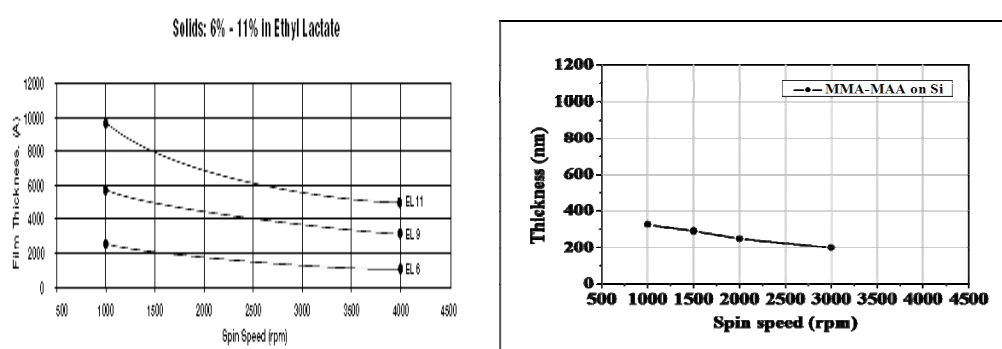


Figure 3.29 Comparison of tabulated (left) and experimental (right) spin curves for copolymer (MMA-MAA EL6).

The clearing dose determination is again studied with the design described in 3.2.2, for 10 and 20 keV beam energy. Clearing dose dependence with the beam energy coincides with the expected behaviour, for lower beam energy, lower delivered doses are needed to completely develop the total resist thickness (Figure 3.30). At 10 and 20 keV for a layer of $325\ \text{nm}$ thick on Si, required doses are, respectively, 35 and $75\ \mu\text{C}/\text{cm}^2$, which also confirms the increase of copolymer sensitivity with respect to high MW PMMA. In addition, resist sensitivity with film thickness (Figure 3.30, right) and feature inhomogeneities at higher beam energies are also equivalent to the performance of PMMA (Figure 3.30, left).

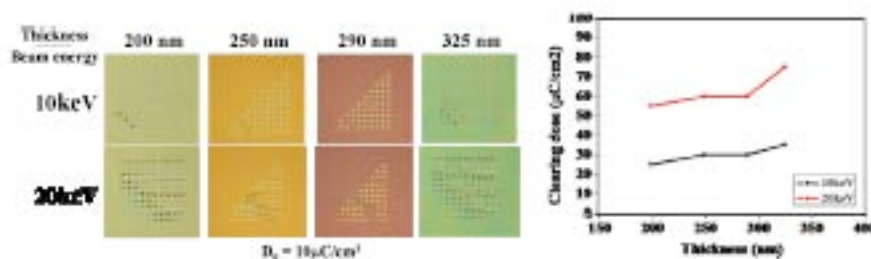


Figure 3.30 Clearing dose determination for copolymer films of different layer thicknesses at 10 and 20 keV. Sensitivity is higher than high MW PMMA and slightly depends on layer thickness.

A thicker layer (650 nm) of MMA-MMA EL9 (9% in Ethyl Lactate) on Si is exposed to 10 keV beam energy (Figure 3.31, left). AFM characterization is used to measure the resist thickness for the different doses that are plotted on Figure 3.31, right. As a result, copolymer contrast is about 3.3, thus lower than the one of PMMA. Again, resist sensitivity decreases with the increase of resist thickness.

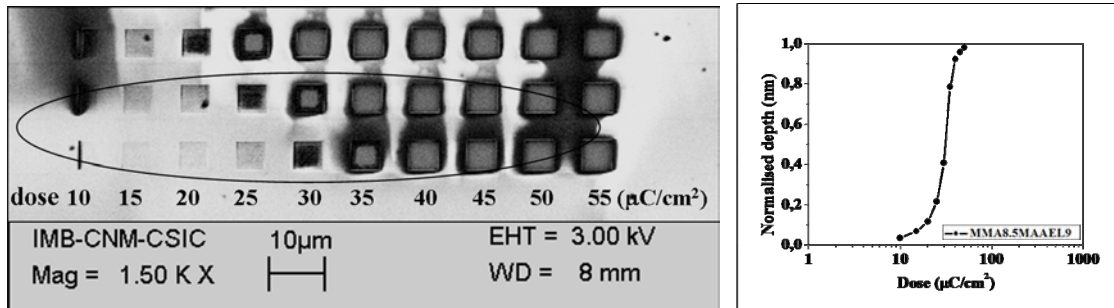


Figure 3.31 For thicker layer of copolymer (650nm) at 10 keV clearing dose increases to $\sim 40 \mu\text{C}/\text{cm}^2$. Contrast is lower than high MW PMMA.

The main use of MMA-MAA is to facilitate the resist lift off process by means of undercut and thicker resist layer, without the necessity of dose increase. As an example, in figure 3.32, left, the chess-like pattern irradiated with doses in the range of clearing dose needed for high MW PMMA result in overexposed patterns and bridging features. The undercut profile seems, hence, confirmed. Similar conclusion is obtained from the dose design exposure at 20 keV. At this beam energy, intrashape inhomogeneities where more important than lower energies in high MW PMMA. Although in this case the resist layer is even thicker (650 nm) the non uniform development is lower, which may be in agreement with an undercut tendency of MMA-MAA profile (Figure 3.32, right).

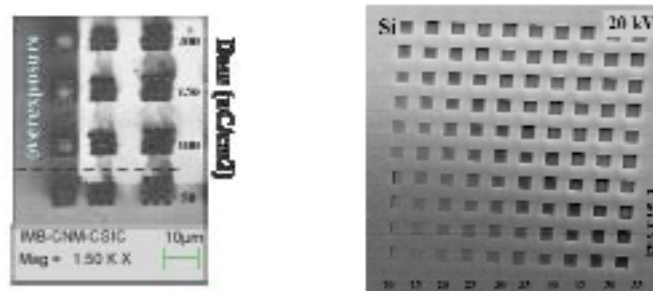


Figure 3.32 Copolymer is often used to facilitate lift off process. Specially, undercut is seen in the left image when overexposure causes the disappearance of central chess-like structure.

The electron penetration depth at 3 keV can be measured from the thick resist films. For the copolymer a higher electron range is found, 310 nm, whereas on PMMA 495k it reached 285 nm (Figure 3.33). It may be directly related with the dose sensitivity and resist composition of lighter and more porous resist materials. On the other hand, the quantitative depth value does not precisely agree with the calculations of electron trajectories, that predicted significantly shorter ranges ($< 200 \text{ nm}$, for PMMA).

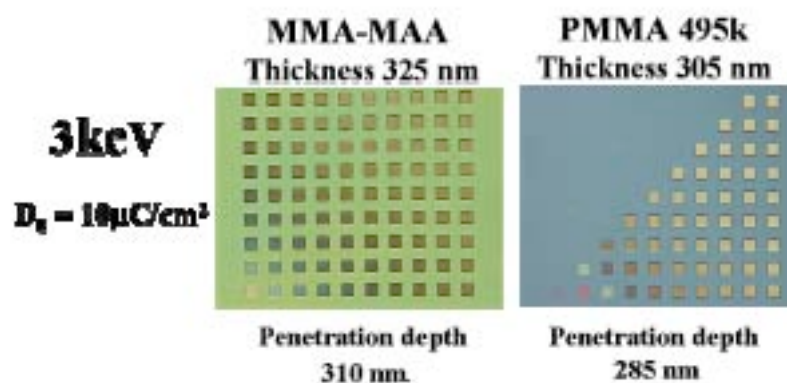


Figure 3.33 Electron penetration range at low beam energy (3 keV) can be experimentally determined on thick resists. For the copolymer, the resist depth that has been developed is higher, as it corresponds to lighter and bigger chain scission products after exposure.

3.3 Epoxy based resists. Negative resists

SU8 is a chemically amplified negative resist that is widely used for the fabrication of microstructures (29). It was developed by IBM to fulfill the necessity of a resist that exhibited both high resolution and high aspect ratios for thick resist layers. The composition is derived from the EPON[®] SU8 resin with the addition of an organic solvent and some onium salts that act as the initiator of the exposure process. Proper exposure dose over the initiator generates a strong acid that facilitates polymerization during PEB. Cationic polymerization leads to the intermolecular cross-linking that produces negative tone structures after development. The cross-linking promoter is sensitive to near UV, but can also be patterned by electron beam and x-rays. SU8 layers can be deposited by spin coating for thicknesses up to 500 μm , which combined with their sensitivity and good thermal and mechanical properties make it ideal for applications in microfluidics, micromechanics or bioscience. Its low MW (~ 7000) causes a high tendency to crosslinking, avoiding swelling, produces high contrast curves and presents high solubility in non exposed areas. After development, it shows excellent adhesion to the substrate and it is chemically very inert and stable with temperature ($T_g = 200 \text{ }^\circ\text{C}$), therefore plasma etching could be used for pattern transfer (27).

However, the use of EBL on SU8 encounters, again, the main limitation from the massive nature of electrons. Electron penetration depth is highly dependent on the incident beam energy and forward scattering across the resist thickness may involve a large beam spreading. In consequence, EBL is not optimal to pattern thick layers with the submicron lateral resolution that characterises EBL performance. The examples found in the literature that apply EBL for patterning SU8 use high beam energies (30) and, even, tend to reduce layer thickness in order to achieve higher resolution (sub-100nm resolution) (31,32).

In the following sections, the performance of EBL on different epoxy based resists is analysed. All the used resists are provided from Microresist within the Novopoly project (33), devoted to the development of novel functional polymer materials and their application for MEMS and NEMS. First, electron beam performance is simulated using the well established SU8 characteristics (density, molecular weight) to

compare with the experimental results on epoxy based negative resists. Then, from the results in thick layers (few microns), many typical phenomena of e-beam interaction with resists become visible. The characteristics and limitations of patterned features, whether in combination with UV exposure or only EBL, are shown. Optimization of EBL performance on epoxy based negative resists is intended on thin layers of a new resist, mr-EBL-6000.1 XP. Characterization of the resist properties under different conditions is examined, before its commercialization. Comparison with existing high resolution negative resists for EBL is also established and performance for their combination with other fabrication methods is determined. Hence, potential applications are suggested or tested.

3.3.1 Simulations on SU8

First, to evaluate expected SU8 performance for thick layers, as presented in Figure 3.34. Similar to PMMA, the pearl shape contour arises when increasing the beam energy, together with a deeper penetration depth. Then, a minimum energy that is required to reach the substrate surface has to be selected for each layer thickness.

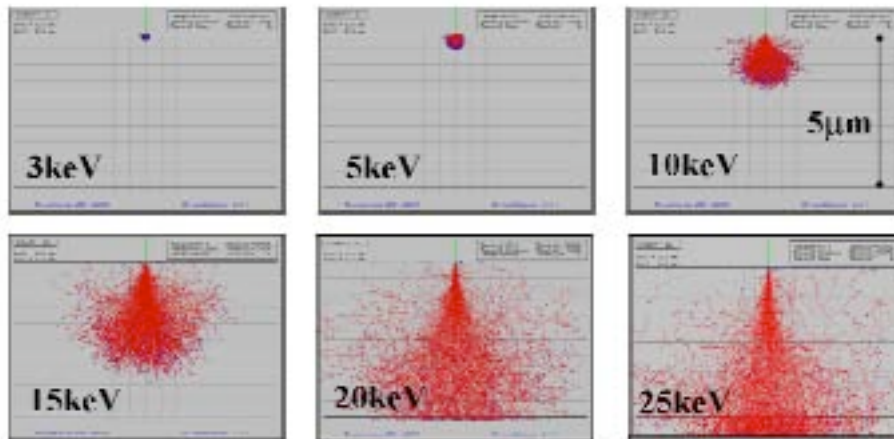


Figure 3.34 Electron trajectories on 5 μm of epoxy based resist (SU8) at different incident beam energies. At 20 keV, the whole layer thickness can be exposed.

The main inconvenient comes from the resist nature. As it is a negative resist, the areas that are efficiently exposed will remain after development process. In consequence, resist profile will not provide stepped profiles on such thick layers. As can be seen in Figure 3.35, simulation of the electron scattering for different thickness with a beam energy of 20 keV, leads to the use of very thin layers, similar to the previous case of PMMA.

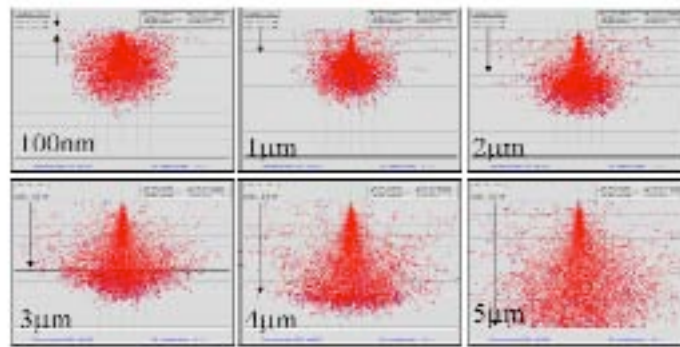


Figure 3.35 Influence of SU8 thickness on electron trajectories for an incident beam energy of 20 keV. Again, thin layers are convenient to obtain high resolution.

Another consequence related with negative tone resists is encountered. On positive resists, isolated electron trajectories on the resist may not cause as much effect as in negative ones. In SU8, all the contributions at the proper energy should be effective in the substrate-resist interface (Figure 3.36). Therefore, many remaining resist spikes may be found after development in not desired locations of the substrate surface, more importantly on high atomic number substrates (Figure 3.36, right).

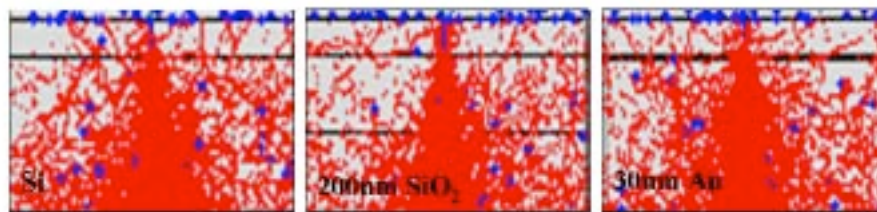


Figure 3.36 The effect of isolated backscattered electrons could cause resist residuals on the surface for the negative resist. Different multilayer substrates can increase or decrease this phenomena.

Comparing both resists, at low energy (3 keV), a slightly different penetration depth is obtained as a direct consequence of their respective composition, whereas beam widening does not seem strongly affected (Figure 3.37).

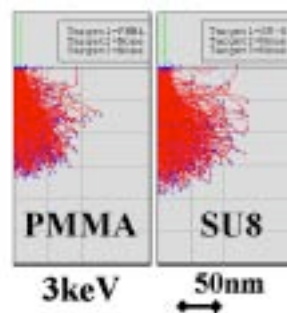


Figure 3.37 Comparison of electron penetration depth for 3 keV in thick resist layer. PMMA (left) has a lower range than SU8 (right).

3.3.2 Electron beam lithography on thick layers of mr-L 5005 XP

EBL experiments are performed in the resist mr-L 5005 XP, which deposited at 2500 rpm spin speed for 45 s provides a resist layer of $\sim 5 \mu\text{m}$. The pre- and post-exposure processing conditions are included in Figure 3.4. Synthesized to be exposed under UV light, the performance for electron irradiation is established experimentally, but the assessment of electron scattering simulations help. Indeed, simulations on SU8 (Figure 3.34) suggest that beam energy strongly determines the electron penetration depth in the polymer, as it is found for other resists.

Based on electron range simulations in a layer of $5 \mu\text{m}$ SU8, beam energies of 18 and 20 keV are used at different doses to expose the thick layer (Figure 3.38). Both achieve to fully expose the whole thickness given an appropriate dose. Required dose should be slightly lower for lower beam energies, but 18 keV may be almost in the limit of electron range. Even at high doses, patterns are more predisposed to be removed from the surface, so 20 keV is established as more convenient.

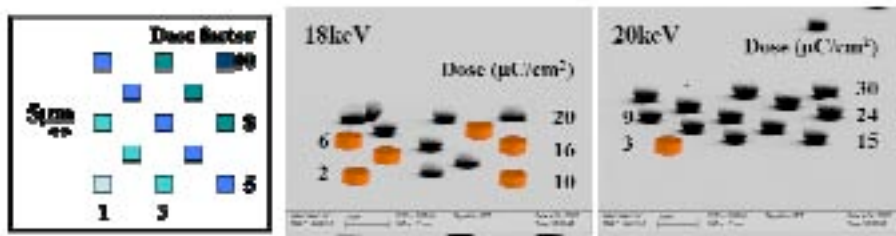


Figure 3.38 (Left) Design of dose test exposure. Internal dose factor ranges from 1 to 10. (Center and right) Experimental results shown that 18 keV is enough to fully expose the resist thickness ($5 \mu\text{m}$). Results at 18 keV and 20 keV are obtained at the dose value specified in each case.

The feature shape distortion is remarkable. Squared patterns become nearly round and it is due to the important deviations that electrons suffer along such thick resist. In Figure 3.39, left a profile of a line of $5 \mu\text{m}$ width shows it in more detail. In the top, a thickness of about 400 nm is the short range where electrons are little deviated from the incoming axis. Simulations are certainly in agreement with this behaviour (Figure 3.39, right). The use of thin resist layers for precise and high resolution patterning by EBL is unavoidable.

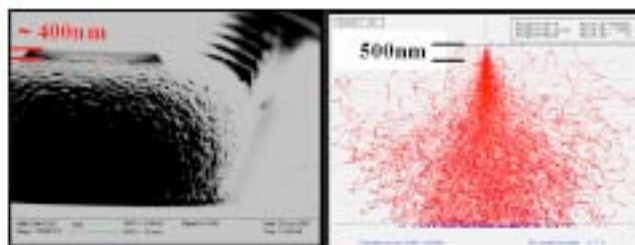


Figure 3.39 Profile SEM image of a line of $5 \mu\text{m}$ in width at 20 keV (left) is in agreement with the beam spread within the resist shown in electron trajectories simulations (right). Low forward scattering is achieved just a few hundred of nm in depth.

The effect of the dose is also important. Exposure of 1 μm width line with enough dose presents distortion (Figure 3.40, bottom), but its excess is directly proportional to the pattern widening (Figure 3.40, to the top). Again, simulations are useful to visualise this phenomena (Figure 3.40, right) and can be used to calibrate feature distances and doses for more complex designs.

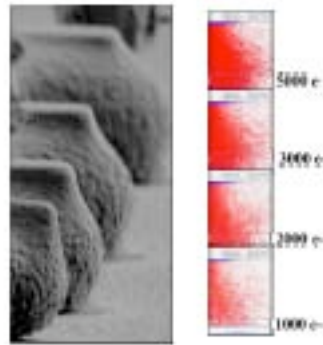


Figure 3.40 (Left) Tilted SEM image shows the dependence of profile with exposure dose. (Right) Assessment with the electron trajectories simulator for increased number of electrons (from 1000 to 5000 electrons) also serves to visualise this phenomena.

From these results, it is clear that design and exposure conditions are crucial, they determine and limitate what can be done. Taking advantage of the strong energy dependence of electron penetration depth, self standing structures can be obtained with the suitable conditions.

The evaluation of energy dependence is realized combining narrow lines at different beam energies (3, 5, 10, 15 and 20 keV) with wide transversal lines exposed at 20 keV to hold them. As an example, lines performed at 5, 10 and 15 keV are shown in Figure 3.41. Not only penetration depth is proportional to the beam energy, but also a strong linewidth dependence is found. At low energies, 3-5 keV, the result of line exposure are more similar to strips than to lines, whereas beyond 15 keV, lines are narrow, but also deeper.

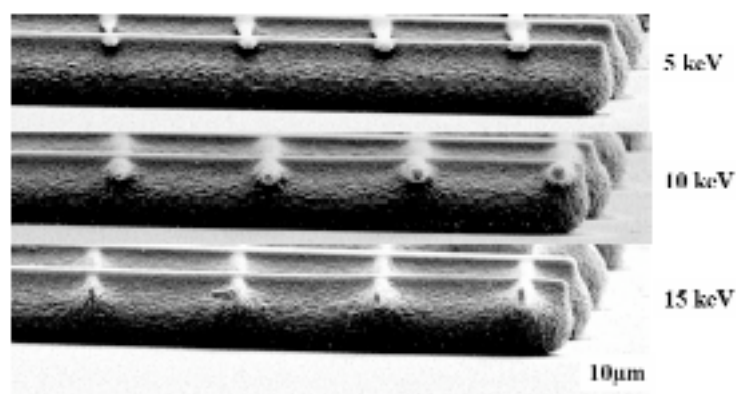


Figure 3.41 Profile SEM images of lines defined at different beam energies. At higher beam energies the penetration range is higher and linewidth increases with dose (from left to right).

Regarding results for 20 keV lines the depth-dose dependence is clear. A factor 1 of dose increase in each line from left to right side leads to correspondingly deeper lines (Figure 3.42), in particular, lines from 0.6 to more than 2.5 μm in depth are found. Same conditions on simulations directly relate a certain quantity of secondary electron generation (density of red lines) to the dose required to form the pattern.

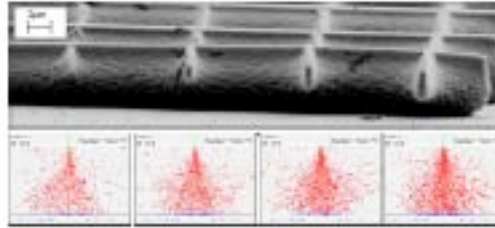


Figure 3.42 Profile SEM image (top) of transversal lines defined at 20 keV. Experimental results corroborate that higher doses directly relate with thicker lines, which can be also visualized by simulations (right)

Concerning to linewidth, resolution is also consequently determined by beam energy and dose. At 20 keV, linewidths of less than 200 nm are achieved with ~ 650 nm in depth (55 nm on the top of the line), whereas at 3 keV, minimum linewidth is around 365 nm, but depth does not reach 200 nm (Figure 3.43). Somehow, resolution seems higher at low energies.

Line resolution results are summarized in the plot of Figure 3.43. For 15 and 20 keV, the two curves represent the measured linewidth on top and bottom, while for 3 and 5 keV uniform width is found for all the depth of the strip. As can be seen, top values follow approximately what is expected in function of beam energy, higher resolution at higher energies, but the line widening with increasing dose has a significantly different increasing rate. Also, electrons at 3 keV beam energy may be so easily stopped that the whole exposure process deviates from the rest of tendencies.

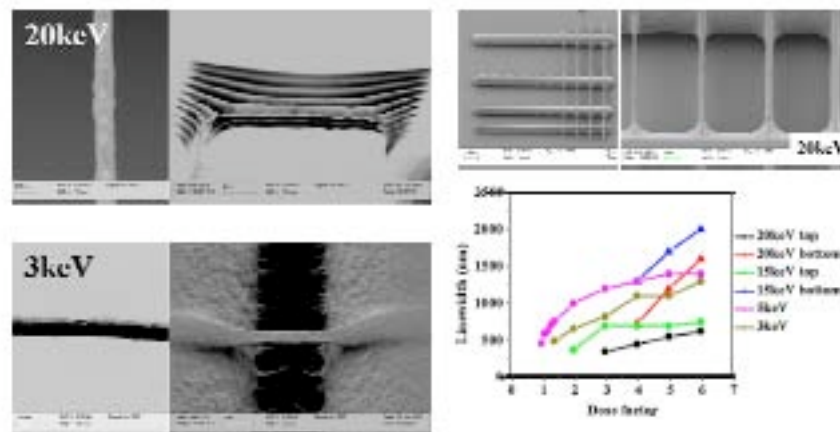


Figure 3.43 (Left) Experimental results for lines defined at 20 and 3 keV. For 20 keV, line is 200 nm in width and 750 nm in depth, whereas at 3 keV linewidth is 0.5 μm and depth is 140 nm. (Right) Dependence of linewidth with dose factor shows that at higher energies forward scattering gets relevant (red and blue lines).

The combination of different beam energies (grey scale lithography) suggest that a great diversity of structures can be fabricated, from single or double clamped beams to channels or many other fancy configurations (Fig. 3.44, top), that could be used for many applications (34). One of the main disadvantages in the EBL system is origin deflection when beam energy is changed. Therefore, misalignment may be encountered, more important with larger changes between beam energies. In addition, a great limitation always exists from the profile of the holding structures (Fig. 3.44, bottom). Certainly, it is not possible to define stepped structures (vertical walls) by EBL with such thick resist layers due to both forward (mainly) and backward scattering. In consequence, bridging occurs between features that are not separate enough to compensate the beam spreading.

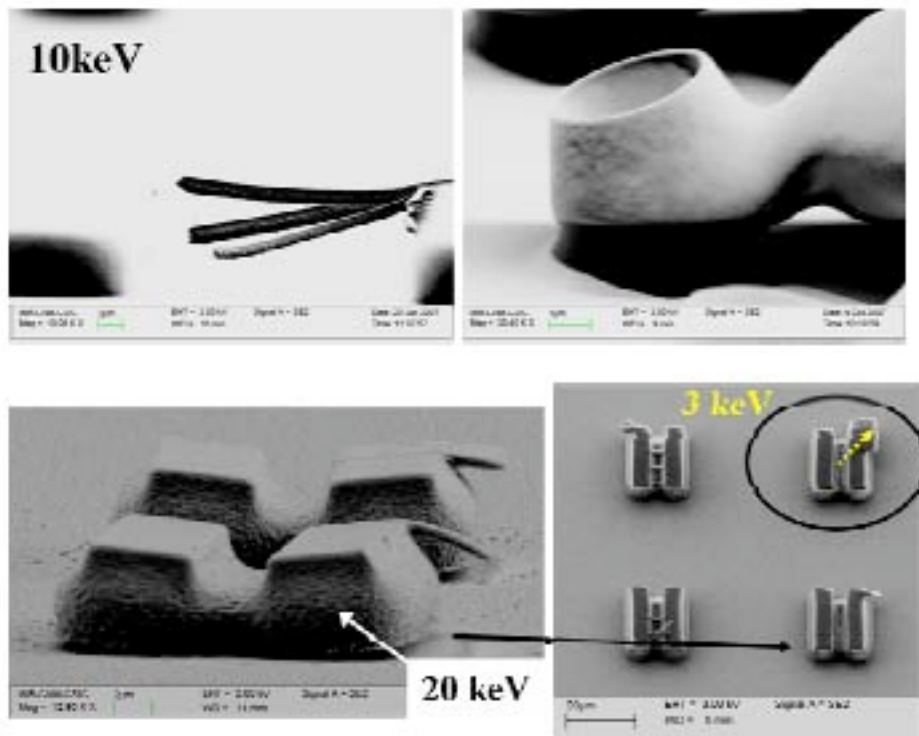


Figure 3.44 (Top) Self standing cantilevers and 3D structures can be defined combining the proper beam energies and design. (Bottom) Bridging occurs as a result of forward scattering. Combining different beam energies might take into account that alignment has to be corrected.

The combination of EBL with UV lithography may be a good solution (35). EBL continues to be suitable to define high resolution features or determined 3D structures, meanwhile UVL is responsible of providing the platform to tight them.

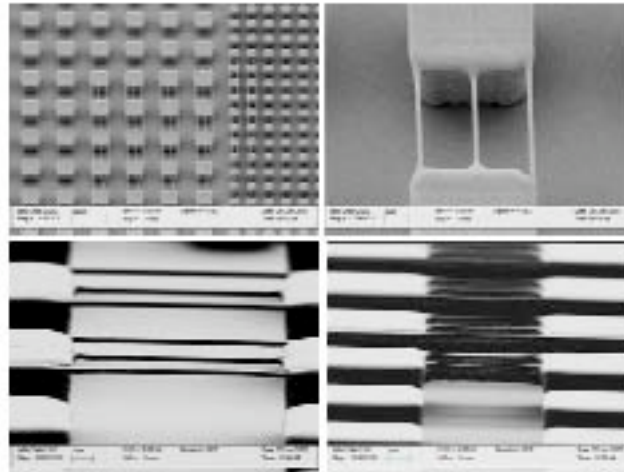


Figure 3.45 Combination of EBL with UV shows that high resolution structures can be obtained. As an example, EBL is used to define high resolution features anchored in UVL defined features.

3.3.3 Electron beam on thin layers: mr-EBL 6000.1 XP and ma-N 2401.

As it has been described in previous section, the main limitation of EBL patterning derives from the electron beam scattering all along the resist thickness. In consequence, it is generally accepted that outstanding results can only be accomplished using thinner layers, typically in the range of 100 nm or less. High resolution in terms of feature size, precise shape control and high pattern densities are obtained in such thicknesses, however a minimum value of film thickness is often required when pattern is transferred to the substrate, whether by etching or metal deposition and resist lift off.

For positive resists, PMMA is the resist with the best performance properties, but an analogous polymer with the inverse tone is also desirable. Due to this, research is still on going to develop new resists capable of filling this gap. MicroResist has synthesized an epoxy based negative for EBL that can be deposited in thin layers: mr-EBL 6000.1 XP (more details about resist composition are confidential and should be requested to the supplier, MicroResist GmbH). The choice of specific formulation and the characterization of its performance is next presented. The set up of the resist and starting parameters for users are established and they will be contained in the product data sheet, soonly marketable.

A basic characteristic of a resist is the sensitivity under irradiation. First, different fractions of PAG in a common polymer/solvent matrix are tested for different energies on a Si substrate (Figure 3.46). The exact values can not be mentioned, as requested from the supplier, therefore different PAG contains are referred as low, medium or high concentrations. The pre- and post- exposure processing conditions are detailed in Figure 3.4. The dose test design described in 3.3.1 (Figure 3.24) is used to evaluate resist remaining thickness in function of delivered dose, for the different PAG percentages at 10 and 20 keV. For 10 keV beam energy, the high sensitivity of the resist is manifested and for full thickness exposure in high PAG resists it occurs at doses even

lower than $1 \mu\text{C}/\text{cm}^2$ (Figure 3.46, left). As might be expected, at higher beam energy (20 keV, layer thickness $\sim 85 \text{ nm}$) sensitivity is lower (Figure 3.46, right). In both cases, two different behaviours are encountered in function of PAG: for the lowest PAG, the contrast is slightly worse in comparison with the rest of formulations. This may be inconvenient in terms of resolution, but could be used for 3D patterning.

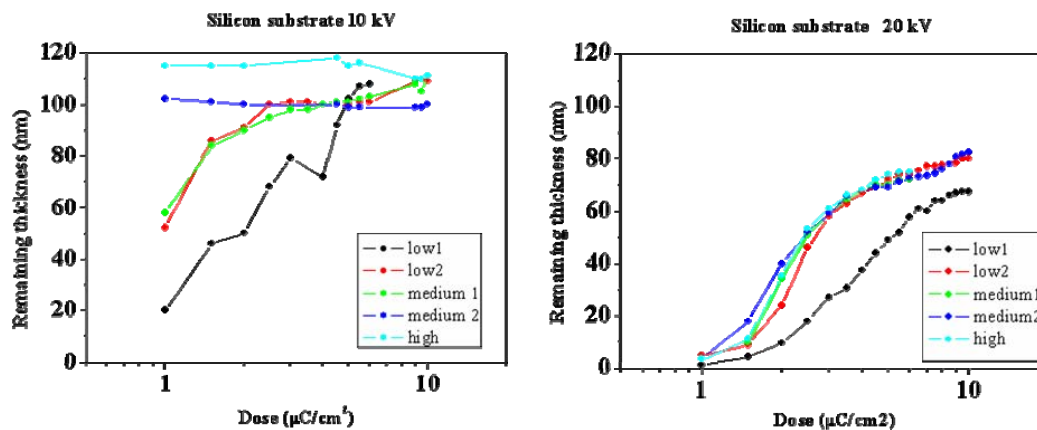


Figure 3.46 Experimental curves for dose test exposures at 10 (left) and 20 (right) keV on Si substrate in function of PAG. Deposited layer thicknesses are 120 and 85 nm, respectively. Sensitivity is directly related with PAG percentage.

Such low doses represent a limiting factor in most of electron beam systems. Beam current (determined by beam energy and aperture size) together with step size and dwelltime restrict the minimum dose that is possible to deliver (Chapter 2). Due to this, low PAG formulations are preferred since wider dose range and more precise control can be realized. Studying more in detail energy dependence with dose (Figure 3.47, left), a $\sim 120 \text{ nm}$ thick film on Si is exposed to 10, 15, 20 and 25 keV. The dose sensitivity decreases with increasing beam energy, contrarily to contrast that is enhanced at higher energies (Figure 3.47, right). Contrast values are calculated as described in (29) and are rather orientative, due to minimum dose limitation mentioned above.

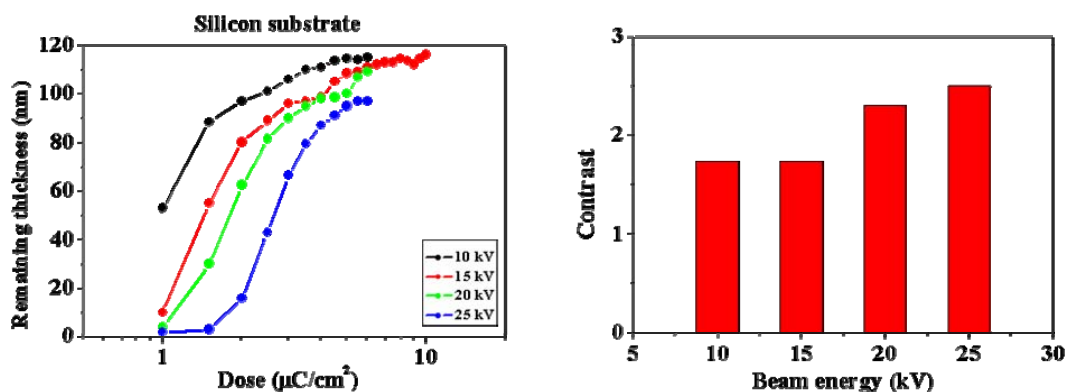


Figure 3.47 (Left) Low PAG resist enable dose tunability. (Right) Exposure at different beam energies on Si reveal an increase of contrast with energy.

High sensitivity is often desired to minimize exposure time. However, the high radiation efficiency is more critical for negative resists. Low energy backscattered

electrons may be a significant portion of exposure dose in the pattern area itself, but also in the near surrounding area (proximity). Different substrate materials have been tested to determine their contribution. Thin layers of SiO₂ (100, 200 and 300 nm) are grown on Si substrates. In Figure 3.48, left, the contrast curves for a beam energy of 20 keV are represented. It seems that sensitivity is slightly increased together with contrast by the introduction of insulating layer. Similar behaviour for 10 keV sensitivity is found, whereas contrast dependence can not be observed in detail.

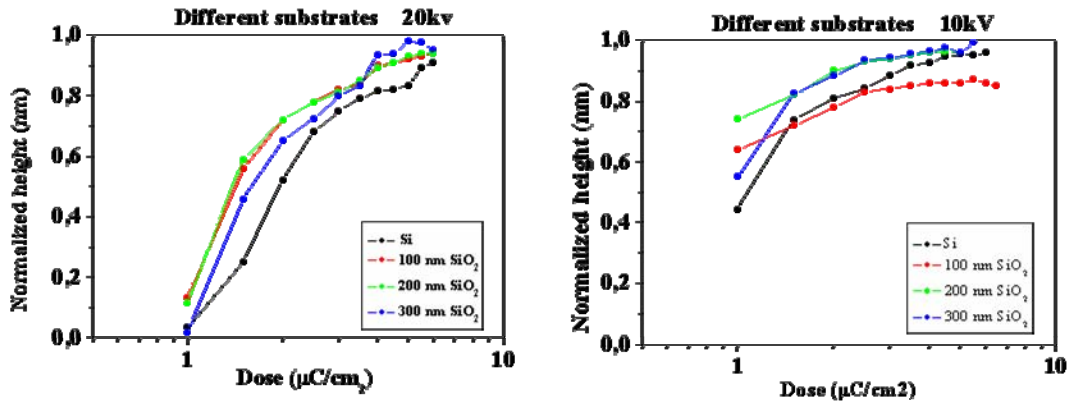


Figure 3.48 Dependence of sensitivity for low PAG concentration resist with different substrates. Thin layers of SiO₂ on Si are compared with bulk Si. Both at 20 (left) and 10 (right) keV beam energies the variability is not significant.

Thin layers of SiO₂ do not seem to cause much difference in resist performance. However, other substrates do. In particular very thin layers of ~ 30, 50 or 32 nm of Ni, Au or Al, respectively, are deposited on Si samples underneath the epoxy based resist. For Ni ($z = 39$) covered substrates, both at 10 and 20 keV beam energy the sensitivity is lower than in Si, so it is the contrast (Figure 3.49, left). Due to the Ni higher Z, electron stopping power is higher. As a result, backscattered electrons are reduced and, hence, absorbed dose rate in the resist is lower than lighter substrate materials. Electron range is reduced in the substrate and consequently charge is almost confined to the delivered area, which results in almost no pattern distortion (Figure 3.49, right). Probably, higher resolution and more densely packed structures can be obtained. Those results are absolutely in agreement with simulations for heavier substrates seen in Figure 3.13.

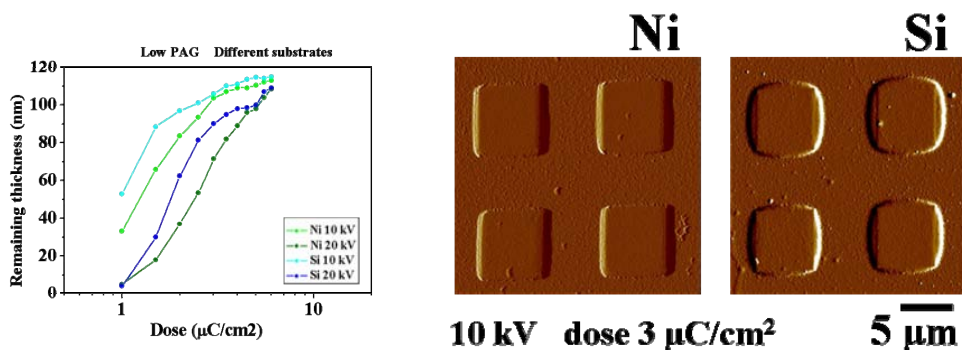


Figure 3.49 (Left) In the case of high Z substrates, the dose sensitivity clearly differs from the Si substrate. (Right) In addition, charge confinement due to higher stopping power in Ni reduces feature intraproximity effect.

However, studying the effect of Au ($Z = 59$) thin layer, results are not as expected. The dose seems almost independent of beam energy and the squared features are again very distorted (Figure 3.50). Although this test is done on 1.5 % PAG resist, this is not the cause of the anomalous phenomena and additional contributions have to be determined. It is possible that resist heating due to the collisions of electron and heavy atoms has accelerated the exposure process. Indeed, chemically amplified resists are highly dependent on PEB and the scattering with the Au layer may be the cause of additional polymerization. What is more, conductive thin layer of Al also covered with low PAG concentration resist does follow the typical dose/beam energy dependence, what reinforces previous statement (Figure 3.51).

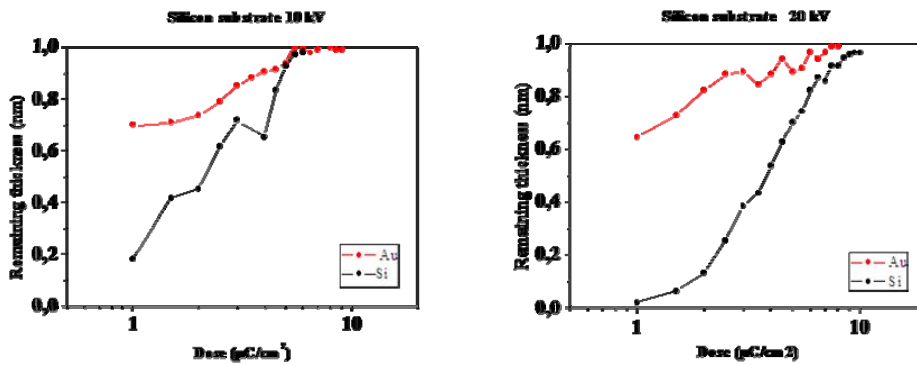


Figure 3.50 Experimental results on Au substrate reveal a unexpected nonlinearity with energy. It is attributed to heating of substrate that induces additional exposure.

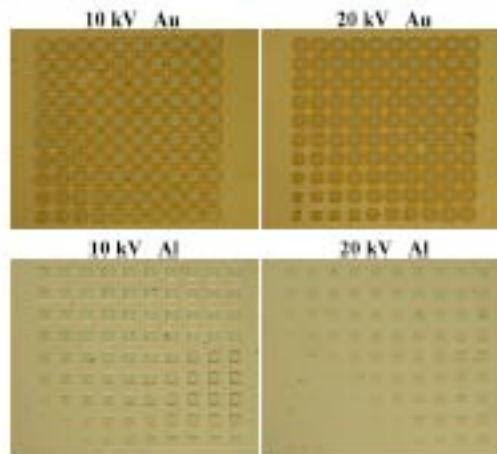


Figure 3.51 Comparison of exposures performed on low PAG concentration epoxy resist on Al (bottom) or Au (top). For the Al substrate, resist shows the typical performance, sensitivity inversely depends on beam energy.

All previous experiments for dose determination are tested for a squared pattern of $5 \times 5 \mu\text{m}^2$. Using different shapes or varying feature sizes accounts for their importance in the determination of exposure dose. In order to find the dose value that is required for exact patterning sizes and remaining thickness, the resist performance is evaluated as presented in Figure 3.52, left. The design consists of an array of rectangles

of increasing X size in horizontal direction and increasing Y size in the vertical one. As it is summarized in Figure 3.52, right, remaining thickness is highly dependent on pattern size. For a same exposure dose and both at 10 and 20 keV beam energy, remaining thickness increases with higher feature size.

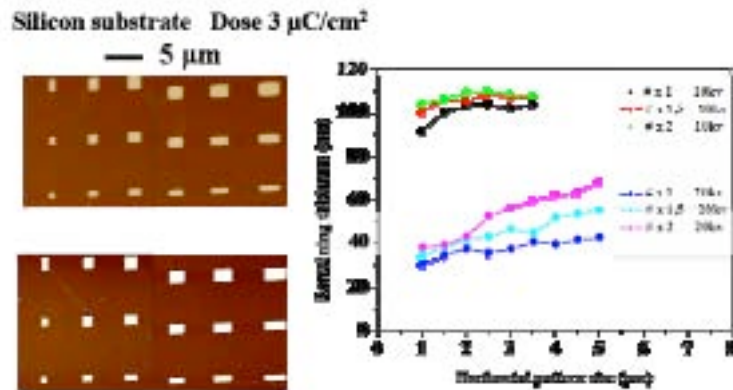


Figure 3.52 Dependence of remaining thickness with feature dimensions. Increasing width or length implies higher remaining thickness for the same exposure dose. AFM topography images (left) are 40 x 20 μm in size, and correspond to 10 keV (top) and 20 keV (bottom) beam energy.

Also, exposure strategy in terms of beam control and deflection is relevant. In Figure 3.53, non uniform resist thicknesses are obtained and it is clearly seen that beam is addressed from left to right, resulting in higher delivered dose at the starting point, where beam is stopped for positioning. In consequence, nonuniform and rough resist remaining thickness is found and using infraexposed patterns to preserve feature shape may be inconvenient if combined with pattern transfer.

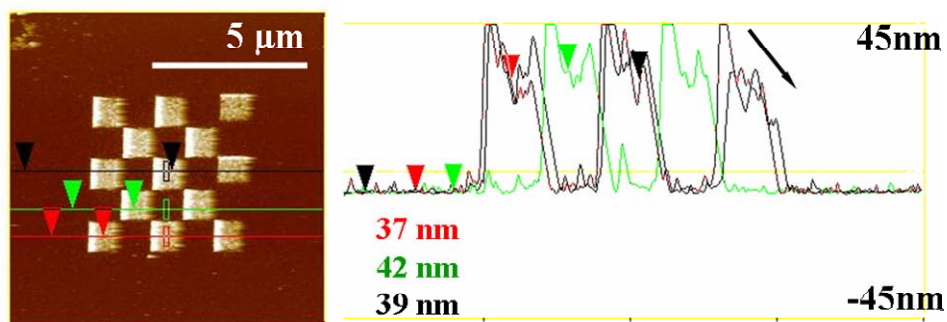


Figure 3.53 Chess-like pattern shows non-uniform remaining thickness and high roughness. Features are defined in 110 nm layer of mr-EBL 6000.1 XP, low PAG, at 10keV on a Si substrate. Exposure dose is $3.5\mu\text{C}/\text{cm}^2$.

Another example of this aspect in the Figure 3.54, where the edges have clearly lower resist thickness. But the important aspect is the good definition of the features, which allows to infer that high resolution can be obtained with the appropriate exposure conditions.

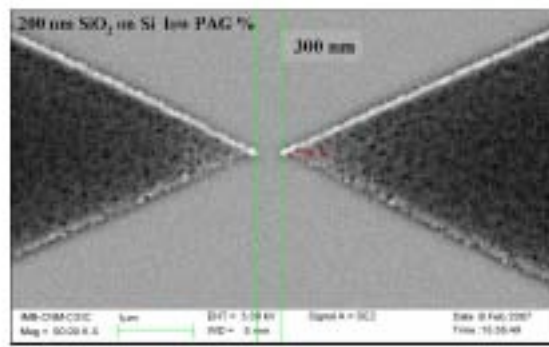


Figure 3.54 High resolution patterning is achievable with proper choice of exposure conditions and design. Arrow-like features are defined at 10keV in 110 nm layer of mr-EBL 6000.1 XP, low PAG, on a 200 nm SiO₂ layer upon Si substrate.

In order to determine resist resolution, some preliminary tests have been done with line patterns. Isolated SPL (periodicity 1 μm) are defined with different PAGs and beam energies on different exposure conditions and doses. As an example (Figure 3.55, right), narrower lines are obtained when higher energies are used, however also remaining thickness diminishes. Hence, further optimisation is required and, in order of doing it, increasing dose and PAG are evaluated (Figure 3.55, left).

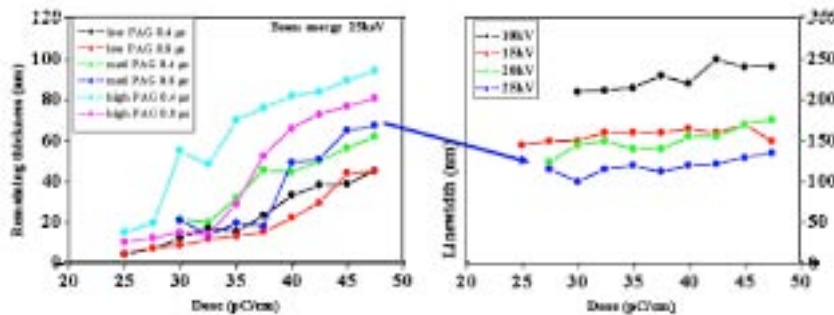


Figure 3.55 Lines are defined in the design as SPL (zero linewidth) and a separation of 1 μm . (Left) Dependence of remaining thickness on dose for different PAG content and beam speed. (Left) Analysis of beam energy dependence on resulting linewidth. Higher energies allow to obtain higher resolution.

As a matter of fact, the characterization method for linewidth results decisive. Standard AFM inspection gives precise information of the resist thickness, but may introduce linewidth deviations due to lateral convolution. The denser and thicker the lines, more important is the linewidth determined distortion (ultra sharp tips give more precise results). Therefore, SEM linewidth determination (sample and resist features are covered by a thin layer of Au to enhance imaging contrast) in high PAG concentration resist at 10 keV on Si, show that lines under 150 nm and reasonable remaining thickness (< 80 nm) are obtained (Figure 3.56). Also dose increment does not increase significantly linewidth. In consequence, promising result can be expected if beam energy, dose and PAG are properly chosen as a whole.

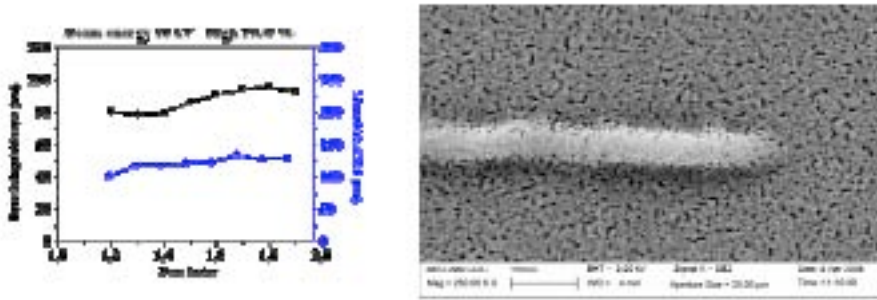


Figure 3.56 Lines are defined at 10 keV in 100 nm layer of mr-EBL 6000.1 XP, high PAG, on Si substrate. Linewidth measured by SEM imaging is more precise, but AFM determines remaining thickness. Submicron lines are systematically obtained.

For many applications feature density is very important and often represents a big challenge in terms of lithography. Arrays of dots and lines for different exposure conditions and periodicities are presented in Figures 3.57 and 3.58. As can be seen for both cases, decreasing interfeature distance results in increased residuals. For dot exposure, increasing dot dwelltime allows to control dot diameter, while for line exposure, design linewidth can be similarly used. For both, combination of design characteristics with dose and periodicity lead to define patterns in the 100 nm range.

Epoxy low PAG % on 200nm SiO₂ Beam energy 10kV

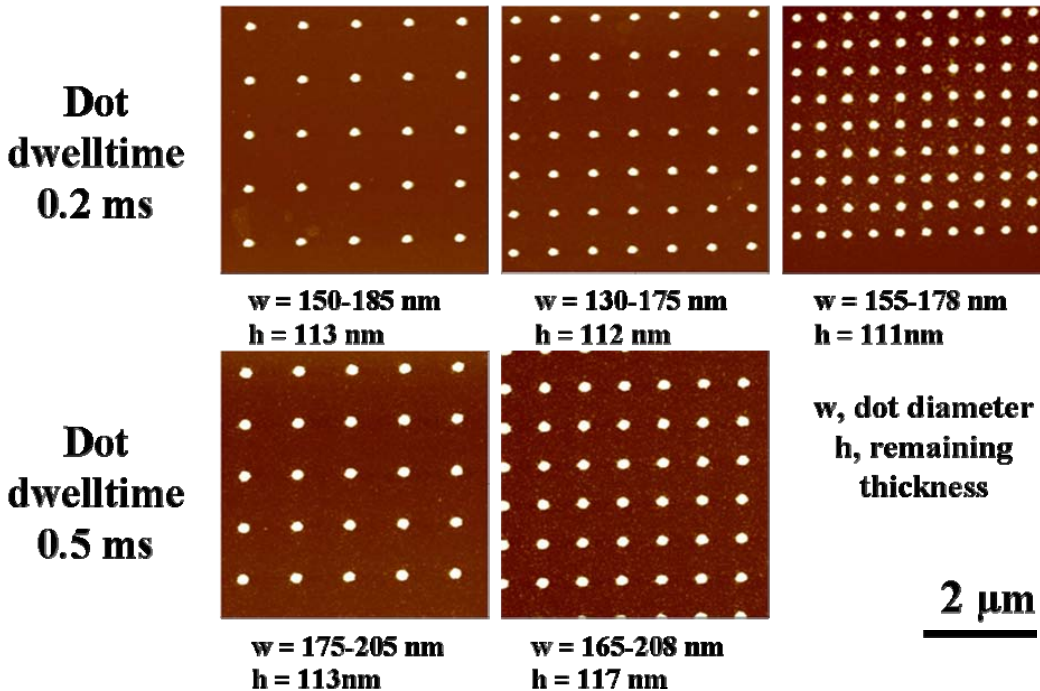


Figure 3.57 Dot diameter can be controlled by the exposure dwelltime. They are defined on 120 nm thick mr-EBL 6000.1 XP, lowest PAG concentration, in a 200 nm SiO₂ layer at 10 keV.

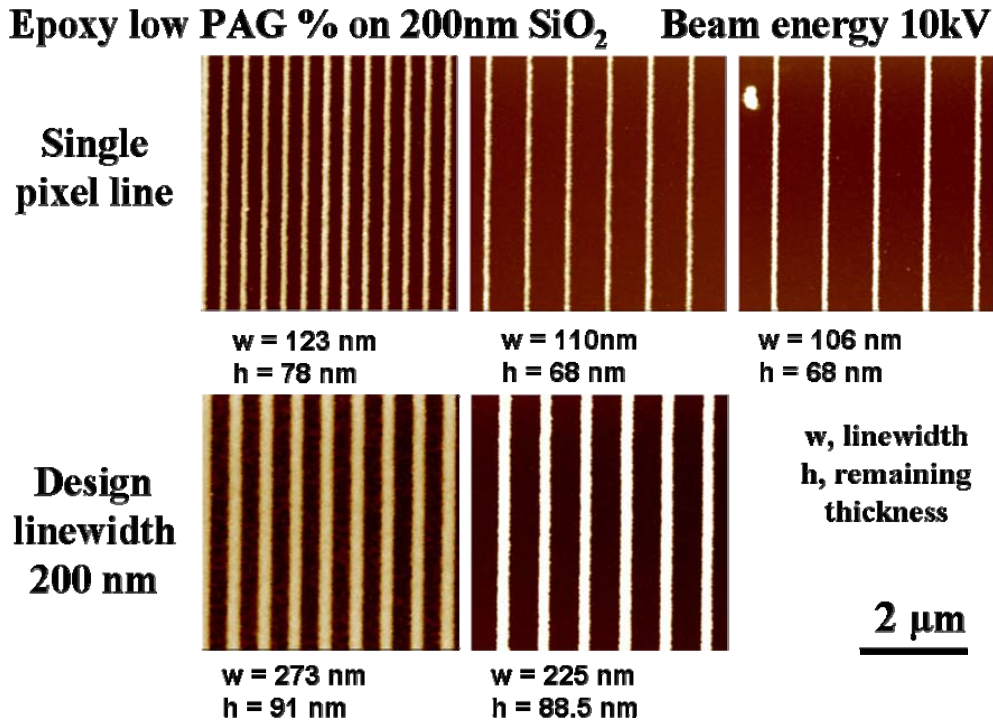


Figure 3.58 Linewidth can be controlled by design linewidth. Decreasing interfeature distance increases resulting linewidth. Lines are defined on 120 nm thick mr-EBL 6000.XP, lowest PAG concentration, in a 200 nm SiO₂ layer at 10 keV.

The continuous research in polymers is not sustainable if the novel materials do not bring enhanced properties. Therefore, comparison with already existing resists is not only convenient, but necessary. It may lead to establish a field and the range of applications where it contributes to fill uncovered demands or to introduce higher performance or specific characteristics for specific processes.

The presented mr-EBL 6000.1 XP is put side by side with ma-N 2401 (36), both polymers from MicroResist GmbH. Ma-N 2400 series is also a negative tone resist for EBL (and DUVL) that can be deposited in thin layer thicknesses (several viscosities are available). Their outstanding characteristics are based on their high resolution and good etch resistance, completed with relatively high sensitivity. Different from the polymer described above, it is not a chemically amplified resist, thus simple processing is always advantageous.

Deposition of ma-N 2401 is realized by 3000 rpm spin coating and preparation for exposure consists of hot plate bake at 90 °C for 60s. Data sheet sensitivity is 120-200 μC/cm² at 20 keV beam energy, dependent on pattern size and resolution (clearing dose ~ 80 μC/cm²). After EB exposure, development is short time immersion in aqueous alkaline solution (10 ± 3 s in ma-D 532), thoroughly rinsing in deionized water for 5-10 min and drying.

The experimental sensitivity is determined as in previous cases. Contrast curves are obtained in ~ 120 nm polymer layers deposited upon Si substrate. For exposures at 10 and 20 keV beam energy, again 5 x 5 μm² areas at different doses are used and thicknesses after development are determined by AFM inspection (Figure 3.59).

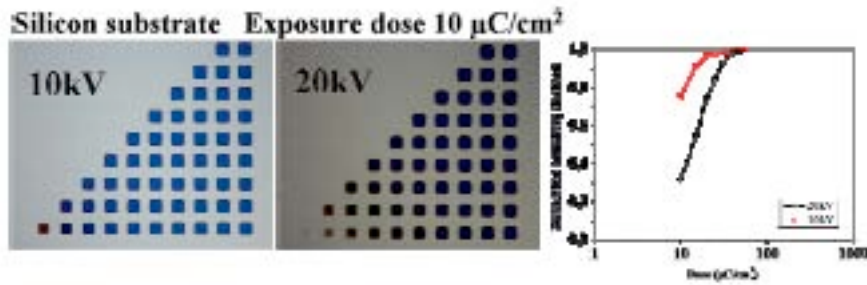


Figure 3.59 Dose test exposure for 120 nm of ma-N 2401 on Si substrate at 10 keV (left) and 20 keV (center), sensitivities are 35 and 50 $\mu\text{C}/\text{cm}^2$, respectively.

The sensitivities are established as 30-40 and 50 $\mu\text{C}/\text{cm}^2$ for, respectively, 10 and 20 keV, which is slightly lower than data sheet reported values and reinforces the necessity to test the resist for every different system that is used.

Contrast is automatically derived from this trial and allows to the first resist comparison in terms of performance (Figure 3.60). The newly synthesized polymer, mr-EBL 6000.1 XP, exhibits a higher sensitivity and better contrast than ma-N 2401, which may indicate a global performance improvement in terms of resolution.

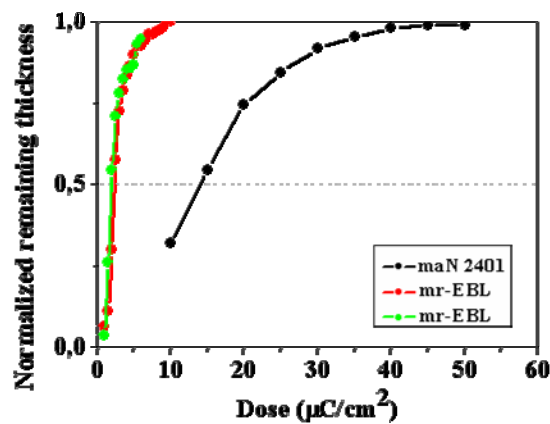


Figure 3.60 Comparison of contrast curves for mr-EBL 6000.1 XP and ma-N 2401. New resist has higher contrast and lower sensitivity. The results of dose test for two different exposures on the new resist are plotted and show absolutely equivalent sensitivity.

As an example of comparative resolution for both resist types, the results of EBL on Si substrates for same patterns are presented in Figure 3.61. Same ring designs are exposed on Si substrates at 10 keV beam energies. Although resulting structures are similar in thickness, ring widths are considerably higher for ma-N 2401 than for the new polymer, mr-EBL 6000.1 XP (in particular, lowest PAG concentration is used). For instance, epoxy based left ring is about 350 nm in width for a thickness of 55 nm, whereas, for the other, width of 550 nm is encountered even with a lower resist height, 44 nm.

Preliminary results concerning to etching resistance are evaluated in the next section. In addition to the mentioned properties, it is noteworthy the importance of the pre- and postirradiation treatments. For mr-EBL 6000.1 XP, PEB process that has been used is common for all the experiments. The difference in resist thickness and substrate heating respect to ordinary UVL in negative resists, together with the specific EB

exposure reaction mechanism may imply that PEB is not so critical in EBL irradiation process. On the other hand and concerning to ma-N 2401, the rinsing after development appears to be very certainly determining to obtain a clean patterned surface. As a result, both resists may need similar processing accuracy.

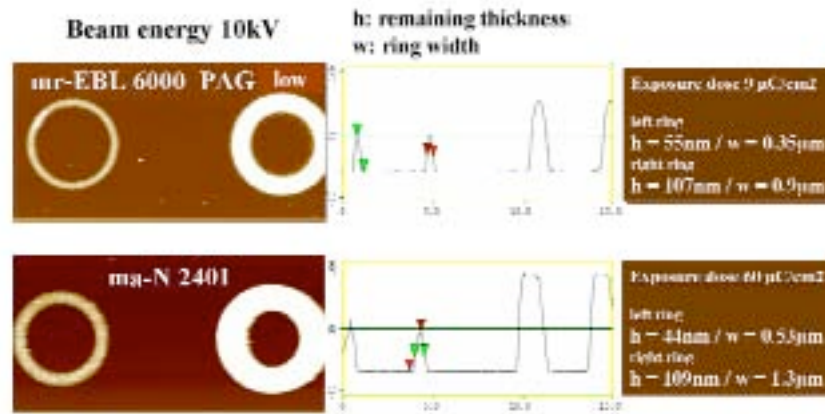


Figure 3.61 For equivalent design, exposure conditions (beam energy, substrate) and similar remaining thicknesses, resolution is considerably higher for mr-EBL 6000.1 XP (top).

3.3.4 Post-lithography processing: etch resistance

From the point of view of resist research in chemistry, polymers are often evaluated and developed mainly concerning to composition, exposure reaction mechanisms, etc. However, for further application these characteristics are secondary if they do not allow to compatibilize chained fabrication processes. In consequence, etch resistance and, related to this, thermal and chemical stability is most appreciated. One of the main uses of negative polymers is the etch masking.

Wet etching

In general, wet etching is widely used since it is simple, cheap and rather controllable. Also, it is considered very convenient for applications where isotropic etching can be admitted or when selective stopping is done by different layers of determined thicknesses.

SiO_2 etching with buffered HF (37) is tested with mr-EBL 6000.1 XP, lowest PAG concentration, as a mask to evaluate its use for fabrication. A sample with a 200 nm layer and resist features is immersed in SiOetch solution for 2 min, the time necessary to eliminate such layer thickness. Some of the results are presented in Figure 3.62. In the left, it is shown that effectively the new resist can be used as a mask, since it remains after the process. However, in the center, the effect of the resist thickness and of solution penetration in smaller apertures is present. In addition to this, such etching depth is a limitation for submicron features due to the isotropy of the process as can be seen in the right, namely underetching. Resist is unsticked and as a result feature height is been reduced or even shape is distorted (Figure 3.62, right).

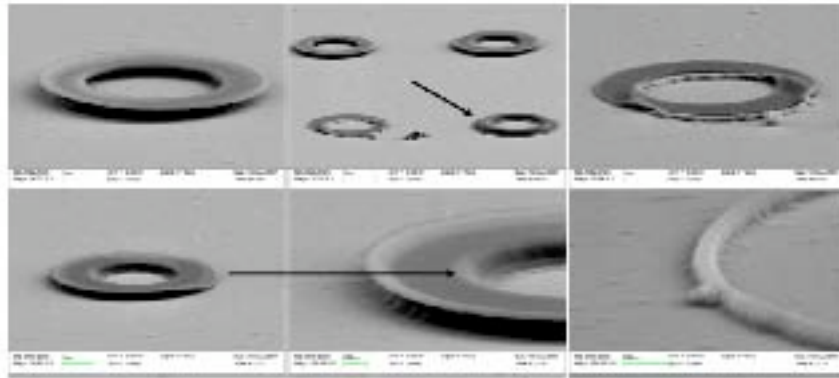


Figure 3.62 (Left) Resist layer remains after the wet etching. (Center) Non uniform thickness features lead to inhomogeneous results (top) and etching solution penetration can be difficult (bottom). (Right) Undercut can cause de-sticking of resist and feature distortion (top), but can be also used to define features under 100 nm in width (bottom).

More in detail, the result of resist thickness can be seen in the dose test pattern. In the left side of Figure 3.63, insufficient and inhomogeneous resist thickness cause that the feature is not completely nor uniformly transferred to the SiO_2 layer. But excessive exposure dose that implies certain pattern distortion is not a good solution neither, since it is indeed replicated.

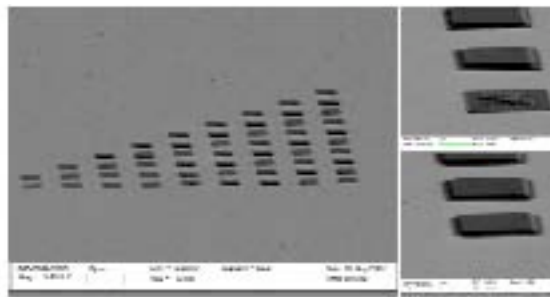


Figure 3.63 SEM images of etching of 200 nm of SiO_2 with mr-EBL 6000.1 XP mask (Left) Results on dose test pattern. (Right) Remaining thickness inhomogeneities are replicated (top) and overexposure results in distorted features (bottom).

Thinner SiO_2 layers may be convenient to reduce etching time and the resulting underetching profile. A Si substrate covered with ~ 40 nm of SiO_2 is patterned again with the same resist and immersed in the etching solution for 20 s. The results in Figure 3.64 show that resist thickness does not seem quantitatively affected by the etching, but many redeposited rests appear in the sample substrate. In this case, a lack of resist thickness may not be so problematic when transferring narrow lines and reliable dot shapes are also found.

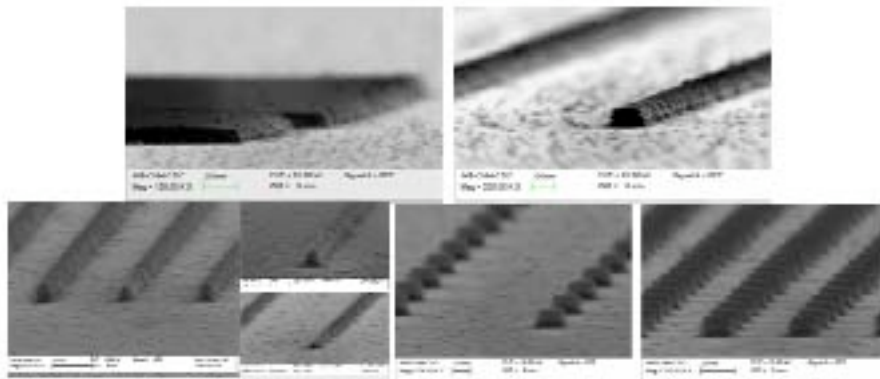


Figure 3.64 SEM images for the etching of 40 nm of SiO₂ with mr-EBL 6000.1 XP mask. Etching selectivity and feature definition are good.

It may be interesting also to have also available other etching processes, such as Silicon etching. Therefore, mr-EBL 6000.1 XP is tested as a mask in TMAH etching. In this case, the epoxy based polymer does not resist the process. As it is shown in Figure 3.65, the squared shapes of dose test pattern are displaced from their original ordered position, which may indicate that the resist features are detached during the immersion in the etching solution. Hence, it seems that is a matter of resist adhesion to the substrate, more than a selectivity issue. Both types of low PAG concentration resists are tried with similar results.

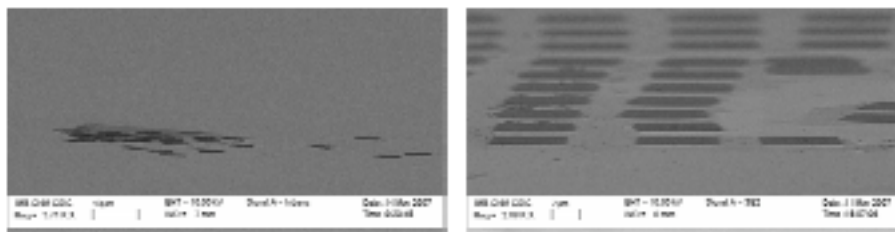


Figure 3.65 Si wet etching using TMAH is not compatible with mr-EBL 6000.1 XP due to adhesion.

Evaluation of SiO₂ wet etching in ma-N 2401 shows a resist performance similar to the one of mr-EBL 6000.1 XP. Enclosed in Figure 3.66 are the results of wet etching of 200 nm of SiO₂ layer with ma-N 2401 mask. However, it seems that the thin resist layer may be consumed within the process. Slightly different feature thicknesses may be related with the original differences in resist thickness mask before the etching.

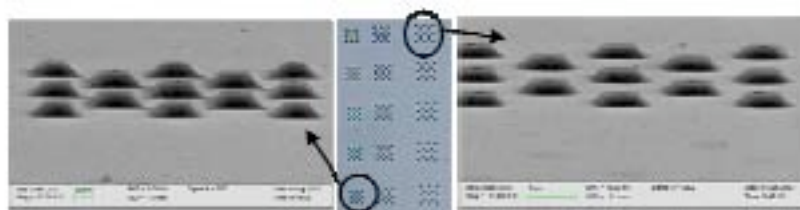


Figure 3.66 Ma-N 2401 is used to mask 200 nm of SiO₂ wet etching. No resist remains after the process.

More in detail, the thickness resistance can be quantified with accurate SEM imaging (Figure 3.67). In particular, for an original resist thickness of 88 nm, no polymer remains (top, left), whereas for ~ 117 nm not all the resist is removed (top right). In addition, the pattern distortion caused by infraexposure (resist thickness inhomogeneity) is present in Figure 3.67, bottom. The performance of ma-N 2401 in SiOetch indicates that mr-EBL 6000.1 XP has a better wet etch resistance.

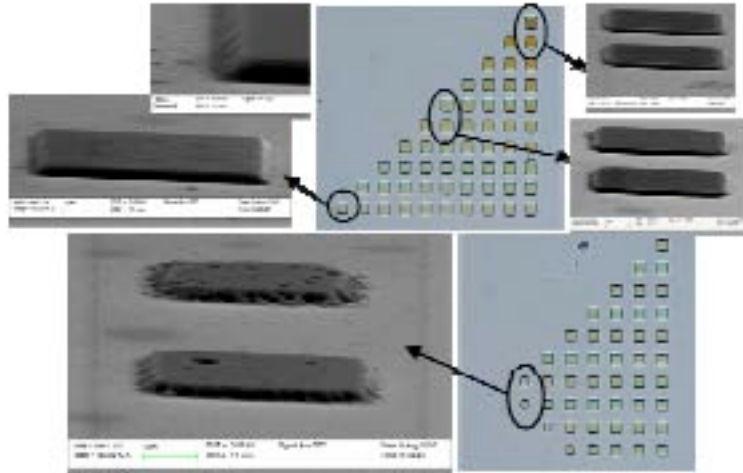


Figure 3.67 Selectivity of ma-N 2401 for wet etching is slightly higher than 2. (Top) SEM images reveal that resist has been etched (left) and some residuals remain (right) for an original thickness 117nm.

Dry etching

An alternative to Si wet etching is the dry etching. Reactive ion etching (RIE) is characterised for its anisotropy, but often is more complicated to determine the optimal conditions of the process (time, gases ratio, power, etc). Due to this, first it is convenient to use a similar case that is ensured to resist the process, as may be ma-N 2401. The results on Figure 3.68 and 3.69 correspond to 30 s in 8 scc/min O_2 and 25 scc/min SF_6 in the RIE equipment Oxford plasmlab 80 plus, placed at the Clean Room of the UAB.

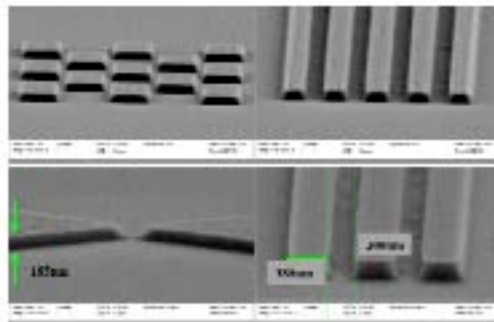


Figure 3.68 Si RIE using ma-N 2401. Some resist remains after the process.

Indeed, the 100 nm thick resist shows enough resistance during the dry etching process, in particular a Si thickness of <185 nm are removed. Process conditions seem suitable to achieve relatively vertical profile with not excessive undercut and used for testing the new resist, mr-EBL 6000.1 XP. Some possibility of using this process to develop specific applications are exemplified in Figure 3.69.

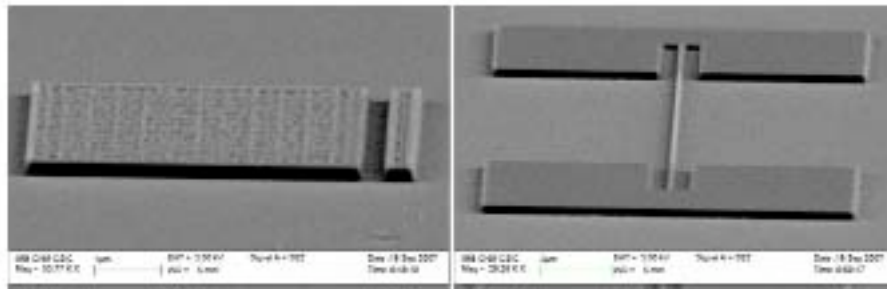


Figure 3.69 Examples of structures defined on ma-N 2401 and transferred to Si by RIE.

It should be convenient to set up also the SiO₂ etching also with the RIE, in order to complement the previous case. However, it seems more difficult to establish good etching parameters as it is presented in Figure 3.70. Whether polymer resistance or etching power is low, but certainly results are not promising.

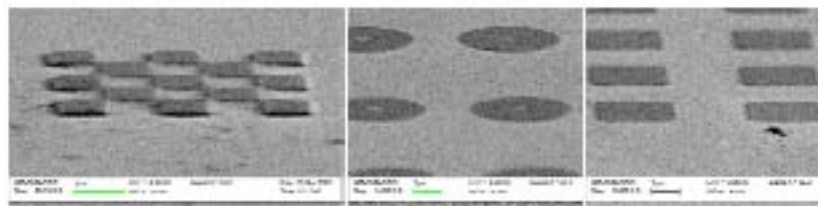


Figure 3.70 SiO₂ RIE presents bad selectivity in the tested conditions.

Si RIE should be tested with mr-EBL 6000.1 XP. Although the polymer partially resists, this process should be optimized to be less aggressive and to guarantee certain integrity of the resist thickness (Figure 3.71).

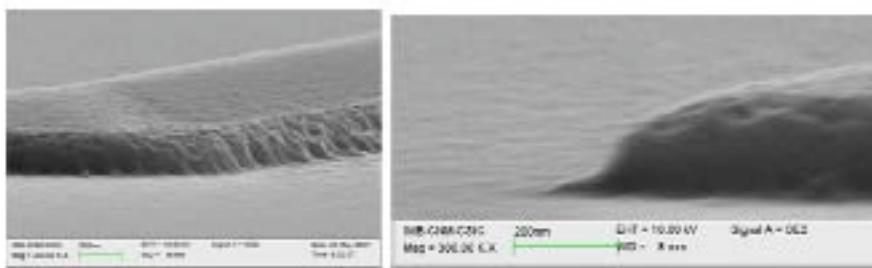


Figure 3.71 RIE using mr-EBL 6000.1 XP as a mask. The etching recipe is equivalent to the RIE used for ma-N 2401: in 8 ssc/min O₂ and 25sc/min SF₆, during 30 s.

Combined etching

A solution for the difficulties encountered in dry SiO₂ and wet Si etching can be tested with the combination of the complementary processes. Thus, ma-N 2401 is used first as a mask for wet SiO₂ etching and subsequently dry Si etching is applied (Figure 3.72). Results are certainly positive and it is interesting to experience this technology with the new resist.

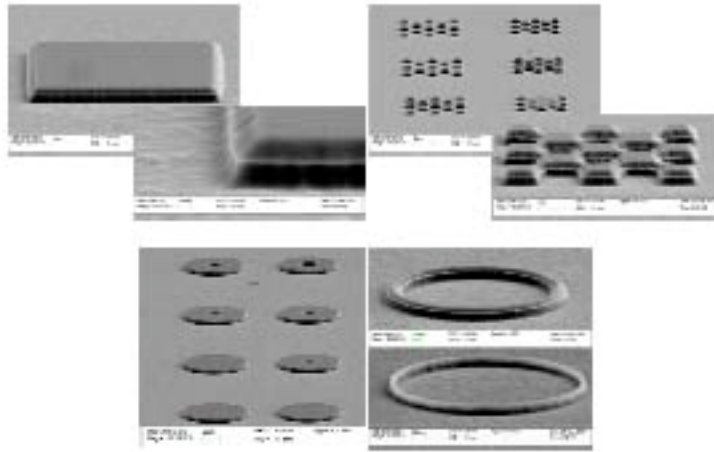


Figure 3.72 SEM images for some examples of combination of SiO₂ wet etching and Si dry etching on ma-N 2401. Original SiO₂ thickness is 200 nm and Si etching is about 200 nm. Ma-N 2401 thickness is completely consumed.

The combination of wet SiO₂ etching and dry Si etching on PAG 3% provides again a valid procedure, but RIE conditions may be certainly adjusted (Figure 3.73). As can be seen, insufficient resist thickness affects the SiO₂ thickness of the feature (RIE conditions are equivalent to previous examples, Figure 3.66, 3.67, 3.72, but etching time is 1 min).

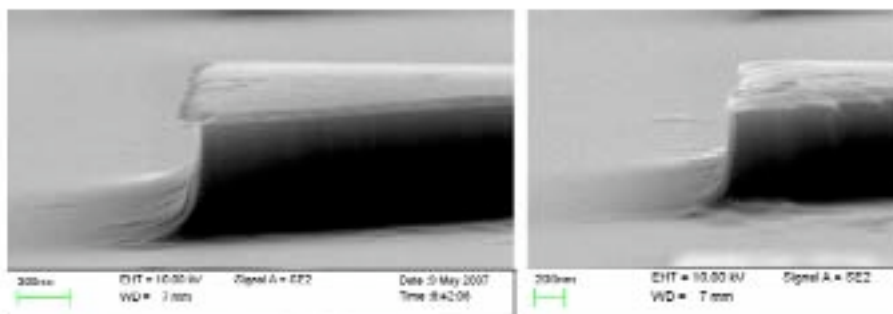


Figure 3.73 Result of combined wet and dry etching using mr-EBL 6000.1 XP as a mask. Etching time is excessive and partially consumes SiO₂ layer.

Resist removal

For some applications, elimination of the resist after the etching process is required. This is the case of functionalization, where some materials are preferentially attached on certain surfaces. Epoxy based resist, SU8, is difficult to be stripped, so it may be convenient to determine if mr-EBL 6000.1 XP is possible to be eliminated. Pyrolysis at 600 °C during 5 minutes in N₂ ambience is capable to completely eliminate the resist. As it is presented in Figure 3.74, completely flat and roughless surfaces are obtained, where the polymer thickness was enough to resist all the etching process (center). On the other hand, a lack of resist may contribute to feature roughness, but does not require resist stripping (left). In this example, since the lines (half width) are, additionally, narrower than the underetching, resist layer is detached and features are partially affected by wet etching with increased surface roughness. Resists rests due to feature density may be also transferred to the substrate (top, right). As can be seen, high feature density cause higher amount of resists rests between dots, due to proximity effect, and these spikes are also transferred by the wet etching. On the contrary, same dots (equivalent dose), being more separate, do not present this limitation (bottom, right).

In summary, a complete series of processes are available to be combined for fabrication of a wide range of applications.

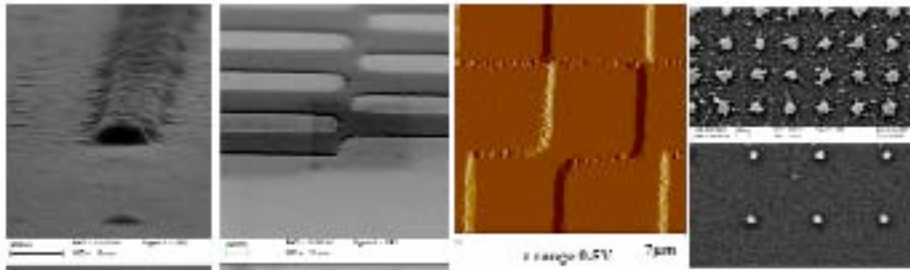


Figure 3.74 Features defined in mr-EBL 6000.1 XP are transferred by wet etching to the 75 nm thick SiO₂ layer. Pyrolysis at 600 °C during 5 min is used to remove the resist.

Other fabrication processes are also interesting to be chained with the precedent steps. Combination of different levels of lithography may be interesting and compatibility with other resists and their processing materials should be tested. As an example, methacrylic positive resists used upon epoxy based resists may allow many specific configurations, such as metallic clamped cantilevers. MIBK developer is tested on epoxy to evaluate this option. Comparing the resist thicknesses of standard EBL processing flow with the same adding the sample immersion in PMMA developer, no effect in MIBK:IPA use is shown, as illustrates Figure 3.75.

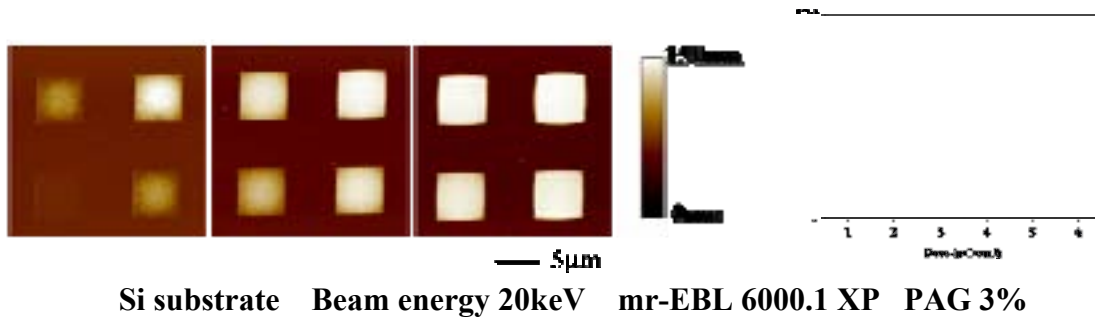


Figure 3.75 Compatibility of mr-EBL 6000.1 XP with MIBK (the developer for PMMA) is tested. (Left) AFM images after immersion in MIBK:IPA. (Right) Comparison of the remaining thickness after exposure (black line) or after additional immersion in MIBK:IPA (red line).

The general processing parameters for mr-EBL 6000.1 are summarized in the following table.

mr-EBL 6000.1 XP	Beam energy (keV)	Dose* ($\mu\text{C}/\text{cm}^2$)	Wet etching		Dry etching	
			SiO ₂	Si	SiO ₂	Si
lowest PAG	10	7	√	x	x	√
	20	10				
low PAG	10	3	√	x	x	√
	20	7				
*Aproximate dose for $5 \times 5 \mu\text{m}^2$ squares on Silicon substrate, layer thickness $\sim 100\text{-}120 \text{ nm}$						
Etching results correspond only to the specific processes that have been tested						

3.4 Proximity effect correction

3.4.1 Proximity effect

An incoming energetic electron beam entering in a solid surface (resist and substrate) forward scatters in small angles. As a result of this inelastic collisions, secondary electrons with low kinetic energy are created. Slow electrons cause the resist exposure and induce a certain delocalisation from the original beam delivery point in a range of few nanometers. But, occasionally, large angle collisions also occur causing high kinetic energy electrons in the order of the primary beam that in turn forward scatters. Again, inelastic collisions drive to the creation of secondary electrons that efectively expose the resist material, if in there. In consequence, far away from the original region where the beam incides, the resist suffers the effect of electron exposure (Figure 3.76).

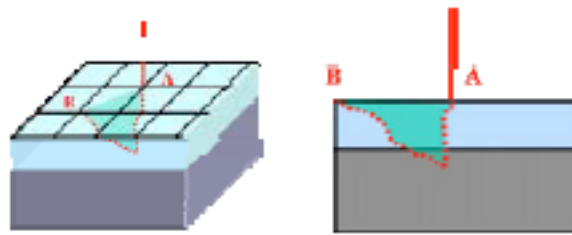


Figure 3.76 Electron effect reaches positions far away from the point of beam impact.

Proximity effect (PE) is the result in the resist of energetic electron trajectories and the energy deposited from the respective secondary electrons. PE causes non uniform absorption of energy densities and, specially, patterning sub-micron features is significantly affected. PE is considered the main factor limiting the EBL resolution.

Two different types of PE can be distinguished in patterned features: intrashape and intershape PE. Intrashape PE arises in isolated features that exhibit smaller dimensions even when they are equally exposed in dose. Smaller features receive lower deposited energy and, hence, they need higher electron doses to be fully exposed or longer development times. If features with significant difference in their dimensions are irradiated with equal dose, non uniform results might be obtained (Figure 3.77, left). Increasing overall dose or longer developments to adjust underexposed features will cause overexposure or overdevelopment in the bigger features. Intershape PE can be even more critical. Densely packed features mutually contribute to the final deposited energy in the exposed area, but PE also could deliver electron energy out of the exposed area, so that the space between shapes does not exist anymore (Figure 3.77, right).



Figure 3.77 (Left) Intrashape proximity effect. (Right) Intershape proximity effect.

There are two simple techniques to correct the resulting non uniform dose exposure: scaling of the delivered dose or adjustment of the design dimensions in the individual features of the patterned area (1). Dose modulation is the most widely used method and consists of scaling up or down dose exposure values of some parts of the design or portions of the features. However, this is not possible for all the EBL systems, so pattern scaling may be an alternative. Compensating some of the feature sizes, for example, reducing individual shapes in dense arrays, can be sufficient to achieve desired results. In both cases, computational approaches are proposed to give solutions that could solve the calculation algorithms in a unique and implementable form. The other correction approach is to manually adjust their doses and sizes by iterating test exposures which could result not always feasible and very time consuming.

Other options to avoid or reduce PE rely in the choice of the configuration and system parameters. A thin resist layer (<50 nm) diminishes forward scattering and can be complemented with a thicker mask underneath, if pattern transfer is needed. Also,

resists with high contrast usually present less sensitivity to the PE. Substrates are also crucial, while low atomic number materials produce less backscattered electrons, the use of membranes is also reliable. Changing the beam energy can be very convenient for many applications, since low voltages (<15 keV) reduce backscattering and high voltages (>50 keV) minimize forward scattering widening.

After all, if proximity effect correction (PEC) has to be necessarily applied, a third option is proposed: the use of computer-based calculations to automatically adjust the dose of the pattern at local level. Commercial software packages exist, such as NanoPECS from Raith GmbH. It was developed in collaboration with ETH Zurich and it will be used here to illustrate the performance of PEC.

A preliminar study of PE is performed to define a general methodology for the PEC. The ultimate goal is the minimization of PE in a negative resist, since its actual performance is often limited due to pattern distortion. First, a well know resist (PMMA) is tested to establish the procedure to determine PEC parameters. The choice of experimental designs and fitting functions is presented and first correction parameters are determined. The method is extrapolated for two negative resists. Afterwards, the obtained results are applied to correct the properties of a design that do show the undesired effect of proximity.

3.4.2 Theoretical model. Proximity function

As it has been mentioned, PE arises from the combination of different phenomena. The mutual influence of, i) electron scattering with the substrate and the resist, ii) the mechanism of interaction between electrons and resist molecules and iii) the specifications of the development process configures such a complex system that is difficult to be analitically solved. Even individually, these three phenomena are not completely understood or quantified. Theoretically, the models are based on simplificate approximations and not always precise and quantitatively adjusted. Experimentally, the result of PEC is only monitored at the end of the whole process (i.e. after resist development), so interpretation is affected by many uncertainties. As a matter of fact, PE is difficult to be expressed in a precise analytical form established from either the theory or the experiment. Due to this, an interpretation of the whole process behaviour leads to express PE in terms of what is called the proximity function ($f(r)$), (38, 39, 40, 41).

As an example, Monte Carlo simulations are used to describe electron trajectories in solid matter (42). The parameters of the model includes beam energy, electron delivered dose and substrate material. The system is modeled attending to a few considerations. The electron-resist interaction causes focused beam spreading, which depends on resist material and thickness. The substrate lying underneath the resist is the main responsible of backward scattered electrons, so PE is directly related with substrate composition and beam energy. Both phenomena seem to be correctly approximated by individual gaussian distributions, one quantifies electron beam effect of forward scattering and the other for backward scattering. Proximity function is then extrapolated as the weigthed sum of two gaussians (Figure 3.78) (43).

$$f(r) = \frac{1}{\pi(1+\eta)} \left(\frac{1}{\alpha^2} \exp \left[-\left(\frac{r}{\alpha} \right)^2 \right] + \frac{\eta}{\beta^2} \exp \left[-\left(\frac{r}{\beta} \right)^2 \right] \right) \quad (3.6)$$

where, r = lateral distance from incident beam

α = standard deviation of forward scattered electron distribution

β = standard deviation of backscattered electron distribution

η = ratio of energy deposited by forward scattered electrons to the energy deposited by backscattered electrons

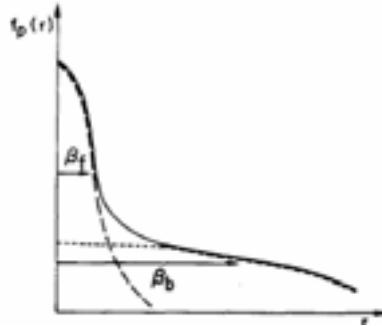


Figure 3.78 Proximity function is the sum of two gaussian contributions corresponding to forward (β_f) and backward (β_b) scattering (43).

The first term is attributed to the contribution of forward scattered electrons, whereas the second term is related with the backward scattered electrons.

The implications to correct PE have indeed been used in many cases and achieved proper results (44). However, specially for some substrates and resists a better match between the experimental results and the model is achieved with the addition of a third contribution. As a matter of fact, deposited energy distribution is not uniquely caused by PE in terms of electron scattering, so, due to this, more accuracy is obtained when an exponential decay modulates proximity function (45, 46).

$$f(r) = \frac{1}{\pi(1+\eta+\nu)} \left[\frac{1}{\alpha^2} \exp \left[-\left(\frac{r}{\alpha} \right)^2 \right] + \frac{\eta}{\beta^2} \exp \left[-\left(\frac{r}{\beta} \right)^2 \right] + \frac{\nu}{2\gamma^2} \exp \left[-\left(\frac{r}{\gamma} \right) \right] \right] \quad (3.7)$$

where, ν = efficiency of exponential function and γ = decay of exponential function

Efficient results are obtained using this proximity function for the correction of PE, for example in photonic crystals (47), although some limitations in correction accuracy are encountered (48). As it occurs in many cases, some terms of the equation can even be neglected since their contribution is reduced and PE may be caused mainly by contributions of the other terms of the equation. In consequence, simplified fitting formulas are easier to work with.

Another expression is proposed to simulate PE in terms of the absorbed dose. In this case, proximity function includes not only the electron trajectories and their slowing-down process, but also the effect of the exposure mechanism on the resist and the mechanism and rate of development process. But this model is even more complicate to apply and PE function parameters have to be measured for each individual part of the process (electron-solid interaction, exposure mechanism of the resist, development process).

3.4.3 Methodology for Proximity Effect Correction parameter

The correction of PE (PEC) is based on the determination of proximity function parameters. Applying them to the design configuration in terms of feature distribution and shape, the modulation of original design should result in uniformly deposited dose and, hence, developed image should coincide with the desired original design.

The determination of proximity function parameters can be undertaken with several strategies from experimental exposure tests. The methodology has to provide unequivocal parameters that allow technically reasonable PEC results in terms of time, design data size and complexity and resolution.

One of the simplest procedure to determine PEC parameters is the so called Doughnuts structure method (49). It is based on the simpler proximity function (3.6), where only α , β , η , are the parameters to be determined. This design takes advantage of the radial symmetry of the structure and relies on the concept of intrashape PE. It consists of an array of rings with variable radius for the inner ring that is exposed at different doses. The parameters of PE are obtained from experimental values: the pair of delivered dose and inner radius (D_i , R_i) that lead to completely clear the central point (P) of the doughnut structure (Figure 3.79) after irradiation and development.

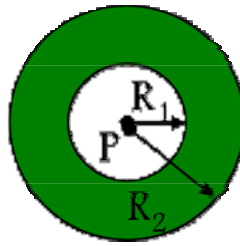


Figure 3.79 Design of the Doughnut structure used to determine PE parameters.

The effective dose, Q_p , that is received in P is,

$$Q_p = 2\pi Q \int_{R_1}^{R_2} r \cdot f(r) \cdot dr \quad (3.8)$$

where, Q = exposure dose

In the case of the ring structure, if R_2 is much larger than β and P is fully developed, then,

$$Q_p = D_0 = \frac{Q}{(1+\eta)} \left(\exp \left[-\left(\frac{R_1}{\alpha} \right)^2 \right] + \eta \exp \left[-\left(\frac{R_1}{\beta} \right)^2 \right] \right) \quad (3.9)$$

where D_0 is the actual dose that is required to clear out the resist when it is directly irradiated.

Identification of which dose causes inner circle disappearance allows to determine proximity function parameters by fitting experimental data pairs with the simple formula ($Q_p = D_0$) (Figure 3.80). The recognition of such boundary condition is

performed by optical inspection, but more accurate results may be obtained by SEM and AFM imaging or pattern transfer by metal deposition and lift off or etching. However, pattern transfer often generates additional uncertainties to the measurements, due to the process itself and its resolution. Another option is coverage of the exposure result with a gold thin layer, which facilitates inspection by SEM contrast enhancement. On the other hand, this method (Doughnuts structures) does not accurately describe α , so refined PEC parameters have to be determined by alternative designs.

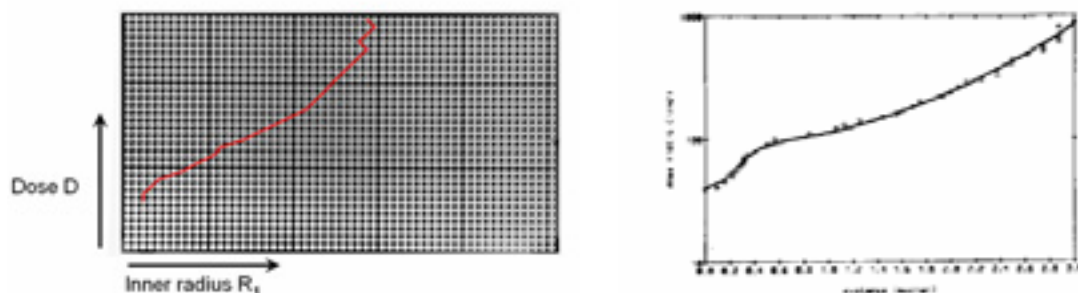


Figure 3.80 Procedure for PE parameters determination. (Left) Experimental determination of D_i/R_i data pairs (red) using Doughnuts structure. (Right) Fitting experimental data pairs with the theoretical expression allows to determine PE parameters values (49).

Other options for the determination of PEC parameters are based on the test cells proposed by Grobman (50), Machida (51), or Shaw (52). The designs go from rectangular shapes to arrays of lines that are optically evaluated, but curve fitting formula is rather complicate.

In the case of the evaluation system proposed by Jackel (53) and Dix (46), very small rectangles are used and SEM inspection enables to determine resulting linewidths. Precise metrology is needed, which difficults the realization of this technique, although the curve fitting formula is simpler than the one above.

Accurate results are obtained with the method described in (54), where α , β and η are obtained individually with separated test cells. Original matrix of bars with different doses is corrected with different proximity parameters. Corrected designs are exposed and, hence, parameters are determined when homogeneous results are obtained (Figure 3.81).

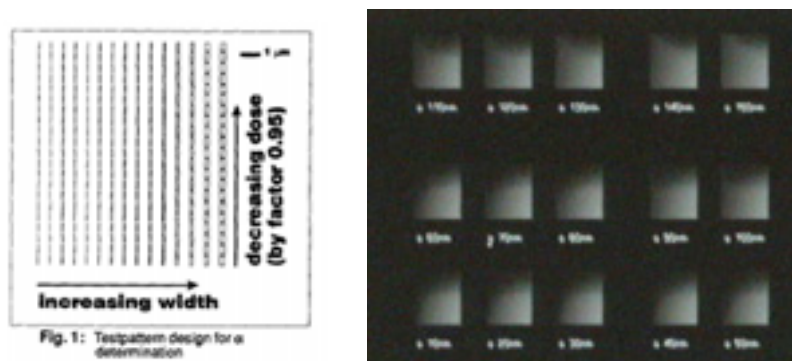


Figure 3.81 (Left) Specific design to determine α parameter. (Right) Correct PEC parameters are found when the boundary condition of horizontal line uniformity is achieved (54).

3.4.4 Experimental Proximity Effect Correction parameters

A preliminary approach to the use of PEC is performed. The aim of present study is to acquire a basic overview of the PEC parameters with different resists and under several EBL conditions. The choice of parameter determination method is done as a function of it, this is, with the simplest approach.

Therefore, doughnuts structures are used to obtain experimental data pairs (D_i , R_i) and they are fitted by the simpler equation (3.9). Eventhough it is reported that advanced proximity function (equation (3.7)) describes experimental points more accurately (Figure 3.82, left), a first general behaviour is established. In section 3.5.5, PEC parameters are used to perform subsequent process of design correction and use of it in real designs where PE arised and distorted pattern results.

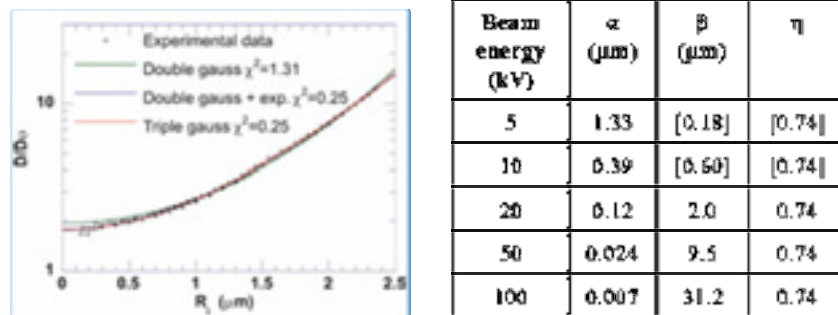


Figure 3.82 (Left) Fitting experimental data with the advanced proximity function is more accurate (55). (Right) Results of PEC parameters determination from (56).

First, the study is performed for single layer of PMMA 950k MW (~120 nm) on a Si substrate. The pattern design consists of five rows of rings of decreasing inner radius which are modulated by a dose factor (Figure 3.83, left). This design is exposed with different exposure doses and at both 10 and 20 keV beam energy. A set of starting values for (D_i , R_i) are obtained and they serve to give an idea of which are the ranges of radius and doses that is convenient to expose for each incoming beam energy. Hence, more designs are executed with smaller step variations (Figure 3.83, center and right) for the inner radius and at several different exposure doses.

Figure 3.83 (Left) Example of starting design for the determination of experimental data pairs (D_i , R_i) on Si substrate. (Center and right) In refined designs, inner radius variation is 0.1 μm . Circumferences indicate the R_i/D_i pairs where central point is completely developed.

As a result, a set of experimental data allows to observe the behaviour difference as a function of the two beam energies. In Figure 3.84, left, the longer electron range at 20 keV is clearly seen, but also a certain difference in their tendencies. For a beam energy of 10keV, the curve seems to correspond to a single exponential curve, whereas a kind of “shoulder-shape” is encountered for 20 keV. This accounts from the limitation of the Doughnuts structure approach to precisely determine α , but also highlights the convenience to establish PE parameters separately for different ranges for 20 keV (49).

The effect of the substrate on PE has been not only predicted, but experimentally observed and reported (57). As an example, the use of a 200 nm layer of SiO₂, instead of the bare Si substrate, already shows a slight variation in the experimental determination of (D_i, R_i) pairs for the fitting of PEC parameters (Figure 3.83, right). As seen in previous sections, this insulating layer does not cause a great variation, however, it has to be taken into account when high precision of EBL results are required.

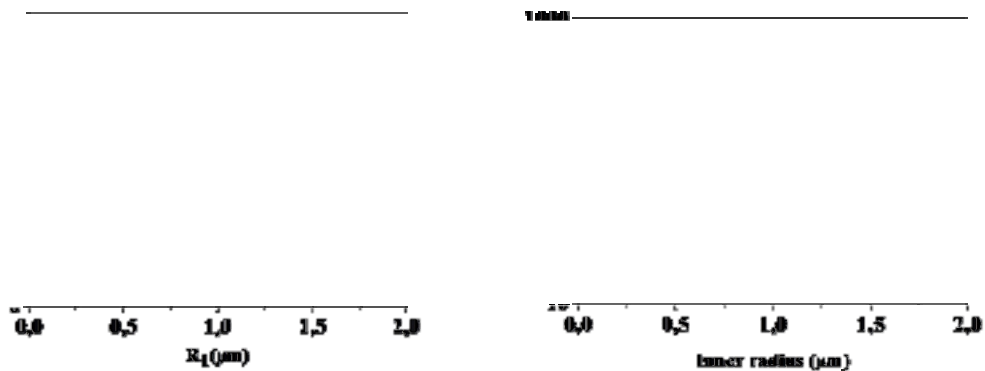


Figure 3.84 Plottings of experimental data pairs (D_i, R_i).
 (Left) Values for 950k MW PMMA on Si substrate at 10 and 20 keV beam energy.
 (Right) Comparison of results obtained in Si vs SiO₂, on 950k MW PMMA upon Si.

Determining PEC parameters from the experimental data is not trivial. The fitting formula (3.9) is used to adjust simultaneously three variables (α , β , η) and also clearing dose (D₀) needs to be fixed. As mentioned in section 3.3, clearing dose is not uniquely determined, since it can depend on design and also on the imaging method. Taking advantage of tabulated parameters (56), a first estimation of PEC parameters in the present configuration and EBL system are shown in figure 3.85. On the left, a good fitting is achieved for 10 keV beam energy and agreement with the values in the literature is found, even when the resist thickness is very different (Figure 3.82, right). It seems that is the whole set of PEC parameters what is important to balance, not the individual parameters. Similarly for 20 keV, on the figure 3.85, right, fitting PEC parameters adjust rather well with experimental points, but again a certain deviation for higher ranges is encountered and dividing the fitting in two different regions should be convenient. In addition, experimental PEC parameters are not similar to the reported ones. The necessity to adjust α with a more refined method arises and even PE is to be considered specially sensitivity to the 20 keV beam energy. Possibly, since this energy is between high (>50 kV) and low voltages (<15 kV), for PE it is manifested as more variable results. The close proximity between rings in the desing may cause additional deviations, since it is in the range of the lateral spreading (5 μ m) and larger external radius should match better with the premises of doughnuts structures method (i.e. R₂ > β).

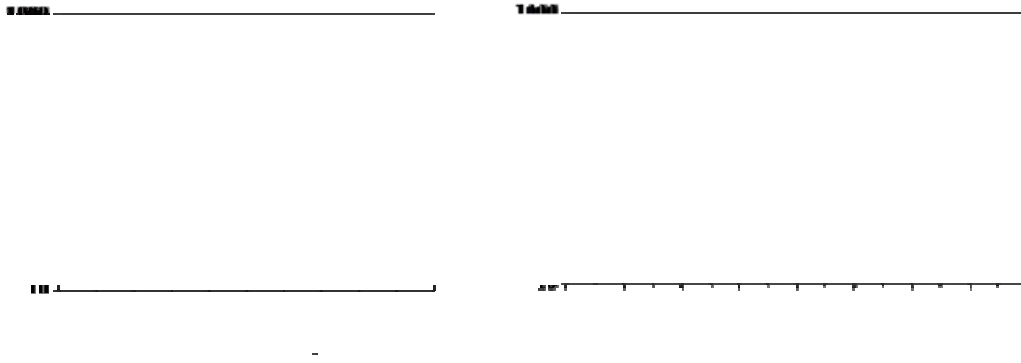


Figure 3.85 Examples of fitting curves for the experimental results on 950k MW PMMA upon Si at 10 keV (left) and 20 keV (right).

The PEC parameters are: $\alpha = 0.4$; $\beta=0.6$; $\eta=0.75$ for 10 keV and $\alpha = 0.3$; $\beta=2$; $\eta=0.8$ for 20 keV.

Paying attention to the change in the fitting curves with the variation of the different parameters, the convenience of some starting values to have an *a priori* idea of which are the correct ones becomes clear. In figure 3.86, left, 10 keV experimental points are plotted together with four fitting curves from different combinations of (α , β , η , D_0) sets. In red, the fitting showed in previous figure is considered the more adequate for describing the system performance, this is $\alpha = 0.4$, $\beta = 0.6$, $\eta = 0.75$, $D_0 = 50 \mu\text{C}/\text{cm}^2$. The green fitting does not differ a lot from experimental points and corresponds to reducing α to half the previous value, 0.2. In fact, also D_0 has to be adjusted in order to achieve a better match $D_0 = 35 \mu\text{C}/\text{cm}^2$. It is not exactly that forward scattering (β) contribution has been precisely determined, but reasonable values for clearing dose are to be used. The importance of the balance of the four parameters is reinforced. Fitting C, in blue, is obtained changing β to 1 and it seems clear that backscattering is the main contribution. It determines the slope of the curve and even when changing D_0 to $70 \mu\text{C}/\text{cm}^2$ can compensate curve Y position, this set of PEC parameters does not coincide at all with experimental points. Last case is $\alpha = 0.4$, $\beta = 0.6$, $\eta = 1.5$, $D_0 = 50 \mu\text{C}/\text{cm}^2$, so fitting D differs from A just in the ratio that accounts from the efficiency of backward versus forward scattered electrons. A 50% change in η value does not cause much difference in the good fitting agreement, compared to curve A. As mentioned, determination of the whole set of PEC parameters does not result easy to be unequivocally defined, but it will be crucial in their application to correct design dose modulation. An idea of which are the correct values can be assessed from the representation of resulting clearing dose using different sets of α , β and η in (3.9). The dispersion of the resulting points from the D_0 value used in α , β and η determination gives an idea of how good they are. Fitting A, with $\alpha = 0.4$, $\beta = 0.6$, $\eta = 0.75$, gives the smallest dispersion around $D_0 = 50 \mu\text{C}/\text{cm}^2$ (Figure 3.86, right). Together with the inherent dispersion from any experimental data, it has to be remarked that no experimental data pairs are removed. It is obvious that the points from first designs, that serve to establish the subsequent more refined measurements, will increase data dispersion from the ideal fitting.

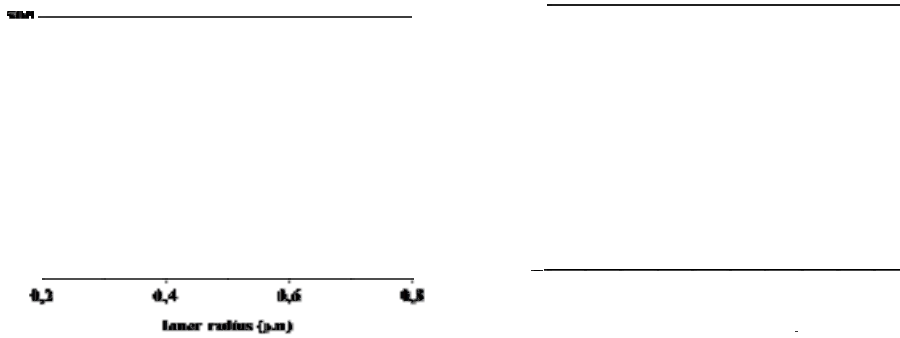


Figure 3.86 (Left) Examples for the variation of PEC parameters on fitting curves
(Right) Dispersion of calculated D_0 using fitting A parameters.

[A: $\alpha = 0.4$, $\beta = 0.6$, $\eta = 0.75$, $D_0 = 50 \mu\text{C}/\text{cm}^2$; B: $\alpha = 0.2$, $\beta = 0.6$, $\eta = 0.75$, $D_0 = 35 \mu\text{C}/\text{cm}^2$;
C: $\alpha = 0.4$, $\beta = 1$, $\eta = 0.75$, $D_0 = 75 \mu\text{C}/\text{cm}^2$; D: $\alpha = 0.4$, $\beta = 0.6$, $\eta = 1.5$, $D_0 = 50 \mu\text{C}/\text{cm}^2$].

Additional difficulties are to be encountered when applying this method to determine PEC parameters in the negative resists (and, in consequence, to successfully correct pattern designs). First, because it is not sure that the same methodology can be extrapolated from the positive resists methodology, in terms of theoretical background, boundary conditions for experimental data pairs determination, etc. Second, due to the intrinsic nature of the resists: tone, high sensitivity, low contrast, etc. And third, owing to the fact that no reference parameters exist for proximity effect, neither commonly accepted exposure conditions are defined.

Equivalent exposure strategy to the one of PMMA is performed both for epoxy based resist (mr-EBL-6000.1 XP) and for commercial ma-N 2401, at 10 and 20 keV beam energy and with the same previous designs (Figure 3.87). The extraction of experimental data pairs for (D_i, R_i) is also analogous to the case above and results are summarized in figure 3.87. Again the same performance difference is found when beam energy is changed from 10 to 20 keV and only more experimental data should be convenient, specially for ma-N 2401, in order to develop a more detailed study.

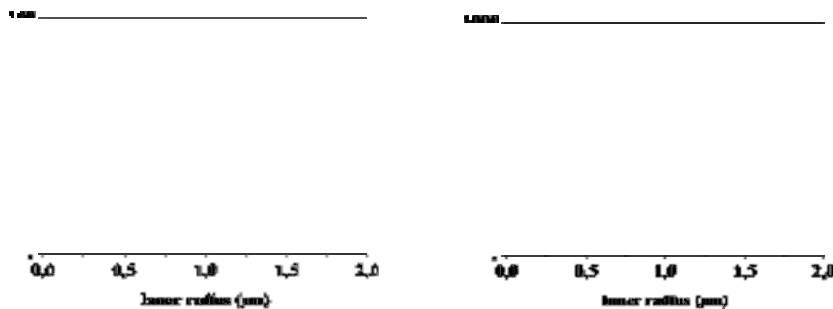


Figure 3.87 Experimental data pairs (D_i, R_i) obtained for mr-EBL 6000.1 XP (left) and ma-N 2401 (right).

However, a simple comparison between the two negative resists can be done if doses are normalised, using the actual exposure doses determined by dose tests (section 3.2.2). Indeed, figure 3.88 shows that similar PE performance is found, owing to the parallel slope of the experimental points and even divergence could be attributed to the normalization values themselves.

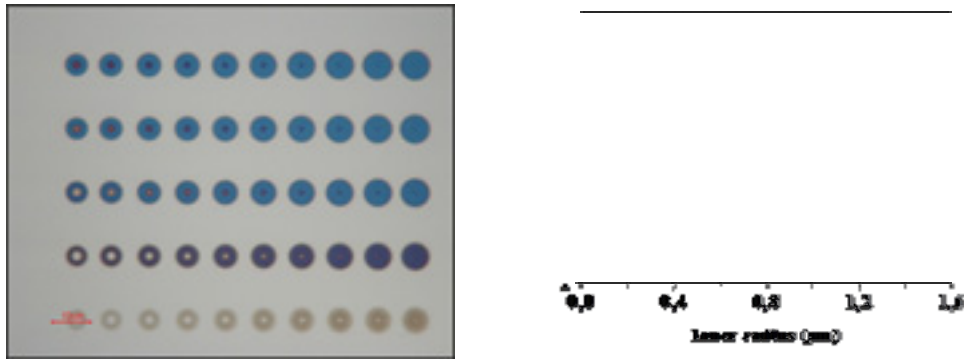


Figure 3.88 (Left) Optical image of Doughnuts structure test in mr-EBL 6000.1 XP at 20 keV on Si substrate. (Right) Comparison of experimental data pairs (D_i , R_i) for the two negative resists on Si exposed at 10 keV. Performance is similar.

Next step consists of establishing the fitting that will enable the determination of PEC parameters for the subsequent design correction. As mentioned, no starting data values exist. Therefore, considering the general performance similar to PMMA, extrapolation of parallel behaviour is also applied. In figure 3.89, the experimental results, together with fitting curve, for mr-EBL 6000.1 XP at 10 keV are plotted. In particular, fitting corresponds to $\alpha = 0.3$, $\beta = 0.6$, $\eta = 0.75$, which values coincide with the ones for PMMA except for α . As a matter of fact, β is attributed to be mainly dependent of substrate material, so it makes sense that this value is equivalent to the one of PMMA. The final evaluation to know if correct determination of PEC parameters is done is not possible to be established until PEC parameters are applied to a practical design correction.

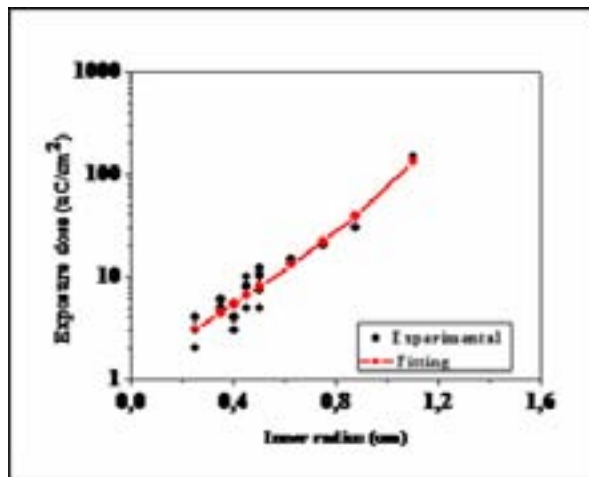


Figure 3.89 Fitting experimental results with $\alpha = 0.3$, $\beta = 0.6$, $\eta = 0.75$, for the resist mr-EBL 6000.1 XP.

3.4.5 Computer-based Proximity Effect Correction. NanoPECS

A large number of calculation algorithms and correction approaches for PE can be found in the literature, both for general applications or for particular designs. In addition to the minimization of PE by means of the system configuration or manual adjustment by dose modulation or pattern biasing, computer-based PEC programs can compensate PE.

Some examples are PowerProx (58), PROXY (13) or CAPROX (59) but here NanoPECS is used. NanoPECS is the PEC software supplied by Raith GmbH as an optional tool to support EBL capabilities. It has been developed in close collaboration with ETH Zurich. The correction consists of the dose scaling of fractured pattern (Figure 3.90). The different parts of the original design is deconstructed in smaller areas that are modulated with individual dose factors. The entire methodology starts with the determination of PEC parameters, selection of the elements or areas to be corrected and final manual tuning with some dose exposures tests or small variations of PEC parameters to re-correct design.

The program is based on two mathematical concepts. Each continuous element in the design is transformed into a discrete number of points. Representing them in matrix form by the proximity function, the crossed contribution of doses between discrete points is established. Hence, a set of linear equations that relate PE and structural parameters equals to the clearing dose. The inversion matrix gives the transformation of doses to compensate PE. The use of the program enables to interact in most parts of the calculation process to adjust to each specific case. It allows to choose the proximity function to be used (simple or advanced version), to establish new PEC parameters or use the ones existing in the database and definition of many other technical variables (partitioning, fracturing, algorithms, accuracy, etc) (55).

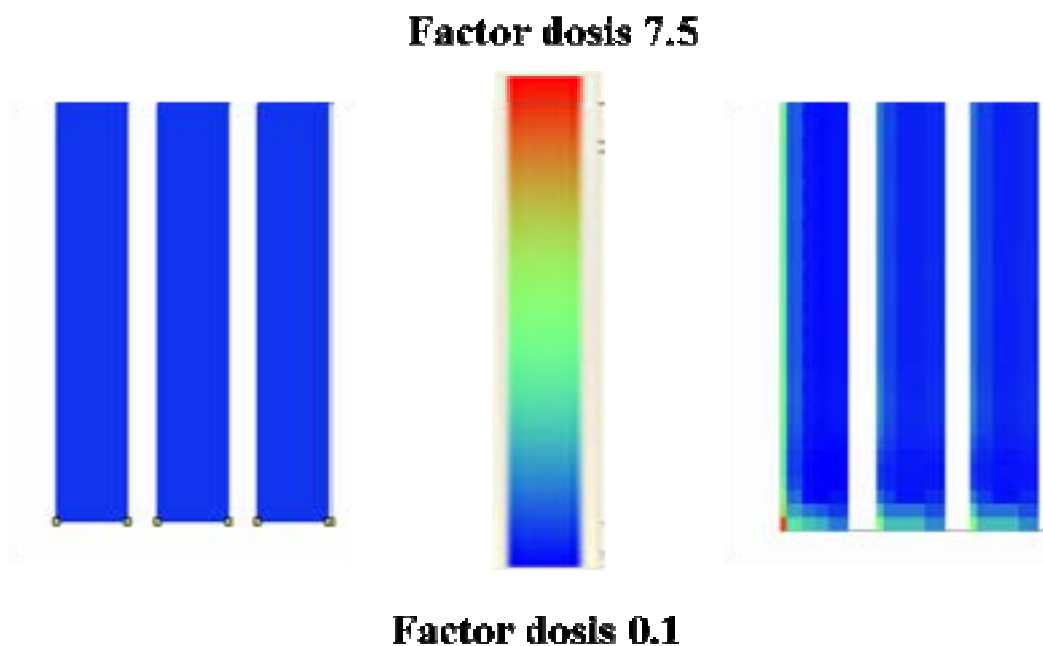


Figure 3.90 Example of the original (left) and corrected (right) design using NanoPECS. Lines are 500 nm in width and separated by 200 nm.

3.4.6 Results of Proximity Effect Correction on PMMA

The correct determination of PEC parameters cannot be demonstrated until they are able to correct an experimental case where PE is present. Since it is the first time at CNM that NanoPECS is used, many issues are to be solved and launched.

The experiments are always performed on a 100 nm PMMA 950k MW layer and with 10 keV electron beam energy. Standard development is used and AFM characterization assists the control of the results.

The first proposed design consists of an array of 500 nm width lines with 200 nm spacing. Exposure with commonly established clearing dose at this energy and resist type and thickness, $100 \mu\text{C}/\text{cm}^2$, leads to overexposure and disappearance of the resist in the space between the lines (Figure 3.91, left). Lower dose, $70 \mu\text{C}/\text{cm}^2$, is not the solution and also highlights the inhomogeneity in the real absorbed dose (Figure 3.91, center and right).

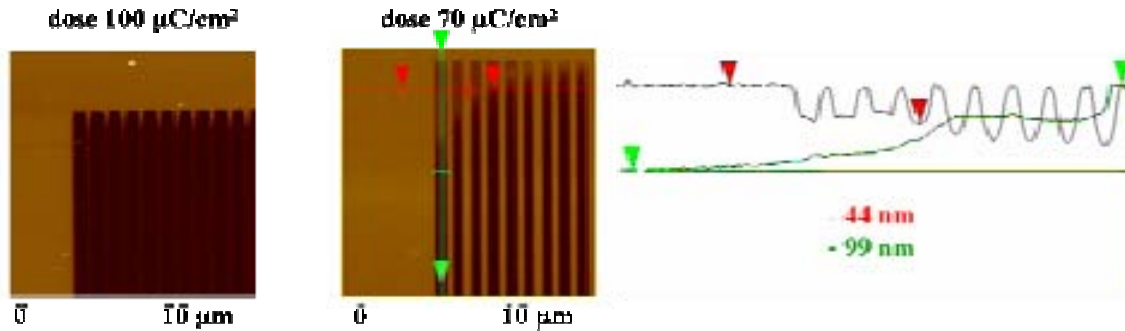


Figure 3.91 AFM images of an example of PE (scan size $10 \times 10 \mu\text{m}^2$). Inhomogeneous absorbed doses for exposures doses of (left) $100 \mu\text{C}/\text{cm}^2$ and $70 \mu\text{C}/\text{cm}^2$ (center) are registered. AFM profiles account for the non uniform resist development (right).

As presented in the discussion of the determination of PEC parameters, the choice of the correct values is not easy from the fitting. In figure 3.92, center and right, the results after exposure of two corrections using different PEC parameters is shown. In the left, fitting curve with $\alpha = 0.4$, $\beta = 0.6$, $\eta = 1.2$, $D_0 = 55 \mu\text{C}/\text{cm}^2$ seems correct and its application to design modulation leads to the central image. On the right side of figure 3.92, the outcome from other parameters correction is significantly different, even when the values do not differ so significantly ($\alpha = 0.4$, $\beta = 0.6$, $\eta = 0.75$, $D_0 = 50 \mu\text{C}/\text{cm}^2$). In consequence, it is not only difficult to decide which are the suitable parameters, but it is crucial and dramatic effects occur when design correction is not well driven.

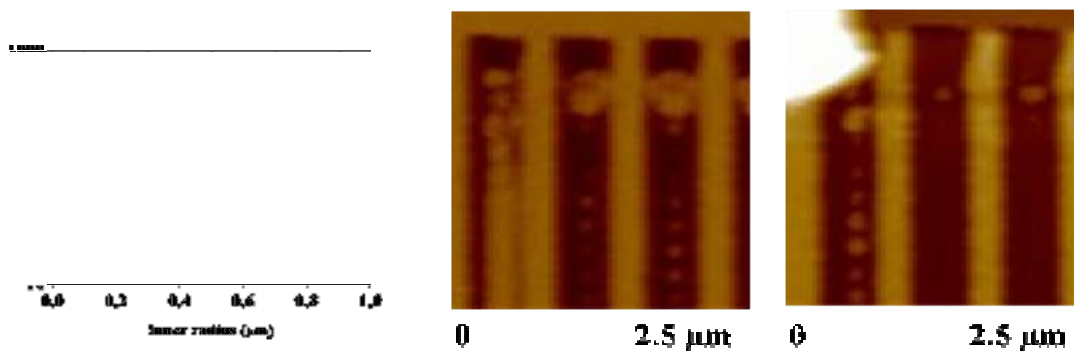


Figure 3.92 (Left) Fitting curve determines the PEC parameters. Corrected design is exposed and corresponds to the center image. (Center and right) Examples of results obtained with design correction for different PEC parameters.

The second set of parameters seems a better orientation and it is similar to the tabulated parameters of NanoPECS database. However, it does not succeed to completely solve PE consequences and the results suggest that certain dependence on the scanning strategy is also present. A possibility to compensate this relies on testing other scanning options, such as line vs meander mode or forcing scan direction to X or Y vs the automatic option. Results are summarized in figure 3.93 and indeed a strong dependence on these parameters is found.

Figure 3.93 Testing of same corrected design and constant dose with the different scan options: (top left) meander mode and scan direction automatic; (top right) meander mode and scan direction Y; (bottom left) line mode and scan direction Y; (bottom right) meander mode and scan direction X.

At this point, it seems that the main problem is originated from the intrinsic correction of the doses. The original non uniformity of the deposited dose comprised a big part of the design corners, but now corrected pattern has mainly solved these XY spatial inhomogeneities leaving what seems the effect of excessive dose factor scaling. One of the limitations of EBL systems comes from the finite speed of data transfer and restrictions in the beam movement and control. As shown in figure 3.90, corrected pattern is splitted in very small areas and precise dose factor is assigned to each one of them. Starting value for the original uniform design dose is 1, whereas corrected design presents a wide dose factor range after the calculation, between 0 and 76. During the exposure, these factors are multiplied by the exposure dose that is fixed in the exposure parameters window (Chapter 2), so a high dose contrast is expected and also some areas will not be correctly irradiated by design dose due to the limited minimum dwelltime (and in consequence, limited minimum dose). In order to compensate this, an alternative strategy for dose correction is proposed.

Changing the starting dose factor of the original design to 0.1, the range of corrected dose factors is reduced ten times (from 0 to 7.6), so the dose contrast effect may be reduced. The second problem, the impossibility to expose doses with zero or very low dose factors is solved easily. The corrected pattern is replicated several times just adding some dose factors to the whole dose modulated design. Hence, minimum dose limitation disappears or is reduced. Dose exposure value has now to be determined

for achieving correct results. In figure 3.94, two images of the array of lines using this correction methodology are shown. In the left, nearly uniform lines are obtained and, in the right side, the excess of electron dose also corroborates the good PEC with a uniform overdevelopment.

Figure 3.94 Using the strategy of dose factor the results are uniform along the whole pattern, even for different exposure doses.

Just with a refined final adjustment of dose exposure values, the presented methodology and strategy for correction seems to be capable of completely establishing the better design and exposure conditions (Figure 3.95).

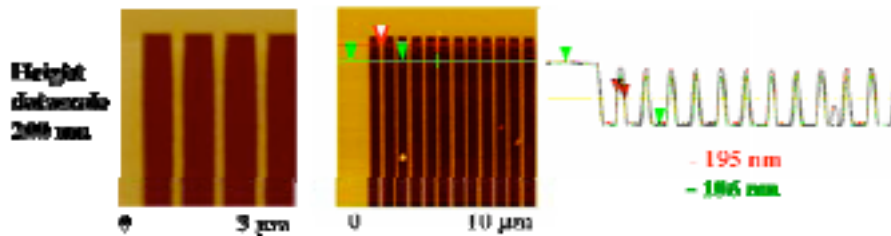


Figure 3.95 Optimization of PEC using final adjust of exposure dose and dose factor strategy.

As another example, a simple structure formed by a $5 \times 5 \mu\text{m}^2$ area close to a 500 nm width line is proposed (Figure 3.96). The same methodology that has been described above is used for the design correction and determination of exposure conditions.

Figure 3.96 Design used to corroborate the PEC methodology.

As can be seen in the left side of figure 3.97, again PE causes the shrinking of the separation and resist thickness between the line and the area, particularly in the central part. PE leads to variable width along the line and distortion of area shape. It is possible to compensate such phenomena with element fracturing and proper dose scaling (Figure 3.97, right).

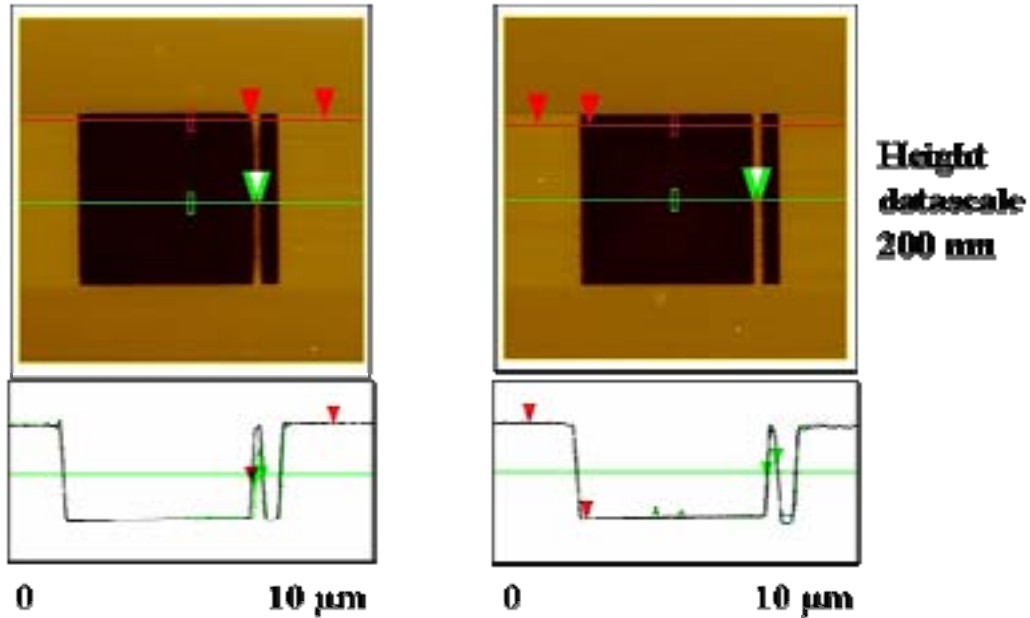


Figure 3.97 (Left) Result of exposure using uniform dose in all the design area. (Right) Result of exposure after design correction and adjustment of exposure dose.

In order to remark the necessity of PE correction a third design is tested and this pattern will be used also as a demonstrator for the negative resist in the next section. It consists of a long line that passes from being an isolated element to be confined between two large areas with small separation. As can be appreciated in the figure 3.98, left, the arrow points out that the final edges are overexposed (loss of resist thickness) and shape distorted, and also a slight linewidth widening is found. On the right, the results of PEC again corroborate that used PEC parameters are suitable and that the correction strategy leads to good results.

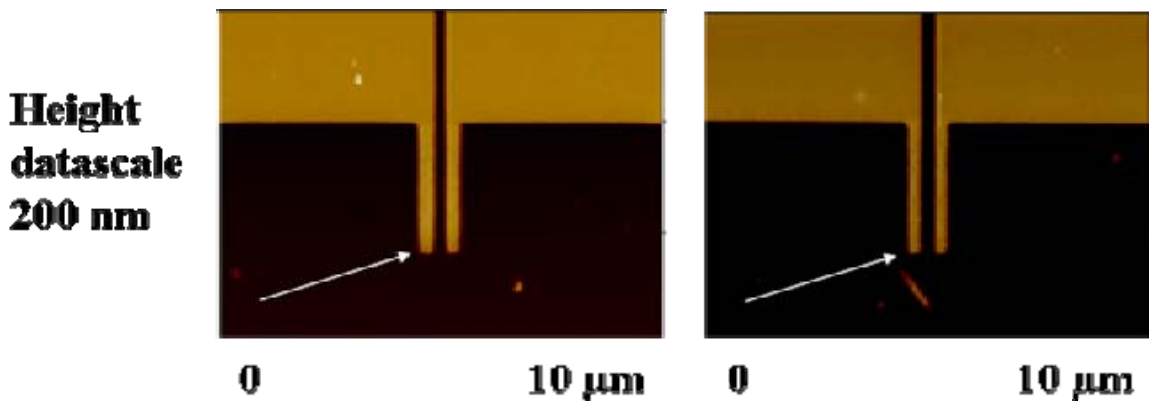


Figure 3.98 Design that will be used to apply the established PEC method on mr-EBL 6000.1 XP. (Left) Result of the exposure using uniform dose. (Right) Result of the exposure after PEC.

3.4.7 Results of Proximity Effect Correction on mr-EBL 6000.1 XP.

The final goal of this study of PEC is to define a methodology of correction of nonuniformities in the deposited/absorbed dose for the negative resists under electron beam exposure. The motivation arises from the strong inhomogeneities and distorted patterns that result from irradiation of this kind of resists and specially due to their high sensitivity and rather low contrast (Figure 3.99).

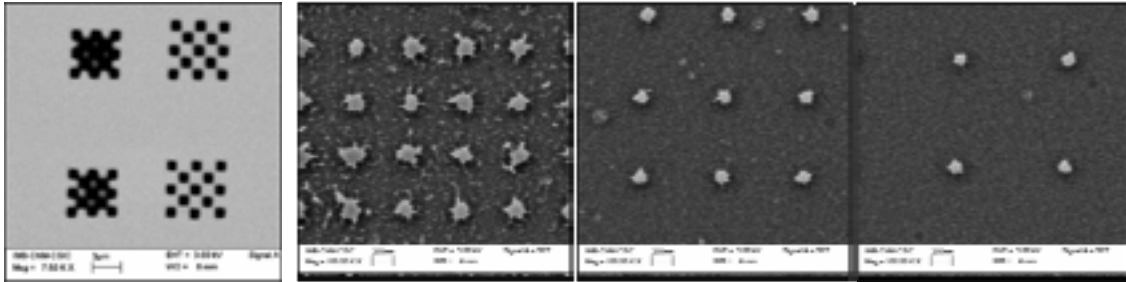


Figure 3.99 SEM images evidence the necessity to compensate PE on mr-EBL 6000.1 XP. (Left) Chess-like structure presents exposed resist in non-directly irradiated areas. (Center and right) Densely packed arrays are susceptible to PE, which may be inconvenient also for pattern transfer.

As another proof of presented PEC methodology, the modulation of mr-EBL 6000.1 XP is shown in Figure 3.100. The procedure is absolutely equivalent to the previous case. Last design example that has been tested on PMMA is used. Again electron beam energy is 10 keV and resist thickness layer is ~ 100 nm on a Si substrate. In figure 3.100, left, the result of EBL corroborates the necessity to adjust resist absorbed dose to make the pattern clean and reliable to the original structure. In noncorrected design, large areas (placed in the upper part of Figure 3.100, left) are slightly convex and present a decrease in resist thickness the more they approach to the edge. The central line also is nonuniform all along its length, respect to both its resist height and width. In addition, significantly big rests of resist are found in the spaces between the line and the areas. Here, PE seems magnified by resist high sensitivity.

The design correction is performed starting with the values of PEC parameters shown in section 3.5.3. The dose correction strategy is analogous to PMMA. Final dose exposure tests are performed to find the more suitable value. It is clear from figure 3.100, right that uniformity improves. AFM image demonstrates almost regular resist height along the areas and better edge shape, together with constant line width and height. In addition, rests in the gap are appreciably reduced not only in number, but also in size.

Figure 3.100 AFM images show the results of uniform dose exposure (left) and PE corrected design (right). The validity of PEC methodology, from PEC parameters determination to final exposure dose adjustment, is confirmed.

Summarizing, this chapter includes general information about the performance of different resists under the irradiation by electron beam, but also specific values of proper exposure conditions. The study of conventional methyl methacrylate-based resists as a function of resist material, substrate, beam energy, etc serves to establish the general behaviour of EBL technique. Two negative tone resists are also tested. Experimental exposures on thick layers of mr-L 5005 account for the characteristics and limiting factors that result when they are exposed to the electron beam. A new electron beam negative resist, mr-EBL 6000.1, is exhaustively characterized in terms of exposure and etching, which allows its use for nanofabrication. This section ends with the establishment of the complete methodology for the correction of proximity effect, the main limitation of EBL resolution. Correlation with simulations of electron trajectories within the resist layer and substrate is found all along the discussion of the experimental results.

References

- (1) M.A. McCord
Handbook of Microlithography, micromachining and microfabrication. Volume 1: Microlithography. Chapter 2: Introduction to Electron Beam Lithography
SPIE (1999)
- (2) S. Babin, I. Y. Kuzmin, and C. A. Mack
Comprehensive simulation of electron-beam lithography processes using PROLITH/3D and TEMPTATION software tools
Microelectronic Engineering **57-8**, 343-348 (2001)
- (3) M. Isaacson and A. Murray
Insitu Vaporization of Very Low-Molecular Weight Resists Using 1-2 Nm Diameter Electron-Beams
Journal of Vacuum Science & Technology **19** (4), 1117-1120 (1981)
- (4) C. G. Willson, H. Ito, D. C. Miller, and T. G. Tessier
Poly(Methyl Alpha-Trifluoromethylacrylate) as a Positive Electron-Beam Resist
Polymer Engineering and Science **23** (18), 1000-1003 (1983)
- (5) J. N. Helbert, G. J. Iafrate, C. U. Pittman, and J. H. Lai
Effect of Chemical Composition Upon the Radiation and Electron-Beam Resist Behaviors of Vinyl-Polymers
Polymer Engineering and Science **20** (16), 1077-1081 (1980)
- (6) E. Gipstein, A. C. Ouano, D. E. Johnson, and O. U. Need
Parameters Affecting Sensitivity of Poly(Methyl Methacrylate) as a Positive Lithographic Resist
Polymer Engineering and Science **17** (6), 396-401 (1977)
- (7) H. Elsner, H. G. Meyer, A. Voigt, and G. Grutzner
Evaluation of ma-N 2400 series DUV photoresist for electron beam exposure
Microelectronic Engineering **46** (1-4), 389-392 (1999)
- (8) H. Yamamoto, T. Kozawa, A. Nakano, K. Okamoto, S. Tagawa, T. Ando, M. Sato, and H. Komano
Study on acid generation from polymer
Journal of Vacuum Science & Technology B **23** (6), 2728-2732 (2005)
- (9) T. Kozawa, H. Yamamoto, A. Saeki, and S. Tagawa
Effects of low energy electrons on pattern formation in chemically amplified resist
Journal of Photopolymer Science and Technology **19** (3), 361-366 (2006)
- (10) A. Charlesby

- Atomic radiation and polymers**
London: Pergamon (1960)
- (11) V. M. Bermudez
Low-energy electron-beam effects on poly(methyl methacrylate) resist films
Journal of Vacuum Science & Technology B **17** (6), 2512-2518 (1999)
- (12) L. F. Thompson and R. E. Kerwin
Polymer Resist Systems for Photolithography and Electron Lithography
Annual Review of Materials Science **6**, 267-301 (1976)
- (13) PMMA
www.microresist.de/pmma_en.htm
- (14) A. Bross
Interlayer and intershot charged-induced pattern distortion on GaAs substrates exposed with a high throughput shaped beam EBL system
Available at www.gaasmantech.org/Digests/2004/2004Papers/3.3.pdf, 131-142 (2004)
- (15) G. Owen
Electron Lithography for the Fabrication of Microelectronic Devices
Reports on Progress in Physics **48** (6), 795-851 (1985)
- (16) M. Yasuda, H. Kawata, K. Murata, K. Hashimoto, Y. Hirai, and N. Nomura
Resist Heating Effect in Electron-Beam Lithography
Journal of Vacuum Science & Technology B **12** (3), 1362-1366 (1994)
- (17) J. Goldstein, D. Newbury, D. Joy, C. Lyman, P. Echlin, E. Lifshin, L. Sawyer, and J. Michael
Scanning Electron Microscopy and X-ray Microanalysis (3rd Edition)
Springer Science + Business Media, Inc, ISBN 0 306 47292 47299 (2003)
- (18) A. N. Broers, A. C. F. Hoole, and J. M. Ryan
Electron beam lithography - Resolution limits
Microelectronic Engineering **32** (1-4), 131-142 (1996)
- (19) M. G. Rosenfield and A. R. Neureuther
Exploration of Electron-Beam Writing Strategies and Resist Development Effects
IEEE Transactions on Electron Devices **28** (11), 1289-1294 (1981)
- (20) D. Joy
Monte Carlo modelling for electron microscopy and microanalysis
Oxford University Press, NY (1995)
- (21) M. Kotera, K. Murata, and K. Nagami
Monte Carlo simulation of 1-10-keV electron scattering in an aluminum target
J. Appl. Phys. ; Vol/Issue: 52:12, Pages: 7403-7408 (1981)

- (22) N.F. Mott
The scattering of fast electrons by atomic nuclei
Proc. Royal Society (London) **A124**, 425-442 (1929)
- (23) R. Browning
Universal elastic scattering cross sections for electrons in the range 1-100 keV
Appl. Phys. Lett. **58** (24), 2845-2847
- (24) I. Haller, M. Hatzakis, and Srinivas.R
High-Resolution Positive Resists for Electron-Beam Exposure
IBM Journal of Research and Development **12** (3), 251 (1968)
- (25) E. Reichmanis and A. E. Novembre
Lithographic Resist Materials Chemistry
Annual Review of Materials Science **23**, 11-43 (1993)
- (26) I. Gitsov and N. A. Madjarova
Synthesis and Evaluation of Methyl-Methacrylate Copolymers and Terpolymers as Electron-Beam Resists .1. Poly(Methyl Methacrylate-Methacrylic Acid-Methacryloyl Chloride)
Journal of Applied Polymer Science **41** (11-12), 2705-2710 (1990)
- (27) Z. Cui
Micro-Nanofabrication
Higher Education Press, ISBN 7 04 017663 017667 (2005)
- (28) S. A. Rishton
PhD Dissertation
University of Glasgow (1984)
- (29) M. J. Madou
Fundamentals of microfabrication: the science of miniaturization (2nd edition)
CRC Press, ISBN 0 8493 0826 8497 (2002)
- (30) S. Balslev, T. Rasmussen, P. Shi, and A. Kristensen
Single mode solid state distributed feedback dye laser fabricated by gray scale electron beam lithography on a dye doped SU-8 resist
Journal of Micromechanics and Microengineering **15** (12), 2456-2460 (2005)
- (31) M. Aktary, M. O. Jensen, K. L. Westra, M. J. Brett, and M. R. Freeman
High-resolution pattern generation using the epoxy novolak SU-8 2000 resist by electron beam lithography
Journal of Vacuum Science & Technology B **21** (4), L5-L7 (2003)
- (32) A. Pepin, V. Studer, D. Decanini, and Y. Chen
Exploring the high sensitivity of SU-8 resist for high resolution electron beam patterning

- Microelectronic Engineering **73-74**, 233-237 (2004)
- (33) Novopoly
Novel functional polymer materials for MEMS and NEMS applications
NMP3-CT-2005-013619
- (34) P. Mali, A. Sarkar, and R. Lal
Facile fabrication of microfluidic systems using electron beam lithography
Lab on a Chip **6** (2), 310-315 (2006)
- (35) V. Kudryashov, X. C. Yuan, W. C. Cheong, and K. Radhakrishnan
Grey scale structures formation in SU-8 with e-beam and UV
Microelectronic Engineering **67-8**, 306-311 (2003)
- (36) ma-N2400
www.microresist.de/ma-N2400_2005_en.htm
- (37) SioetchH 06/01 VLSISelectipur
worldaccount.basf.com/wa/EU~en_GB/Catalog/Chemicals/pi/BASF/PRD/30268479
- (38) M. Parikh
Corrections to Proximity Effects in Electron-Beam Lithography .1. Theory
Journal of Applied Physics **50** (6), 4371-4377 (1979)
- (39) M. Parikh
Corrections to Proximity Effects in Electron-Beam Lithography .2. Implementation
Journal of Applied Physics **50** (6), 4378-4382 (1979)
- (40) M. Parikh
Corrections to Proximity Effects in Electron-Beam Lithography .3. Experiments
Journal of Applied Physics **50** (6), 4383-4387 (1979)
- (41) M. Parikh and D. F. Kyser
Energy Deposition Functions in Electron Resist Films on Substrates
Journal of Applied Physics **50** (2), 1104-1111 (1979)
- (42) D. F. Kyser and N. S. Viswanathan
Monte-Carlo Simulation of Spatially Distributed Beams in Electron-Beam Lithography
Journal of Vacuum Science & Technology **12** (6), 1305-1308 (1975)
- (43) T. H. P. Chang
Proximity Effect in Electron-Beam Lithography
Journal of Vacuum Science & Technology **12** (6), 1271-1275 (1975)
- (44) W. Patrick and P. Vettiger

- Optimization of the Proximity Parameters for the Electron-Beam Exposure of Nanometer Gate-Length Gaas Metal-Semiconductor Field-Effect Transistors**
Journal of Vacuum Science & Technology B **6** (6), 2037-2041 (1988)
- (45) S. A. Rishton and D. P. Kern
Point Exposure Distribution Measurements for Proximity Correction in Electron-Beam Lithography on a Sub-100 Nm Scale
Journal of Vacuum Science & Technology B **5** (1), 135-141 (1987)
- (46) C. Dix, P. G. Flavin, P. Hendy, and M. E. Jones
0.1-Mu Scale Lithography Using a Conventional Electron-Beam System
Journal of Vacuum Science & Technology B **3** (1), 131-135 (1985)
- (47) R. Wuest, P. Strasser, M. Jungo, F. Robin, D. Erni, and H. Jackel
An efficient proximity-effect correction method for electron-beam patterning of photonic-crystal devices
Microelectronic Engineering **67-8**, 182-188 (2003)
- (48) R. Wuest, F. Robin, C. Hunziker, P. Strasser, D. Erni, and H. Jackel
Limitations of proximity-effect corrections for electron-beam patterning of planar photonic crystals
Optical Engineering **44** (4) (2005)
- (49) L. Stevens, R. Jonckhere, E. Froyen, S. Decoutere, and D. Lanneer
Determination of proximity parameters in electron beam lithography using doughnut structures
Microelectronic Engineering **5**, 141-150 (1986)
- (50) W. D. Grobman and A. J. Speth
Exposure Wedge for Electron-Beam Lithography Development Control and for Determination of Resist Development Rate and Proximity Effect Parameters
Journal of the Electrochemical Society **125** (3), C153-C153 (1978)
- (51) Y. Machida, N. Nakayama, S. Furuya, and S. Yamamoto
Enhanced Proximity-Effect Correction for Vlsi Patterns in Electron-Beam Lithography
Ieee Transactions on Electron Devices **32** (4), 831-835 (1985)
- (52) C. H. Shaw
Proximity Parameters Determination for Electron-Beam Lithography Using a Novel Technique
Journal of Vacuum Science & Technology **19** (4), 1286-1290 (1981)
- (53) L. D. Jackel, R. E. Howard, P. M. Mankiewich, H. G. Craighead, and R. W. Epworth
Beam Energy Effects in Electron-Beam Lithography - the Range and Intensity of Backscattered Exposure
Applied Physics Letters **45** (6), 698-700 (1984)

- (54) S. V. Dubonos, B. N. Gaifullin, H. F. Raith, A. A. Svintsov, and S. I. Zaitsev
Evaluation, Verification and Error Determination of Proximity Parameters Alpha, Beta and Eta in Electron-Beam Lithography
Microelectronic Engineering **21** (1-4), 293-296 (1993)

- (55) F. Robin, A. Rampe, et al
Accurate proximity effect correction of nanoscale structures with NanoPECS
Raith application Notes Available at www.raith.de

- (56) G. Owen
Methods for Proximity Effect Correction in Electron Lithography
Journal of Vacuum Science & Technology B **8** (6), 1889-1892 (1990)

- (57) N. Aizaki
Proximity Effect Dependence on Substrate Material
Journal of Vacuum Science & Technology **16** (6), 1726-1733 (1979)

- (58) S. J. Wind, P. D. Gerber, and H. Rothuizen
Accuracy and efficiency in electron beam proximity effect correction
Journal of Vacuum Science & Technology B **16** (6), 3262-3268 (1998)

- (59) U Hofmann et al
Hierarchical proximity correction using CAPROX
Proceedings of SPIE **2621**, 558-567 (1995)